

Report No. CDOT-DTD-R-2004-8 Appendices

DRILLED SHAFT DESIGN FOR SOUND

BARRIER WALLS, SIGNS, AND SIGNALS

APPENDICES A - F

APPENDIX A

**SURFICIAL SOILS AND BEDROCK OF COLORADO
AND GEOLOGIC OVERVIEW, WITH EMPHASIS
ON THE URBAN FRONT RANGE CORRIDOR**

TABLE OF CONTENTS

1.0	INTRODUCTION	A-1
2.0	SUMMARY OF SOIL AND BEDROCK CONDITIONS IN THE URBAN FRONT RANGE CORRIDOR.....	A-1
2.1	Soil Deposits	A-2
2.1.1	General Soil Types.....	A-2
2.1.2	Plasticity	A-3
2.1.3	Moisture Content and Ground Water	A-3
2.1.4	Consistency or Density	A-3
2.1.5	General Distribution of Near Surface Geomaterials	A-4
2.2	Bedrock	A-5
2.2.1	Generalized Distribution.....	A-5
2.2.2	Common Bedrock Types within the Corridor	A-6
2.2.3	Depth to Bedrock.....	A-8
2.2.4	Bedrock Hardness	A-9
3.0	STATE-WIDE GEOLOGY SUMMARY.....	A-10
3.1	Western Great Plains	A-11
3.2	Central Rocky Mountains.....	A-12
3.3	Western Plateaus.....	A-13
4.0	FRONT RANGE URBAN CORRIDOR SUBSURFACE CONDITIONS.....	A-17
4.1	SOILS OF THE CORRIDOR	A-17
4.1.1	Stratigraphic Relationships	A-17
4.1.2	Generalized Distribution.....	A-18
4.1.3	Major Soil Groups, Largely Age Sequential	A-19
4.1.4	Major Soil Groups, Largely Transitional.....	A-24
4.1.5	Special Soil Conditions.....	A-26

4.2 BEDROCK OF THE CORRIDOR..... A-28
 4.2.1 Generalized Distribution..... A-28
 4.2.2 Major Bedrock Groups..... A-29

REFERENCES..... A-35

1.0 INTRODUCTION

Over much of the state, Colorado surficial and shallow soils and bedrock are highly variable due to repeated episodes of mountain building, subsidence, igneous intrusion and extrusion, and glaciation. Within many provinces or trends, however, soil and bedrock character vary within definable limits due to similar geologic history, thus allowing for generalizations of their geotechnical properties. Emphasis in this report is on soil and bedrock conditions likely to affect structures rather than total geologic aspects.

This study concentrates on shallow subsurface conditions of soil and bedrock usually encountered for sound barrier walls, overhead signs, and similar structures along the Urban Front Range Corridor (the Corridor). For our purposes, the Corridor is defined by a combination of geologic/geomorphic and population/transportation factors. From west to east, it covers the far eastern portion of the Rocky Mountains Front Range, the Frontal Hogback, and the valleys and uplands divisions of the Great Plains Western Piedmont Sub-Province. It extends from approximately Fort Collins on the north, including the Greeley area, to Pueblo on the south, thus capturing the State's dominant population centers along Interstate 25. An outline of the statewide geological environment is also presented including a brief overview of soil and bedrock conditions along other (non-Front Range) important highway corridors.

2.0 SUMMARY OF SOIL AND BEDROCK CONDITIONS IN THE URBAN FRONT RANGE CORRIDOR

Soils and bedrock that exist along the Urban Front Range Corridor vary considerably as a result of the geologic processes that formed them. This section provides a brief overview of the soil and bedrock types often found in the Corridor and discusses engineering properties that may affect laterally loaded drilled shafts. More detailed geologic descriptions are presented in later sections of this report.

2.1 Soil Deposits

2.1.1 General Soil Types

Soils in the Corridor vary from clean sands and gravels to clays and silts. Sands and gravels are commonly encountered near existing and historic river channels including the South Platte River, Cherry Creek, Plum Creek, St. Vrain River, Cache la Poudre River, Arkansas River, and many others. Remains of previous valley floors or alluvial fans can be seen in gravel capped terraces in many areas. Alluvial clays and silts are also occasionally present within the river deposits, although the clay soils are much more common than silt soils. Silt is very often present as a minor constituent in alluvial sands and gravels. Eolian sands and clays are often located east of the major historic rivers, coinciding with the prevailing westerly winds. Sometimes these soils compress upon wetting and may require special design considerations. Significant thicknesses of residual surficial soils also exist in some areas, although to a lesser extent than alluvial and eolian deposits. Even less common are soils of colluvial (slope wash) origin which often contain the full range of soil types frequently mixed with bedrock fragments. Most sands and gravels typically encountered are rounded to subangular, and clays possess low to high plasticity. Due to the many geologic processes that created the soil deposits in the Corridor, significant variations in material types are common, often times over relatively short distances both horizontally and vertically.

Man-placed fill soils comprised of the full range of natural soil types, and sometimes bedrock fragments, are common along the Corridor. Cuts and fills are an inherent part of highway development and often have significant thicknesses at overpasses and in areas with moderate or greater topographic relief. Fill soils may also be found in old sanitary landfills, old aggregate pits, and in low lying areas that were raised for development to reduce the risk of flooding. In the case of sound barrier walls, berms are sometimes constructed to reduce the height of the wall so a nominal thickness of fill is typical to most sound barrier projects. Typically, fill soils have been placed under relatively controlled circumstances in recent decades, but there are exceptions. It remains CDOT practice to allow contractors to place construction debris within the right of way outside

of the roadway prism defined by a 1:1 outward slope from the edge of shoulder. These fills are typically uncontrolled.

2.1.2 Plasticity

Plasticity of fine grained soils in the Front Range Urban Corridor ranges from non-plastic to low plastic silts to very high plastic clays. Silt soils are not encountered very frequently. Most of the clays possess medium plasticity with plasticity indexes in the range of 15 to 30. Liquid limits are most often below 50, but higher liquid limits and plasticity indexes are occasionally observed. Liquid limits greater than about 70 are rare. Medium to high plasticity clays have the potential to be expansive when wetted. The swell potential depends on many factors including moisture content, dry unit weight, mineral composition, particle size gradation, and Atterberg Limits. Where swelling soils exist, it is likely that required caisson depths to resist uplift forces will control the design instead of lateral loading conditions. Of course, both conditions would need to be checked.

2.1.3 Moisture Content and Ground Water

Moisture contents of soils in the Corridor usually range from slightly moist to wet below the ground water table. Dry soils, defined for our purposes as not having visible moisture, are occasionally encountered. Saturated soils exist in areas of poor surface drainage, below the ground water elevation, and sometimes several feet above the ground water table due to capillary action in fine grained soils. Depths to ground water are highly variable, and localized perched water conditions frequently exist. Generally, however, the ground water table near permanent flowing water channels is likely to be at approximately the same level as the water surface. Ground water elevations rise further away from the river or creek and often correlate with the ground surface topography, but sometimes the ground water surface is highly variable.

2.1.4 Consistency or Density

The consistency and density of cohesive and cohesionless soils, respectively, also vary considerably. Cohesive soil consistency runs the gamut of the generally accepted

classifications from very soft to hard, and cohesionless soils also vary over the entire density range from very loose to very dense. Most cohesive soils encountered in the Corridor typically are medium (UC strength of 0.5 to 1.0 tsf or SPT of 4 to 8) to very stiff (UC of 2.0 to 4.0 tsf or SPT of 15 to 30). Consistency tends to vary inversely with moisture content; relatively dry cohesive soils are stiffer than soils with greater moisture. Most cohesionless soils range from medium dense (SPT of 10 to 30) to dense (SPT of 30 to 50).

2.1.5 General Distribution of Near Surface Geomaterials

The foregoing discussion categorizes soil types based on whether they are cohesive or cohesionless. In reality, many soils in Colorado do not fit neatly into one category or the other; they have cohesive and frictional components. It is assumed that most soils with greater than 70% passing the #200 sieve in Colorado will behave largely in a cohesive manner, and those with fewer than 30% fines will behave largely in a frictional manner. Estimated proportions of geomaterials likely to be encountered near the ground surface in the more populated areas of the Front Range Urban Corridor at sound barrier wall, overhead sign, or signal projects are presented in the Table A-1 to provide a general idea of the typical soil distribution. Silts are fine grained, but have little cohesion and are not commonly encountered in the Urban Corridor.

Table A-1

Material Type	USCS Symbols Included	Fines Content (% <#200)	Estimated Distribution (%)
Clay, silt	CL, CH, ML, MH	>65	20a
Sand, gravel	SW, SP, GW, GP, SC, SM, SW-SC, etc.	<35	20b
Intermediate soils	SC, SM, CL, CH, MH	35-65	60c

- a. Silt soils are a minor percentage.
- b. Gravel soils are a small percentage.
- c. A majority (est. 75%) of these soils are clay.

d. Estimated total distribution of soils based on USCS criteria is 65% clay (and silt) and 35% sand (and gravel).

The research team was hesitant to provide estimated distributions in the above table because of the great difficulty in selecting and evaluating an appropriate data set. Consequently, these estimates are primarily based on representative values deemed reasonable by several local consulting and CDOT geotechnical engineers that provided their opinions. USGS maps (see references) were also reviewed. The values presented in the table should not be considered absolute, but are presented to provide a relative indication of the frequency of occurrence along the Corridor and to help identify which soil conditions should be targeted for future lateral load tests. A review of exploratory boring logs and laboratory data conducted for several CDOT and Geocal, Inc. projects indicated that the above estimated distributions are reasonable. It is important to bear in mind that any particular project could have several soil types, or it could have only one general type of soil. Therefore, it is critical that site specific subsurface investigations be conducted.

2.2 Bedrock

2.2.1 Generalized Distribution

Except for transitional zones where bedrock is very highly weathered, the interface between soil and bedrock is usually fairly well defined along the Corridor. A major unconformity (period of non-deposition and/or erosion) due to uplift along the mountain front has separated younger soil from older bedrock. Bedrock units in the Corridor are distributed into four major settings (arranged as younger to older for the age of their generally included units):

1. Early Tertiary (Paleocene) coarse sandstone and conglomerate units, the youngest bedrock, are primarily limited to the central part of the Corridor forming major exposures in the Monument Highlands.
2. For valleys and uplands of the Western Plains Piedmont (the dominant portion of the Corridor), upper Late Cretaceous sedimentary rocks are intermittently exposed through soil cover throughout the northern and

southern parts and comprise most of the bedrock likely to be encountered in foundations.

3. The mountain front belt includes a wide age range (Triassic to Pennsylvanian) of diverse sedimentary rocks that are exposed in a variably wide and locally intermittent band immediately east of the mountains. Jurassic to lower Late Cretaceous age shale and sandstone-dominant, tilted strata are intermittently well exposed along the narrow Frontal Hogback and as flatter lying outcrops in the Arkansas River valley near Pueblo.
4. Pre-Cambrian igneous and metamorphic rocks are exposed pervasively in mountainous areas along the west margin of the Corridor.

2.2.2 Common Bedrock Types within the Corridor

Most drilled shafts are likely to be constructed where upper Late Cretaceous sedimentary rocks exist (item 2 above) which includes most of the Denver metro area, Fort Collins, Greeley, Boulder, Colorado Springs, and Pueblo areas. Major bedrock units include the Denver, Arapahoe, & Lower Dawson Formations and the Laramie Formation, Fox Hills Sandstone, and Pierre Shale. Other bedrock types (items 1, 3, and 4 above) are discussed in Section 4 of this report.

2.2.2.1 Denver, Arapahoe, and Lower Dawson Formations

The Denver, Arapahoe, & Lower Dawson Formations encompass a broad, arc-shaped band sweeping from northern Denver around the Monument Highlands with the general arrangement being Denver Formation dominant to the north (under most of the Denver metropolitan area), Arapahoe Formation in the center, and Lower Dawson Arkose to the south (around Colorado Springs). These units, although sometimes separately mapped, are largely age equivalent and interfinger with each other over long distances.

The Denver Formation mostly consists of claystone/shale, over most of the Denver area, with thinner interbeds of siltstone, weakly to well cemented sandstone, and infrequent conglomerate. Claystone/shale, as well as tuffaceous sandstone, are well noted for having major vertical and horizontal zones with high to very high swell potential; non-

sandy claystone is frequently highly plastic when saturated. Claystone clays and ash-derived sandstone clays are montmorillonite rich (frequently termed “bentonitic”) often including seams of nearly pure bentonite. Where unweathered, the formation includes a blue-green-gray claystone (and sandstone in some areas) locally known as the “Denver Blue”. The “Denver Blue’s” upper surface is not a stratigraphic horizon, but rather an irregular weathering/alteration zone that is often transitional. The bluish color has been observed to change to a predominantly grayish color after exposure to air.

The Arapahoe Formation is generally coarser than the Denver Formation. The two are frequently mapped as Denver-Arapahoe Undifferentiated in the Denver area. The formation is generally described as well stratified, interbedded claystone/shale, siltstone, sandstone, and conglomerate. A well-developed lower Arapahoe conglomerate is frequently only weakly cemented and is a significant aquifer. Conglomerate and sandstone units have variable low to moderate swell potential; siltstone and claystone/shale have moderate to high swell potential.

Lower Dawson Arkose also tends to be well interbedded with layers of conglomerate, coarse sandstone, shale, and silty fine sandy shale (termed “mudstone”). The coarser units usually have moderately well graded quartz and feldspar sands with granitic pebbles (“arkose”); local coal beds are noted. Clay rich and clay-dominant zones have moderate to very high swell potential and moderate to high plasticity, particularly in the Austin Bluffs area north of Colorado Springs.

2.2.2.2 Laramie Formation, Fox Hills Sandstone, and Pierre Shale

Laramie Formation, Fox Hills Sandstone, and Pierre Shale formations occur in two broad situations: (1) intermittently exposed in moderately dipping beds east of the mountain front (immediately east of the Frontal Hogback) from Ft. Collins to Denver and (2) with thin soil mantles in gently dipping and near flat lying units in the Louisville area and along Interstate 25 between Colorado Springs and Pueblo.

The Laramie Formation is dominated by thinly bedded shale and siltstone with common hard to friable sandstone interbeds, lesser thin hard conglomerate, and lignitic to sub-bituminous coal beds. The formation is sandier in the lower portion. Most Laramie clays are dominantly kaolinitic with usually low to moderate swell potential; the middle third tends to be montmorillonitic with resulting high swell potential. Sandstones vary from weakly to well cemented.

Foxhills Sandstone units are cross-bedded and quartz sand-dominant. Relatively thin interbeds of claystone/shale, mudstone, and coal occur throughout. The sands are generally weakly cemented and friable; they are important aquifers with medium to high permeability, particularly north of Denver.

The Pierre Shale is a very thick, claystone/shale-dominant formation with numerous thin bentonite beds throughout. The bedrock units are almost always suspect for moderate to very high swell potential, medium to high plasticity, and low slope stability nearly everywhere they are encountered along the Corridor. Thin sandstone interbeds occur throughout the formation. Significantly thick sandstone members are present in several areas at different stratigraphic positions. Hard limestone masses (butte formers in outcrop) occur in the middle portion to the south. To the south, the middle portion also contains appreciable gypsum content that may affect sulfate-susceptible cement.

2.2.3 Depth to Bedrock

Depths to the most common bedrock units are highly variable and depend on geologic processes that have occurred in an area and sometimes man's activities in the form of cut/fill operations. There is a large area of near surface bedrock in the Monument Highlands between southern Denver and northern Colorado Springs. Bedrock predominates the near surface geomaterials closer to the Rocky Mountain Front Range at the western edge of the Urban Front Range Corridor. In other areas of the Corridor, bedrock may exist near the surface or could be much deeper beneath alluvial deposits,

sometimes in the range of 80 to 100 feet. Generally, however, bedrock is likely to be encountered within the upper 50 feet of geomaterials at most sites. Bedrock is intermittently located within the upper few feet in many areas of the overall Corridor.

An estimated percentage of surficial geomaterials likely to be comprised of bedrock at a sound barrier, sign, or signal project in populated areas along the Corridor is on the order of 10 to 15 percent. Even within the population centers of the Corridor, bedrock occurs much more frequently than 15 percent of the projects when the total length of typical sound barrier, overhead sign, and traffic signal caisson depths is considered. It is important to note that the upper portion of geomaterials along a caisson provides the greatest resistance to lateral loads, although this is a function of pier diameter. Overhead sign foundations have the greatest depths because of the loading conditions on this type of structure, with typical depths in the range of 17 to 24 feet according to CDOT standard plans. Bedrock is very often encountered within the upper 25 feet; however, depths to bedrock are highly variable as discussed above.

2.2.4 Bedrock Hardness

The most common bedrock types in the Corridor, discussed in Section 2.2.2, are sedimentary deposits that have been heavily overconsolidated by as much as 1,000 feet of overburden that was subsequently eroded to the present day terrain. The previous overburden pressure, degree of weathering, and amount of cementation of sandstone or conglomerate, are the key factors that largely determine the hardness of the bedrock. Unconsolidated, undrained shear strengths in the Denver Formation range from 3 ksf to 30 ksf, and shear strengths in the Denver Blue range from 8 ksf to more than 30 ksf (Hepworth & Jubenville, 1981). Standard penetration test results generally range from about 30 to 80 for the non-Denver Blue bedrock, although some highly weathered areas may have SPT values in the teens. Denver Blue bedrock normally has SPT blow counts of at least 80. Denver Blue claystone/sandstone bedrock typically has blow count values in the range of 50/8" to 50/2", and sometimes this is the first 6 inches of a drive that would normally not be recorded for a SPT. SPT refusal also occurs. Bedrock hardness varies from very low strength to moderate strength according to International Society of

Rock Mechanics classification criteria. The weaker bedrock is better described in terms of soil consistency terminology in the range of very stiff to hard and tends to behave similar to heavily overconsolidated clay.

Another CDOT study currently underway dealing with axial drilled shaft capacity has yielded some useful data on the bedrock strength of the metro Denver area. As part of this study, Osterberg load cell tests (O-cell), pressure meter testing, and coring with subsequent unconfined compression testing was performed on the weaker brown claystones and the harder, gray “Denver Blue” claystone/sandstone. O-cell tests at two sites with relatively weak bedrock (SPT ranging from about 30 to 60) indicated ultimate caisson end bearing values on the order of 50 ksf, and three O-cell tests in the much harder bedrock indicate ultimate end bearing values of greater than about 250 ksf. Pressure meter tests conducted indicated unconfined strengths in the general range of 10 ksf to 20 ksf for the weaker bedrock and 50 ksf to greater than 150 ksf for the harder bedrock. Unconfined compression (UC) tests on the weaker bedrock generally ranged from 5 ksf to 20 ksf. UC tests on the relatively hard bedrock indicated strengths ranging from 50 ksf to 300 ksf; the higher values are from well cemented, clayey sandstone bedrock.

3.0 STATE-WIDE GEOLOGY SUMMARY

Colorado is situated across three continental-scale geologic and geomorphic provinces, each with remarkably different history and conditions and all with important subdivisions. They roughly divide the state into north-south trending thirds. From east to west they include: (1) The gently structured western margin of the Great Plains including the broad Colorado Piedmont gently sloping east from the Front Range, (2) complexly structured multiple major mountain ranges of the Central Rocky Mountains including significant intermountain valleys, and (3) intermediately structured uplifts and downwarps of the Western Plateaus. For brevity, the following paragraphs in this summary concentrate on present day conditions, especially as related to soil and bedrock distribution, rather than details of geologic history and structure. A simplified guide comparing relative geologic ages to absolute time and common formations is shown on the Colorado Geological

Survey publication “Colorado Geologic Highway Map” included in the envelope at the end of this report.

3.1 Western Great Plains

Colorado’s geologic share of the Great Plains is basically a broad, stable shelf floored by an unexposed metamorphic “basement” and a relatively uniform layer of Paleozoic through Early Mesozoic clastic (transported particles, *e.g.*, sandstone, siltstone, & claystone/shale) and carbonate (limy precipitates and particles, *e.g.*, limestone & dolomite) sedimentary rocks. The later have only limited exposure in the southeast corner of the state and along a narrow mountain front band immediately east of the Front Range. The shelf is gently deformed as a relatively wide, deep trough paralleling the Front Range (the Denver and Raton Basins) that has preserved a thick accumulation of Cretaceous age claystone/shale-dominant sedimentary rocks with significant sandstone, and much lesser limestone, members. Older portions of these Cretaceous units extend more thinly eastward into Kansas. Cretaceous rocks have major surface exposures or form relatively shallow bedrock along the Front Range Urban Corridor (as detailed in Section 4.2) and along all of Interstate 25, along the broad valleys of the Platte River (Interstate 76 & U.S. 36) and Arkansas River (U.S. 50), high plains drainage basins such as Big Sandy Creek (portions of Interstate 70, U.S. 40 & 287), and the Chaquaqua Plateau (greater Las Animas County area). The Paleozoic through Cretaceous strata are flat lying to very gently dipping throughout the province except for being steeply upturned along the mountain front of the Front Range and moderately folded and faulted in structures of the Canon City embayment west of Pueblo (U.S. 50).

Cretaceous rocks are mantled by a wide range of variably thin to thick Quaternary age alluvial (water transported) soils in the flood plains and terraces of river valleys and major tributaries. They are also commonly overlaid by broad, relatively thin sheets of unconsolidated eolian (wind born) deposits on many upland surfaces between the Platte and Arkansas Rivers. These uplands (or “high plains”, particularly in the northeast, far east, and southeast parts of the state) also include significant mantles of Middle to Late

Tertiary clay, sand, and gravel that are variable loose (soil) to well cemented (bedrock) as typified by the Pawnee Buttes and high terraces along the Platte River near Sterling.

3.2 Central Rocky Mountains

This rugged belt includes numerous major ranges (*e.g.*, the Front Range, Sangre de Cristo Mountains, Mosquito Range, Sawatch Range, and Elk Mountains) of tremendous geologic complexity due to a history of repeated regional mountain building oscillations from the Early Pre-Cambrian to today. They nonetheless have some broad commonalities. The cores of the ranges consist of deeply rooted older Pre-Cambrian age metamorphic material derived from intermediately to highly altered, preexisting sedimentary and igneous rocks (now quartzite, schist, gneiss, and mixed-type migmatites). Except for the less altered quartzite, most have moderately to well developed foliation (preferred alignment of mineral constituents with resulting planes of relative weakness). The metamorphic complexes are widely intruded by younger Pre-Cambrian plutonic igneous rocks of mostly granitic composition. Some of the intrusions (*i.e.*, the Pikes Peak Batholith west of Colorado Springs) are so large as to dominate much of a range leaving only smaller metamorphic remnants exposed. The granitic rocks tend to be massive (non-foliated). Both the metamorphics and granitics tend to be pervasively fractured with multiple intersecting joint sets. Both small and major faults are common; a few, particularly in Summit-Lake Counties and along the west side of the Sangre de Cristo Mountains have been active in the Quaternary Period. The granitic masses are noted for weathering deeply on gentle to intermediate slopes and where well fractured, forming granular and porous residuum and colluvium. Transportation corridors crossing Pre-Cambrian-dominated bedrock include Interstate 70 from just west of Golden to near Dillon, U.S. 50 from west of Canon City to near Coaldale, and U.S. 50 over Monarch Pass.

During periods of uplift of the Rocky Mountain ranges, large amounts of sediments, particularly coarse clastics, were shed onto adjacent lowlands. When erosion or tectonic sagging lowered the mountains, marine incursion resulted in thick finer clastic and carbonate deposits. Substantial remnants of these Paleozoic through lower Early

Cretaceous sedimentary rocks are preserved in fault blocks within the mountains and on their flanks. These are frequently steeply dipping, highly faulted, and occasionally highly folded. These remnants tend to be aligned in narrow, north-south trending bands. Example areas include: (1) The S.H. 9 corridor from the Blue River Valley and Kremmling on the north, through Dillon and Breckenridge, to Fairplay on the south, (2) S.H. 160 over La Vita Pass, (3) S.H. 50 from Coaldale to near Salida, and (4) along Interstate 70 in the greater Vail area. Depressions in the foundering surface of the ancestral Rockies created some enclosed basins that promoted relatively thick evaporite deposits (calcium sulfate/gypsum in particular). These evaporite-rich sediments are unstable, tend to flow under pressure, and create highly contorted zones where overlaid by, or interbedded with, clastic and carbonate rocks (as exemplified by Pennsylvanian age interbedded units along Interstate 70- in the Eagle Valley between Eagle and Dotsero). They are also soluble and may cause sinkholes to develop.

Superimposed on the Pre-Cambrian ranges and Paleozoic-Cretaceous remnants are several relatively flat lying Tertiary age volcanic fields with thick, layered deposits of tuff (hardened ash) and andesitic lava. The lava is often very resistant to erosion resulting in, for example, the Rabbit Ears Range (U.S. 40 southeast of Steamboat Springs). Less resistant tuff exist in the floors of some valley areas such as much of South Park (S.H. 9 south of Hartsel). Well-faulted and folded Early Tertiary conglomerate, sandstone, and coaly shale units mantle older rocks in a large area of North Park and the Rabbit Ears Range (U.S. 40 and S.H. 9).

3.3 Western Plateaus

West of the Central Rocky Mountains, a series of gently to moderately structured geologic basins and uplifts are broadly termed the Plateau Province due to the frequently high, similar elevation of much of the surface. This surface is occasionally punctuated with relatively more complex mountains that are more localized than the Rocky Mountain ranges. Features of this province (generally from north to south) include the following the following major subdivisions:

Sand Wash Basin in the northwest corner of the state (including the U.S. 40 corridor west of Craig) is dominated in the surface and shallow subsurface by thick sequences of mixed clastic sedimentary rocks ranging from conglomerate to claystone/shale including oil shale and some coal. The basin tends to be rimmed with Cretaceous shale-dominant units that include significant sandstone members, major coal beds, and swell-prone claystone/shale portions (U.S. 40 between Steamboat Springs and Craig). The large Piceance Basin to the south is situated between S.H. 64 west of Meeker and S.H. 92 north of Delta and including the Interstate 70 corridor from Glenwood Springs to Grand Junction. It has a very similar sequence of Tertiary sedimentary rocks ringed by Jurassic-Cretaceous sedimentary units. The narrow Grand Hogback on the east side includes major ridge-forming sandstone units as well as thick coal deposits (*e.g.*, the Newcastle area along Interstate 70 between Glenwood Springs and Rifle). The west and southwest sides of the Piceance Basin are defined respectively by the uplifts of Douglas Creek Arch (along S.H. 139, Grand Junction to Rangely) and Uncompahgre Plateau (Southwest of Interstate 70 at Grand Junction). These uplifted flanks have created some of the most extensive Cretaceous sedimentary rock exposures in the state.

The Uncompahgre Plateau, centered in Montrose County, was created by gentle arching of Pre-Cambrian granitic rocks that have limited exposure along the crest (*e.g.*, along S.H. 114 between Whitewater and Gateway). Deep incisions of the uplift have created striking cliff exposures of the thick mantling and very resistant red-brown Triassic age sandstone, siltstone, and shale. Less resistant Jurassic to Cretaceous mixed clastic rocks cover most of the flanks of uplift.

The southwestern portion of the state includes portions of two major and remarkably different basins (Paradox and San Juan Basins) separated by the Colorado Plateau (that sometimes gives its name to the entire Western Plateaus Province). The Paradox Basin contains a series of large, well-defined folds trending northwest-southeast with unique “reversed topography”: the anticlinal (upwards) folds tend to be valleys due to evaporite dissolution while the synclinal (downward) folds are higher. The basin is composed of thick sections of Permian to Pennsylvanian age arkosic sandstone-conglomerate, shale,

limestone, and evaporities (salt, gypsum, potash, etc.). The evaporities have tended to flow towards the basin center to form large unstable masses less dense than the surrounding rock. Paradox Valley along S.H. 90 (centering at Redrocks) is an example of a trend with salt at and near the surface. Portions of the folds and basin flanks have Triassic-Permian cliffs of very hard siltstone and sandstone (same as the Uncompahgre Uplift) as well as thick Cretaceous shale (including bentonitic layers) and sandstone units (as along U.S. 141 from Placerville to Uravan).

Rocks of the Colorado Plateau are very gently structured and deeply incised by the west-flowing Dolores River and major tributaries. Triassic age cliff-forming conglomerate (limestone pebble), sandstone, siltstone, and shale are exposed in deeper canyons. They are thickly mantled by Cretaceous shale, calcic shale, and resistant sandstone units (including the cliffhouse ledges at Mesa Verde National Park). The area along U.S. 160 from Mancos to Cortez typifies much of the Plateau. Thick eolian (wind born) sandy soil has developed in large patchy areas along U.S. 160 from Northdale to Cortez.

The San Juan Basin extends south from Durango (*e.g.*, along U.S. 550 and S.H. 511) into New Mexico. The northern upturned rim (Pagosa Springs to Durango, U.S. 160) exposes the same Cretaceous clastic units as the Colorado Plateau in alternating sandstone hogbacks and shale valleys. The main, very gently south sloping basin has thick Tertiary arkosic sandstone/conglomerate, volcanoclastic (volcanic particles) sandstone/conglomerate, and shale exposed at the surface.

There are two major sub-provinces in the southwest quarter of the state that are geologically separate from the Central Rockies and Western Plateaus that surround them: The Needle Mountains/San Juan Mountains and the San Luis Valley. The Needle Mountains are cored by an uplifted, intensely faulted complex of metamorphosed volcanic-sedimentary rocks intruded by large gabbroic (ferro-magnesium rich) intrusive masses. This complex is surrounded by thick, well-structured layers of Permian-Pennsylvanian age arkosic sandstone/conglomerate, siltstone, shale and lesser limestone, and Mississippian limestone-dolomite. U.S. 550 from Hermosa to Silverton cuts through

the center of the area. The adjacent San Juan Mountains are deeply underlain by Cretaceous sedimentary rocks, but owe their existence to widespread Tertiary volcanic flows of varying rhyolite-andesite-basalt composition. These hard, resistant units tend to be well-fractured (often well-jointed in columnar patterns) and vuggy. They are interbedded with frequently thick, less resistant ash, tuff (granular volcanics), and inter-flow conglomerates (frequently water bearing). The entire San Juan Volcanic Field is well-faulted and flows are frequently cut by intrusive dikes of rhyolitic-andesitic composition. The flows vary from flat lying to moderately dipping except for large, circular areas of volcanic collapse/explosion that are highly structured (called caldara, as with the Silverton, Lake City, and Creede mining districts). Slopes at higher elevations contain thick soil deposits of glacial drift and down-slope colluvium; both tend to be relatively well-graded and commonly contain unweathered boulders. Transportation corridors crossing the volcanics include U.S. 160 (Pagosa Springs to Del Norte, including Wolf Creek Pass), S.H. 149 (South Fork to Lake City), and U.S. 550 (Silverton to Ouray).

The San Luis Valley is a major geologic basin with thick unconsolidated sediments covering most of the valley floor (as U.S. 285 and S.H. 17 south of Villa Grove to Antinito and U.S. 160 from Ft. Garland to Monte Vista). These include some of the oldest soils in the state ranging in age from Tertiary through Holocene and are composed of mixed alluvial gravel, sand, and silt as well as eolian sand (the most noteworthy deposits being Holocene age dunes at Great Sand Dunes National Monument). The valley is frequently rimmed with coarser Pleistocene gravel-dominated alluvial deposits including sand, silt, and clay interbeds; west and south side gravels contain abundant volcanic clasts and ashy clays. The southeast side of the valley (U.S. 16 east of Ft. Garland) has Tertiary age conglomerate, sandstone, and siltstone exposed on faulted terraces. These sediments were derived from the east-adjacent Sangre de Cristo Mountains and include small boulders.

4.0 FRONT RANGE URBAN CORRIDOR SUBSURFACE CONDITIONS

Soils and bedrock of the Front Range Urban Corridor (defined in Section 1.0) are the focus of this section. Emphasis on the Corridor is made because a large percentage of sound barrier, overhead sign, and signal projects occur in this region of the state. Whereas Sections 2.0 and 3.0 presented a general overview of the distribution of soils and bedrock, basic engineering characteristics of the typical deposits, and a statewide geology synopsis, this section provides more descriptive geology characteristics and geographic distribution of the various geomaterials in the Corridor.

4.1 SOILS OF THE CORRIDOR

4.1.1 Stratigraphic Relationships

Unconsolidated materials were deposited and later modified under a relatively limited group of conditions along the Corridor during Pleistocene to Holocene time. Except for the greater output of coarse sediment and water flow during intermittent periods of Pleistocene glacial melting, the depositional settings were very similar to those of today. These conditions were related to each area's distance from the mountain front, position along or between streams that cut into the pediment (sloping bedrock surface), and the steepness of the slope. Bedrock exposure in the uplifted mountain front of Front Range igneous and metamorphic rocks and Frontal Hogback sedimentary rocks has been a feature of the Corridor since early Pleistocene time. They have supplied clastic debris in a variety of environments that resulted in today's soil cover. These depositional and non-depositional (weathering) environments and their related processes have been active throughout this period with some being more dominant than others depending on whether the process occurred during a glacial or an inter-glacial period.

Along the Corridor, these soils have been generically grouped and mapped according to relative age, constituents, and interpreted depositional environment of the material. The larger portion are generally named "alluvium" (dominantly water-borne mixed sediments) and identified with a name whose area typifies the group as a whole. Flood plain (river

and stream channels, overbanks, and areas within stream meanders including very low terraces) alluvium was deposited along rivers and larger tributary stream valleys (Post-Piney Creek and Piney Creek Alluvium). Terrace alluvium resulted from slightly older mixed deposits having been cut through by the streams with progressively older benches occupying progressively higher positions above the streams (Piney Creek, Broadway, and Louviers Alluvium).

Between areas of the active stream influence, the pediment uplands are mantled by still older mixed environment deposits (streams, alluvial fans, soil creep, etc.) that have been subject to longer periods of limited deposition or non-deposition, less focused erosion, and more diagenetic (post-depositional) chemical change (Slocum, Verdos, Rocky Flats, and Nussbaum Alluvium).

It is also recognized that, since depositional environments extend through geologic time, some non-alluvial groups are time transitional resulting in one group extending through the time range of other groups. This is common in dominantly wind born deposits (Eolian Sand and Loess) and soils resulting from a combination of gravity and slower water flow (particularly, slope wash Colluvium). Gravity dominant processes have resulted in geologically instantaneous and areally restricted soil bodies (Landslide and Talus Deposits) along some very steep slopes.

4.1.2 Generalized Distribution

Except for the complex rolling uplands of the Monument Highlands (where Tertiary bedrock outcrops are dominant over a large area), the overall north-south distribution of soil along the Corridor is similar. Relatively unweathered flood plain, terrace, and pediment alluvium deposits are common east of the Frontal Hogback although thicknesses of the groups vary considerably depending on distance from the original stream valleys (many of which closely parallel modern stream flood plains). Variably unweathered to slightly weathered wind born deposits are spotty over wide areas and are commonly pervasive and thick east of major streams and rivers. Gently sloping upland surfaces between stream valleys are commonly mantled by pediment alluvium that is

weathered proportional to its age and that frequently has characteristics strongly influenced by bedrock source material. Steeper slopes, including the east face of the Frontal Hogback and narrow valleys west of the Hogback, are commonly covered with unweathered to moderately weathered slope wash colluvium with material derived from, and strongly influenced by, near upslope bedrock and soil. Colluvial, alluvial, and mass wasting/gravity deposits in the mountainous areas are generally scattered and thin over metamorphic bedrock; colluvium/residuum is common and occasionally thick over granitic-type bedrock.

A common situation along the corridor is, within the distance of a mile or two, to have very young flood plain alluvium near valley center, progressively older alluvial terraces on the valley slopes, further older pediment alluvium capped by eolian material on the adjacent uplands, and colluvial slope wash grading from one to another. In some areas, terrace deposits underlie flood plain soils where the present day stream has not cut into the older deposits. Age ranges for the groups vary along the Corridor; for simplification, the following sections use the most commonly reported ages in the greater Denver area (north central portion of the Corridor).

4.1.3 Major Soil Groups, Largely Age Sequential

4.1.3.1 Lower Level, Flood Plain Alluvium

Post-Piney Creek Alluvium (Late Holocene): These deposits are generally centered along major drainages and larger tributaries, including very low terraces, and are characterized by moderately to well stratified (layered and interbedded) sand, silt, and clay with minor small gravel. The accumulations are noted as commonly having zones of humic bog clay, particularly in the upper portions. Thicknesses of 3 to 10 feet are most common. Permeability is usually poor to moderate. Water tables are frequently high, especially in the spring and early summer. Stability of shallow foundations has been reported in the literature as generally fair to good except for being very poor to poor in organic-rich clay zones.

Piney Creek Alluvium (Early to Middle Holocene): This unit is found in the bottoms of most valleys and tributaries and as low level terraces; with well stratified sand, silt, and clay having interbedded sandy (and sometimes clayey) small to medium gravel, particularly in the basal portions. The upper part is frequently finer and more humic than the lower; lower level gravels occasionally contain cobbles and small boulders, particularly when closer to the mountain front or along rivers and larger streams. The coarser fractions tend to be unweathered. These sediments commonly extend under younger Post-Piney Creek material. Thicknesses commonly range from 5 to 20 feet. Permeabilities are usually moderate in sand and gravel-rich sections and poor elsewhere. Water tables tend to be high in the lower valleys and deeper in upper tributaries and terraces. Clay swell potential is usually considered as low, but may grade to moderate in non-sandy clay zones. Foundation stability is generally poor in areas with significant clay and humic content and good in coarser deposits.

4.1.3.2 Upper Level, Terrace Alluvium

Broadway Alluvium (Late Pleistocene): This material was deposited in multiple stream, terrace, and slope environments and is usually found today on frequently well defined, intermediate-level terraces above rivers and major tributaries. These are generally well stratified, lightly weathered sand and coarser gravel accumulations with silty interbeds. The entire group tends to be more clayey and silty (and humic north of Denver) in its upper portion. Clayey gravel zones are developed at the base in some areas, which occasionally include sound (unweathered) cobble-size material. Very bouldery and cobbly gravels are noteworthy along Monument and Fountain Creeks in the Colorado Springs area. Thickness is commonly in the 8 to 25 foot range with moderate to high permeability except in more silty and clay-rich zones. Water tables are usually intermediate to lower with frequently high yields in wells. Foundation stability is generally considered good.

In areas of lower rainfall and low water table, dry and silt-rich areas of Broadway and Piney Creek Alluvium have been found to exhibit variably slight to marked tendencies

for subsurface piping and the formation of shallow cavities. These areas tend to collapse and create small to moderate sized depressions and sinkholes up to 15 feet deep. Settlement is greatest and most common in areas of very intermittent storm water runoff and is accelerated by man-caused interruptions to the natural drainage process (creating standing water). Areas particularly prone to such collapse include portions of the I-25 corridor between Colorado Springs and Pueblo and along U.S. 50 near Pueblo. This condition may have potential for post-construction instability in otherwise stable soils.

Louviers Alluvium (Middle to Late Pleistocene): Louviers Alluvium is found mostly on higher level terrace remnants and often extends onto upland surfaces as pediment remnants frequently having a strong colluvium aspect. The group is typified by being coarse sand-dominant with common cobble gravels. Soils of the group tend to be more cobbly and contain a few boulders in deposits closer to the mountain front. Similar to the younger Broadway Alluvium, bouldery cobbly gravels are common along Monument and Fountain Creeks. Weathering tends to be light to moderate with some oxide cementation locally common; cobbles and boulders tend to be sound. Thicknesses most commonly range up to 10 to 15 feet, although they locally may be as much as 35 feet. Permeabilities are usually high to very high if cementation is absent. Water tables are usually intermediate to lower; flows may be high. Soils of the group are generally considered to have high foundation stability.

4.1.3.3 Upland Surfaces, Pediment Alluvium

Slocum Alluvium (Middle Pleistocene): These predominantly stream and alluvial fan-deposited soils are positioned on dissected pediments and often contain material derived from underlying and nearby bedrock. They are commonly eroded on their upper surface substantially from original maximum thickness. This erosion has resulted in the most common thickness ranging up to 6 to 15 feet with local, un-eroded areas having as much as 40 feet of accumulation. Deposits are frequently laterally extensive. The group is usually composed of well-stratified pebble clay, silt, sand, and gravel with a few cobbles and boulders. Locally, the group includes significant zones of coarse sand and gravel

with common large cobbles and small boulders; such units may be silty in the upper portion. Soils in this group are frequently moderately to well weathered with some of the gravel through boulder component no longer sound. These coarser fractions are commonly calcium carbonate coated. Zones with a thick calcareous silt component are noted in the southern end of the Corridor. Permeabilities are usually high in uncemented sand and gravel intervals and low elsewhere. Foundation stability is usually considered good except for the moderate swell potential of some very clayey or silty intervals or where the expansive bedrock claystone fragments make up a significant portion of the gravels. Water tables tend to be highly variable.

In many areas, the Slocum Alluvium, particularly in the upper portion, contains 1 to 3 feet thick, wide-spread, calcium carbonate-enriched layers interpreted to represent paleosols (relict or “fossil” soil surface weathering horizons). The constituents are cemented to bedrock-like hardness. This hardness is particularly noteworthy where the cementation occurs in cobble-boulder interbeds. This has created conditions where the vertical soil profile goes from soft, through hard to very hard (“false bedrock”), then back into relatively soft to intermediate material. This same condition of well-developed paleosols is also common in the Verdos and Rocky Flats Alluvium.

Verdos Alluvium (Lower to Middle Pleistocene): These more diverse alluvial deposits are typically found on dissected pediment surfaces above the Slocum Alluvium and have frequent wide areal extent. They are typified by (1) poorly stratified gravel with clay to sand lenses locally common, (2) interbedded gravel to cobbly gravel and silty pebbly sand, or (3) sandy coarse gravel with cobbles and small boulders. The entire formation tends to be more silty and/or clayey in the upper portion. Calcareous silt is common throughout these soils in the southern portion of the Corridor. Local thin volcanic ash beds are noted, particularly in the north central portion of the Corridor. Like the Slocum Alluvium, the upper Verdoso surface has commonly been eroded. Thickness ranges up to 20 feet except for some un-eroded areas with up to 40 feet present. Hard, calcareous-cemented paleosol layers are noted in the upper portion, very similar to those in the

Slocum Alluvium. Permeabilities are usually high in cleaner, uncemented sand and gravel and low elsewhere. Foundation stability is usually fair to good except for being poor to fair in the more clayey zones where weathered clays exhibit moderate swell potential. The more ashy layers may be suspected of having relatively high plasticity. Water tables tend to be highly variable.

Rocky Flats Alluvium (Later Early Pleistocene): These coarsely granular, near mountain front deposits attain significant thickness (averaging approximately 15 feet) and areal extent only in the Highway 93 area of the north central Corridor between Boulder and Golden. They are composed of poorly graded bouldery, cobbley, sandy gravel (likely of alluvial fan origin) and commonly calcium carbonate-enriched and sometimes moderately cemented. Many of the included stones are moderately to well weathered and unsound.

Nussbaum Alluvium (Early Pleistocene): These uppermost pediment soils are likely alluvial fan remnants that occupy only small scattered sites along the mountain front and around isolated topographic highs from Denver to just south of Colorado Springs. They have a similar composition and character to Rocky Flats Alluvium and are in the 8 to 15 feet thick range.

Up to 100 feet thick deposits of age-equivalent pebble gravel have been mapped over an extensive area on Baculite Mesa northeast of Pueblo, however the area is well way from immediate highways or significant population. Geotechnical characteristics for this unusually thick soil have not been found to be described in the literature.

4.1.4 Major Soil Groups, Largely Transitional

Because of the nature of their deposition, several types of soil accumulations (other than the previously described alluvial deposits) were often laid down in multiple environments and over a range of older soils.

4.1.4.1 Eolian Sand (Holocene to Late Pleistocene)

These sand soils were transported by wind and tend to be thickest east of rivers and major stream tributaries. They are most common on lower upland surfaces. The sands, and their downwind Loess equivalents, are particularly common in the Greater Denver and Longmont-Loveland-Greeley areas and east of the I-25 corridor between Colorado Springs and Pueblo. The soils are dominated by very fine to medium grained quartz sand and zones of sandy silt or sandy clay (particularly near the eastern margins). Although locally cross-bedded, they are generally massive (non-stratified) overall. These dune and sheet sand deposits are usually less than 10 feet thick, but in numerous areas extend to 30 feet thick. Permeability is high to very high in the cleaner sands with resulting frequently low water tables. Foundation stability tends to be good under moderate static loads and moderate to poor under heavy or vibratory loads. Low to moderate compression upon wetting is sometimes observed.

4.1.4.2 Loess (Early Holocene through Late Pleistocene)

These soils are also derived from wind born particles, but are the finer equivalents of the Eolian Sands. They are silt and clay-dominate, frequently with a very fine sandy component, and often are found to grade laterally into Eolian Sand. The deposits tend to be massive. They are usually less than 10 feet thick, but occur locally as thick as 25 feet. Vertical permeability is usually moderate with the horizontal component being low. Water tables tend to be low. Foundation stability is usually moderated when loesses are dry, but poor when wet. Uneven wetting of these silty soils frequently results in marked differential settling. Swell potentials are low to moderate except when very clayey where they may grade to high. Significant deposits are usually found on upland surfaces in the same general areas as Eolian Sands. Loess soils are often porous and consequently may exhibit low to high compression upon wetting.

4.1.4.3 Colluvium (Early Holocene through Middle Pleistocene)

These deposits form on moderate slopes throughout the Corridor as a result of the weathering of underlying and upslope soil and bedrock. A combination of gravity (soil creep) and water runoff (sheet wash) moved the weathered material down slope and contributed to further weathering. Colluvial soils are the clay-enriched equivalent of the material from which they were derived and are therefore highly variable from area to area. Common characteristics are a wide size range of components, non-stratification, and the tendency to have very gradational lateral contacts with other soil types. A frequently found accumulation is sandy silty clay that is slightly to commonly gravelly. A common field occurrence is where older upslope terrace deposits grade down slope into colluvial soil that in turn grades down into younger flood plain alluvium. The down slope creep aspect of the depositional process often results in substantial cobbles and small boulders being included in a dominantly clay matrix.

Thicknesses are highly variable. All except the hardest, steepest bedrock exposures usually have at least a thin layer of colluvial soil. As slopes decrease, colluvial components tend to further accumulate and weather, thereby becoming more clayey and thicker (up to 20 feet, but more commonly 10-foot maximum). Vertical and horizontal heterogeneity is common. Permeability is generally low to very low, although permeability largely depends on the clay content. Stability characteristics are greatly dependent on the original source material and degree of clay alteration from the weathering process. Deposits closely derived from expansive bedrock claystone/shale, ashy/bentonitic sandstone, or montmorillonite-rich soils may have low strength and moderate to very high swell potential.

4.1.4.4 Residual Soils

The term Residuum is frequently applied to soils resulting from bedrock or older soil weathering, usually on very gentle slopes that have not undergone significant “colluvium-like” movement. These soils are usually very thin and are often considered the normal

topsoil and not separately mapped. A locally important exception along the far western margin of the Corridor is the occurrence of Grus or Decomposed Granite (Late Pleistocene to Holocene) over granitic bedrock in mountainous areas of the Front Range. This soil is highly porous and consists of coarsely granular, angular (frequently near cubic) fragments of quartz and feldspar. Transition from underlying deeply weathered bedrock is gradual, frequently over a considerable distance. Deposits may be as thick as 5 to 8 feet and commonly thicken further into downslope colluvium.

4.1.4.5 Steeper Slope Deposits (Late Holocene to Middle Pleistocene)

Landslide Deposits are rock and soil debris mixes, usually bouldery to sandy silt and clay, some of which may still be active. These accumulations are spotty, but numerous along the Frontal Hogback, mountain front, and flanks of isolated mesas throughout the Corridor. Like Colluvium deposits, these soils are non-stratified, heterogeneous throughout, and with a wide range of component sizes. Unlike colluvium, they usually have sharp upslope and side margins; down slope toes frequently grade into colluvial materials. Thicknesses are most commonly less than 15 feet. Engineering stability depends on the degree of current slope, water saturation, percent clay, and swell-prone component content; higher values of any equate to lower stability.

Talus Deposits are direct rock fall accumulations at the base of cliffs and very steep slopes. They are typified by a high portion of large, angular to subangular rock fragments with few fines. They tend to be relatively homogeneous and are non-stratified with sharp upslope and lateral margins. The downslope toes often grade into colluvium. These bodies may be laterally numerous and cover a substantial cumulative area. Permeability is almost always high to very high. Stability is usually considered low, even in older deposits.

4.1.5 Special Soil Conditions

4.1.5.1 Artificial Fill (Recent)

Areas with substantial thicknesses and areal extent of man-placed materials are moderately common along nearly the entire Corridor and are very common in some

locales. Except for modern engineered fills, composition and physical character are as varied as the reasons they were placed and each must be separately evaluated. Most fills are likely to be in the 5 to 20 foot maximum thickness range, however highway embankments to 90 feet are known. Some areas or situations of known or suspect significant fills along the Corridor include:

- Old aggregates pits along the flood plains of rivers and major tributaries near metropolitan areas that have been backfilled for development (*i.e.*, numerous sites along the South Platte River immediately north of Denver and eolian sand quarries in Colorado Springs).
- Metropolitan area major highway interchanges.
- Near modern riverbanks in population centers where mixed debris were placed for waste disposal and soil for leveling off for development (e.g., Cache la Poudre River in Ft. Collins, South Platte River and Cherry Creek in Denver, Fountain Creek in Colorado Springs, and the Arkansas River in Pueblo.).
- Mine dumps, particularly Laramie Formation coal mine sites, most of which are thought to have been non-engineered (*i.e.*, extensive dump fields from sub-bituminous coal mines in the Greater Broomfield area including Highway 36 and Interstate 25).
- Smelter dump areas (*i.e.*, Globeville neighborhood/I-25 in Denver and the major CF&I slag pile in southeastern Pueblo).
- Old sanitary landfills in low-lying areas formerly on the margins of population centers (*i.e.*, Commerce City near Sand Creek and Interstate-270).

4.1.5.2 Bedrock Definition, Potential Problems

Two geologic conditions exist in multiple soil groups that may make the definition of the soil-bedrock interface difficult in auger borings. One is the occurrence of sound crystalline boulders or beds of large cobbles within soil deposits (especially 1- Piney Creek Alluvium near the mountain front and near larger streams, 2- Louviers, Slocum, and Verdos Alluvium, and 3- some Colluvium deposits). The other situation is the presence of frequently widespread, thoroughly cemented paleosol (relict weathering

horizons) gravels within otherwise normal soil intervals (especially Slocum, Verdos, and Rocky Flats Alluvium).

4.2 BEDROCK OF THE CORRIDOR

4.2.1 Generalized Distribution

Except for transitional zones where bedrock is very highly weathered, the interface between soil and bedrock is usually well defined along the Corridor. A major unconformity (period of non-deposition and/or erosion) due to uplift along the mountain front has separated younger soil from older bedrock and represents most of the entire Tertiary Period of geologic time in most areas. Bedrock units having likely potential impact on drilled shafts in the Corridor are distributed in four major settings (arranged as younger to older for the age of their generally included units):

5. Early Tertiary (Paleocene) coarse sandstone and conglomerate units, the youngest bedrock, is primarily limited to the central part of the Corridor forming major exposures in the Monument Highlands.
6. For valleys and uplands of the Western Plains Piedmont (the dominant portion of the Corridor), upper Late Cretaceous sedimentary rocks are intermittently exposed through soil cover throughout the northern and southern parts and comprise most of the bedrock likely to be encountered in foundations.
7. The mountain front belt includes a wide age range (Triassic to Pennsylvanian) of diverse sedimentary rocks that are exposed in a variably wide and locally intermittent band immediately east of the mountains. Jurassic to lower Late Cretaceous age shale and sandstone-dominant, tilted strata are intermittently well exposed along the narrow Frontal Hogback and as flatter lying outcrops in the Arkansas River valley near Pueblo.
8. Pre-Cambrian igneous and metamorphic rocks are exposed pervasively in mountainous areas along the west margin of the Corridor.

4.2.2 Major Bedrock Groups

4.2.2.1 Early Tertiary Bedrock of the Monument Highlands

Upper Dawson Arkose (Paleocene): Outcrops of this formation dominate the area along I-25 from the southern suburbs of Denver to northern Colorado Springs. Soil cover is generally limited to thin colluvium/residuum on gentle slopes and thin to moderate alluvium restricted to a few valleys. Younger (Oligocene) Castle Rock Conglomerate is common and highly visible in the area, but is limited to mesas/highlands above most major transportation routes. The Upper Dawson consists of an intricately interfingering, lensing series of members including quartz-feldspar sandstone, sandy and bouldery well cemented conglomerate, friable (weakly cemented) clay-rich sandstone, and claystone-siltstone. Well-cemented zones are very hard. Clayey horizons (including clay matrix sandstones) have high swell potential; less silty or sandy claystone layers may be very plastic when saturated. Other layers are considered stable to very stable.

4.2.2.2 Bedrock of the Piedmont (Western Plains Valleys and Uplands)

Denver, Arapahoe, & Lower Dawson Formations (Paleocene to Latest Cretaceous): These non-marine units, although sometimes separately mapped, are largely age equivalent and interfinger with each other over long distances. All are limited to a broad, arc-shaped band sweeping around the Monument Highlands with the general arrangement being: Denver Formation dominant to the north (under most of the Denver metropolitan area), Arapahoe Formation in the center, and Lower Dawson Arkose to the south (around Colorado Springs). Except for harder sandstone outcrops near Colorado Springs, most of the material is mantled by variably thin to very thick soil.

The Denver Formation is claystone/shale-dominant over most of the Denver area, with thinner interbeds of siltstone, tuffaceous (volcanic ashy) sandstone weakly to well cemented, and lesser conglomerate commonly with volcanic rock clasts. Cemented sandstones may be very hard. Claystone/shale, as well as tuffaceous sandstone, are well noted for having major vertical and horizontal zones with high to very high swell potential; non-sandy claystone is frequently highly plastic when saturated. Claystone

clays and ash-derived sandstone clays are montmorillonite rich (frequently termed “bentonitic”) often including seams of nearly pure bentonite. The formation is a major contributor to unstable conditions in overlying soils where Denver Formation claystone fragments may be common. In the western portion of the Denver area (Morrison Quadrangle), the formation contains thick intervals interpreted as paleo-mudflow deposits containing a jumble of boulder-size claystone fragments in claystone/shale matrix; these units are noted for high swell potential and high plasticity. Where unweathered, the formation includes a waxy, blue-green-gray claystone locally known as “The Denver Blue”. The “Denver Blue’s” upper surface is not a stratigraphic horizon, but rather an irregular weathering/alteration zone that is often transitional.

The Arapahoe Formation is generally coarser, less prone to have volcanic components, and has some slightly older portions than the Denver Formation. The two are frequently mapped as Denver-Arapahoe Undifferentiated in the Denver area. The formation is generally described as well stratified, interbedded claystone/shale, siltstone, sandstone, and conglomerate. A well-developed lower Arapahoe conglomerate is frequently only weakly cemented and is a significant aquifer. Conglomerate and sandstone units have variable low to moderate swell potential; siltstone and claystone/shale have moderate to high swell potential.

Lower Dawson Arkose also tends to be well interbedded with layers of conglomerate, coarse sandstone, shale, and silty fine sandy shale (termed “mudstone”). The coarser units usually have moderately well graded quartz and feldspar sands with granitic pebbles (“arkose”); local coal beds are noted. Clay rich and clay-dominant zones have moderate to very high swell potential and moderate to high plasticity, particularly in the Austin Bluffs area north of Colorado Springs.

Laramie Formation, Fox Hills Sandstone, and Pierre Shale (Late Cretaceous): These formations, listed from younger to older, occur in two broad situations: (1) As

intermittently exposed in moderately dipping beds east of the mountain front (immediately east of the Frontal Hogback) from Ft. Collins to Denver and (2) with thin soil mantles in gently dipping and near flat lying units in the Louisville area and along Interstate 25 between Colorado Springs and Pueblo. In these areas, the upper (Laramie) units are non-marine, the Fox Hills has transitional marine interfingerings, while the lower (Pierre) rocks are generally of marine origin. Unlike younger bedrock, these units are much more widespread and are more consistent within each member over wide areas.

The Laramie Formation is dominated by thinly bedded shale and siltstone with common hard to friable sandstone interbeds, lesser thin hard conglomerate, and lignitic to sub-bituminous coal beds. Coal beds are as thick as 14 feet (although usually much less) and were mined extensively over wide areas and at numerous locations. The formation is sandier in the lower portion; basal sandstone beds may be equivalent to some of the Fox Hills Sandstone. Most Laramie clays are dominantly kaolinitic with usually low to moderate swell potential; the middle third tends to be montmorillonitic with resulting high swell potential. Sandstones vary from weakly to well cemented.

Foxhills Sandstone units are cross-bedded and quartz sand-dominant. Relatively thin interbeds of claystone/shale, mudstone, and coal occur throughout. The sands are generally weakly cemented and friable; they are important aquifers with medium to high permeability, particularly north of Denver. They are considered to have good to very good foundation stability.

The Pierre Shale is a very thick, clay/shale-dominant formation with numerous thin bentonite beds throughout. These rocks are almost always suspect for moderate to very high swell potential, medium to high plasticity, and low slope stability almost everywhere they are encountered along the Corridor. Thin, subordinate, frequently friable sandstone interbeds occur throughout the formation. Significantly thick sandstone members are present in several areas at different stratigraphic positions (the middle level Hygiene Member to the north and the lower Apache Member to the south are noteworthy). Hard limestone masses (butte formers in outcrop) occur in the middle portion to the south. To

the south, the middle portion also contains appreciable gypsum content (Sharon Springs Member) that may affect sulfate-susceptible cement.

4.2.2.3 Bedrock of the Mountain Front, Frontal Hogback, and Arkansas River Valley

4.2.2.3.1 Colorado Group

The Colorado Group is exposed along the immediate east side of the Hogback from the northern end of the Corridor to Denver; dips are too steep for it to be encountered in most foundation situations east of this relatively narrow strip. Constituent formations are also present to the south where they appear as low scattered outcrops or are thinly soil mantled over wide areas (in the Arkansas River valley, west of Interstate 25 and around Pueblo). The formations in this Group are of marine origin and include (from younger to older):

Niobrara Formation (Lower Early Cretaceous): Includes upper chalky shale members (Sharon Springs Shale and Smoky Hill Shale) with thin hard limestone interbeds and thin bentonite and gypsum layers and a lower hard and thick-bedded limestone member (Ft. Hayes Limestone) with limey shale partings and thin bentonite beds.

Benton Shale Equivalents (Lower Late Cretaceous to Upper Early Cretaceous): These include the Carlile Shale, Greenhorn Limestone, and Graneros Shale that contain non-calcareous claystone and siltstone, calcareous shale with hard thin limestone beds, limestone with claystone/shale and siltstone interbeds, and thick clay shale units. The Greenhorn and Graneros formations are noted for common bentonite beds to several inches thick that are vertically numerous in some areas.

Shale units throughout the Group have moderate to very high swell potential and are noteworthy contributors to soil instability in much of the southern portion of the Corridor. Gypsum-rich zones may yield sulfates contributing to breakdown of cement.

4.2.2.3.2 Older Sedimentary Rocks

These diverse units are exposed only along the narrow mountain front and Hogback belt and dip too steeply to be encountered in foundation situations elsewhere in the Corridor. The formations are laterally persistent. Except for the non-marine and frequently conglomeratic members (Fountain Formation), they also tend to have similar content over long distances. They are typically moderately hard to very hard and, except in areas of intense fracturing, usually stable to very stable. Expansive clays are absent. Steep dip and alternating hardness may combine to deflect auger borings out of the vertical. Limestone and dolomitic limestone units (near Colorado Springs and possible north of Ft. Collins) may be vuggy or cavernous. Thick gypsum deposits (Morrison Formation) may affect sulfate-sensitive cement. Noteworthy formations included in this category include (youngest to oldest):

Dakota Group (Early Cretaceous): Ridge-forming sandstone members with lesser shale interbeds; Dakota Hogback and Perry Park are notable exposures.

Morrison-Ralston Creek Formations (Late Jurassic): Thickly interbedded claystone, siltstone, and sandstone with thin limestone beds and thin to moderately thick gypsum layers. Garden of the Gods at Colorado Springs has notable exposures of some of these units (along with Permian Lyons sandstone), and is sometimes mapped together with the Lykins Formation (Jurassic-Triassic; thickly interbedded limestone, shale, siltstone, and sandstone).

Lyons Sandstone (Permian): Persistent, hard quartz sandstone, finely bedded and frequently cross-bedded. Noted for easily parting in 1 to 6 inch layers (“flagstone”); quarried near Lyons for dimension and decorative stone.

Fountain Formation (Permian-Pennsylvanian): Arkosic conglomerate and sandstone with sandy shale interbeds and lenses (“fanglomerate”); great vertically and lateral variability. Notable resistant outcrops are at Redrocks Park and Roxborough Park.

Leadville Limestone, Manitou Limestone, & Peereless Dolomite (Mississippian- Late Cambrian): These hard, carbonate-dominated sedimentary rocks are limited to the area west of Colorado Springs.

4.2.2.3.3 Bedrock of the Mountainous Areas

Older Pre-Cambrian age metamorphic rocks of mixed origins are intruded by younger Pre-Cambrian granitic rocks along the far western margin of the Corridor.

Granitic Plutons: These generally massive, crystalline rocks have a range of compositions generally described as “granitic” (granite, grano-diorite, quartz monzonite, and similar); they are commonly intruded by irregular, coarsely crystalline pegmatite dikes. They are hard where unweathered, but commonly weather deeply (to 50 feet has been reported in the Air Force Academy area) forming thick residuum soil termed “grus”. Multiple systems of well-defined fractures are the rule. Except for highly fractured and deeply weathered areas, foundation stability is good to very good.

Metamorphic Rocks of the Ancestral Rocky Mountains: These generally hard to very hard rocks were derived from a variety of pre-existing sedimentary and igneous units that were subject to heat and pressure of deep burial. They have undergone moderate to moderately severe mineral alteration and consist dominantly of quartzite and metaconglomerate, schist, granitic gneiss, and intensely mixed types (migmatites). Except for the quartzites, they usually have significant foliation (strong preferred alignment of minerals) with resulting planes of relative weakness. In some areas, the original sedimentary bedding planes remain as interfaces of relative weakness. As a whole, these rocks tend to be pervasively fractured with multiple joint sets. In addition to the larger granitic intrusive masses, the metamorphic rocks also commonly contain irregular pegmatite dikes. Foundation stability is generally good except in areas of intense fracturing and where foliation dips as steep (or more steeply) than the slope and in the same direction.

References

Hepworth and Jubenville, “Drilled Pier Foundations in Shale, Denver Colorado Area”,
Drilled Piers and Caissons, American Society of Civil Engineers, October 28,
1981, p. 68.

Publications listed below were reviewed by Geocal to provide a framework for state-wide geology and added detail along the Front Range Urban Corridor. The standard quadrangle scale maps (1:24,000) provided selected engineering characteristics for representative areas along the corridor. This list is not a comprehensive bibliography for the area or state. Abbreviations for common publication agencies are included at the end of the list.

CGS Environmental Geology Series 7: Potentially Swelling Soil and Rock in the Front Range Urban Corridor, 1974.

CGS Map MI-8: Colorado Geologic Highway Map (with GTR Mapping, 1:100,000), 1991 Rev.

CGS Rocktalk V.4-N.4: Ground Subsidence and Settlement Hazards in Colorado, 10/2001.

USGS Map MF-631: Geologic Map & Engineering Data for the Highlands Ranch Quadrangle, CO (1:24,000), 1974.

USGS Map MF-761: Geology, Montrose 1° x 2° Quadrangle, CO (1:250,000), 1976.

USGS Map MF-2347: Generalized Surficial Geologic Map of the Denver 1° x 2° Quadrangle, CO (1:250,000), 2001.

USGS Map MF-2388: Generalized Surficial Geologic Map of the Pueblo 1° x 2° Quadrangle, CO (1:250,000), 2002.

USGS Map OF-78-532: Preliminary Geologic Map of the Greeley 1° x 2° Quadrangle, CO & WY, (1:250,000), 1978.

USGS Map OF-78-878: Map Showing Artificial Fill in the Greater Denver Area, CO, (1:100,000), 1978.

USGS Map OF-80-321: Bedrocked Surficial Engineering Geologic Maps, Littleton Quadrangle, CO, (1:24,000), 1980.

USGS Map OF-80-654: Preliminary Engineering Geologic Map of the Morrison Quadrangle, CO, (1:24,000), 1980.

USGS Map GQ-1229: Geologic Map of the Niwot Quadrangle, CO, (1:24,000), 1975.

USGS Map GQ-1392: Geologic Map of the Lafayette Quadrangle, CO, (1:24,000), 1977.

USGS Map GQ-1413: Geologic Map of the Highlands Ranch Quadrangle, CO, (1:24,000), 1977.

USGS Map GQ-1427: Geologic Map of the Fort Logan Quadrangle, CO, (1:24,000), 1978.

USGS Map GQ-1453: Geologic Map of the Arvada Quadrangle, CO, (1:24,000), 1979.

USGS Map GQ-1524: Geologic Map and Physical Properties of the Surficial and Bedrock Units of the Englewood Quadrangle, CO, (1:24,000), 1980.

USGS Map GQ-1541: Geologic Map of the Commerce City Quadrangle, CO, (1:24,000), 1980.

USGS Map GQ-1567: Geologic Map of the Sable Quadrangle, CO, (1:24,000), 1983.

USGS Map GQ-1625: Geologic Map of the Horsetooth Reservoir Quadrangle, Larimer, CO, (1:24,000), 1989.

USGS Map I-360: Geology, Structure, and Uranium Deposits of the Moab Quadrangle, CO & UT, (1:250,000), 1983.

USGS Map I-408: Geology of the Northwest and Northeast Pueblo Quadrangles, (1:24,000), 1964.

USGS Map I-558: Geologic Map of the Trinidad Quadrangle, South-central CO, (1:250,000), 1969.

USGS Map I-560: Geologic & Structure Contour Map of the LaJunta Quadrangle, CO & KS, (1:250,000), 1968.

USGS Map I-629: Geology, Structure, and Uranium Deposits of the Cortez Quadrangle, CO & UT, (1:250,000), 1972.

USGS Map I-687: Geologic Map of the Lower Cache La Poudre River Basin, North-central CO, (1:62,500), 1972.

USGS Map I-731: Generalized Surficial Geologic Map of the Denver Area, CO, (1:62,500), 1972.

USGS Map I-790-A: Geologic Map of the Morrison Quadrangle, CO, (1:24,000), 1972.

USGS Map I-736: Geologic & Structure Map of the Grand Junction Quadrangle, CO & UT, (1:250,000), 1973.

USGS Map I-764: Geologic Map of the Durango Quadrangle, Southwestern Colorado, (1:250,000), 1983.

USGS Map I-856-H: Geologic Map of the Greater Denver Area, Front Range Urban Corridor, CO, (1:100,000), 1979.

USGS Map I-857-F: Geologic Map of the Colorado Springs – Castle Rock Area, Front Range Urban Corridor, CO, (1:250,000), 1979.

USGS Map I-885-G: Geologic Map of the Boulder – Greeley Area, CO, (1:100,000), 1978.

USGS Map I-944: Geologic Map of the Lamar Quadrangle, CO & KS, (1:250,000), 1976.

USGS Map I-972: Geologic Map of the Craig 1° x 2° Quadrangle, North-western Colorado, (1:250,000), 1981.

USGS Map I-999: Geologic Map of the Leadville 1° x 2° Quadrangle, Northwestern Colorado, (1:250,000), 1988.

USGS Map I-1022: Geologic Maps of the Pueblo 1° x 2° Quadrangle, South-central Colorado, (1:250,000), 1984.

USGS Map I-1092: Maps Showing Geology, Structure, Oil & Gas Fields in the Sterling 1° x 2° Quadrangle, CO, NE, & KS, (1:250,000), 1978.

USGS Map J-1289: Surficial Geologic Map of the Grand Junction 1° x 2° Quadrangle, CO & UT, (1:250,000), 1981.

USGS Map I-1346: Surficial Geologic Map of the Craig 1/2° x 1° Quadrangle, Moffat & Routte Counties, CO, (1:100,000), 1982.

USGS Map I-1526: Geologic Map of the Vernal 1° x 2° Quadrangle, CO, UT, & WY (1:250,000), 1985.

USGS Map MF-631: Geologic Map ang Engineering Data for the Highlands Ranch Quadrangle, Arapahoe and Douglas Counties, Colorado, 1974.

USGS Professional Paper 551: General Engineering Geology of the US Air Force Academy Site, CO, 1967.

USGS Professional Paper 1230: Environmental Geology of the Front Range Urban Corridor and Vicinity, CO, 1982.

USGS & CGS Indidental Map: Geologic Map of Colorado, (Tweto, 1:500,000), 1979, (with companion: Geologic Cross Sections across Colorado, Tweto, 1983).

Abbreviations for common publication agencies:

CGS- Colorado Geological Survey

USGS- United States Geological Survey

Appendix B

Analysis Methods for Lateral Response of Drilled Shafts

Several analytical approaches have been proposed to carry out analysis of laterally loaded piles/drilled shafts. This appendix basically serves as a detailed reference attachment for all the methods that we have discussed in the report.

1. Brinch Hansen Method:

This approach developed by Brinch Hansen in 1961 is recommended for short rigid piles. It is based on earth pressure theory for $c-\phi$ soils. Basically, it consists of determining the center of rotation by taking moment of all forces about the point of load application and equating it to zero.

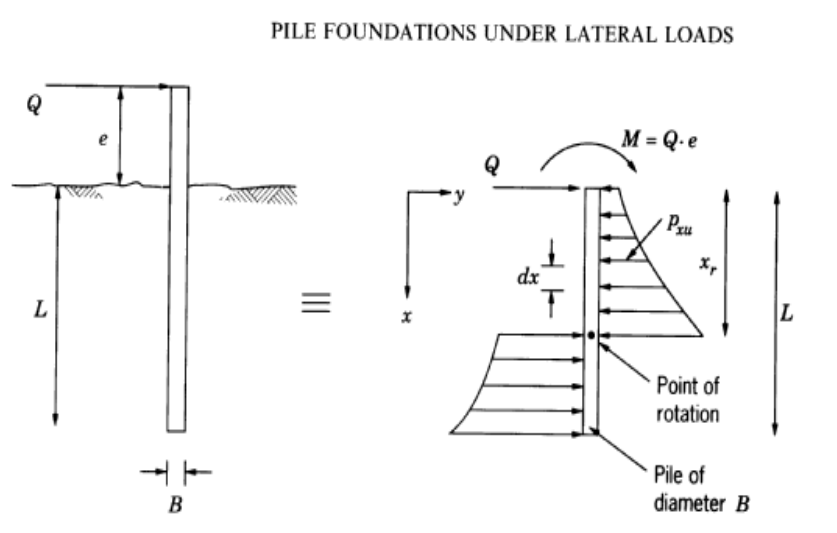


Figure B-1. Mobilization of lateral resistance for a free-head laterally loaded rigid pile

To calculate the ultimate resistance as depicted in Fig. B-1, sum of the horizontal forces are equated to zero. Therefore, the equation for ultimate soil resistance at any depth is given by

$$p_{xu} = \sigma_{vx} k_q + ck_c \quad (B-1)$$

where, σ_{vx} = vertical effective overburden pressure

c = cohesion of soil

k_c & k_q = factors that are function of ϕ and x/B and can be obtained from Fig. B-2.

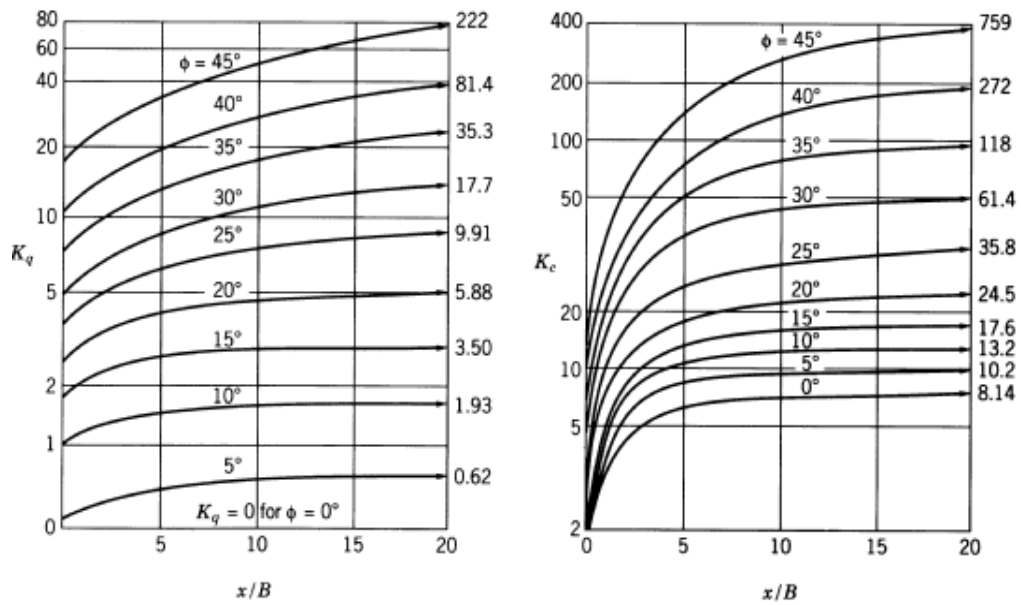


Figure B-2. Coefficients k_q and k_c

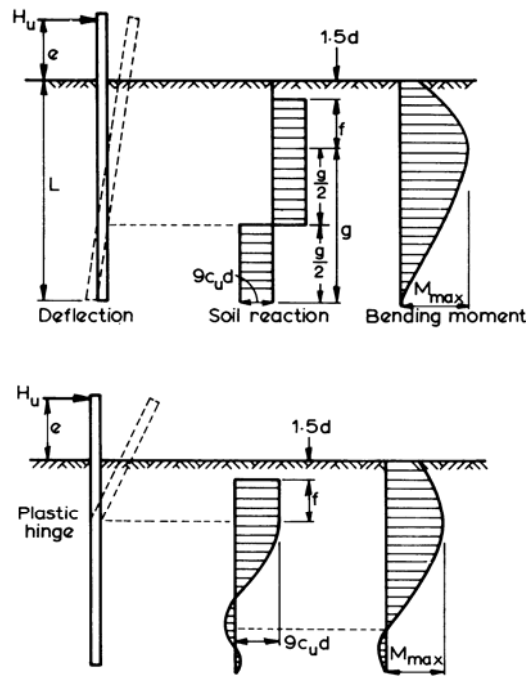
As shown in Fig. B-1, the lateral resistance diagram along the length of the pile and the assumed center of rotation are determined. Moment is taken about the point of application of lateral load Q_u , once the assumption is made for the point of rotation at some depth x_r below ground. If the moment calculated is a small value or near zero, the assumed center of rotation is considered correct. Thus, calculating moment at x_r , we can get the value of lateral load Q_u .

This approach is applicable to c - ϕ soils and valid both for layered and uniform soils. The disadvantages are that the method applies only to short piles and requires a trial-and-error procedure to locate point of rotation in the calculation.

2. Broms Method:

Broms proposed this method in 1964 for lateral resistance of vertical piles. The approach is separately described for piles in cohesive soils and cohesionless soil.

First considering the case in cohesive soil, the assumption is made to consider pile to be equivalent to a beam on an elastic foundation. It suggests a simplified distribution of soil resistance as being zero from the ground surface to a depth of $1.5d$ and constant value of $9c_u$ below this depth, where c_u is un-drained shear strength. The probable failure mechanisms for unrestrained or free head piles are shown for short and long pile along with soil reaction distribution in Fig. B-3 (a). Length of pile is $L = 1.5d + f + g$.



**Figure B-3. Failure mechanisms for a) short and b) long free headed piles in cohesive soil
(after Polous and Davis)**

For the short free-headed pile, failure takes place when the soil yields along the total length of the pile and the pile rotates as a unit around a point located at some depth below the ground surface.

The location of maximum moment and where shear is zero is defined as $f = \frac{H_u}{9C_u d}$, where $H_u =$ ultimate lateral load. The maximum moment at this location is $M_{max} = H_u (e + 1.5d + 0.5f)$, and the part of the pile with length g resists the bending moment $M_{max} = 2.25dg^2 C_u$. Thus, we can calculate the ultimate lateral resistance from the equations given for maximum moment location and maximum moment. The dimensionless ultimate lateral resistance plotted as a function of dimensionless embedment length, as shown in Fig. B-4 (a), can be used directly to determine the ultimate lateral resistance. This dimensionless solution is based on the assumption that $M_y > M_{max}$.

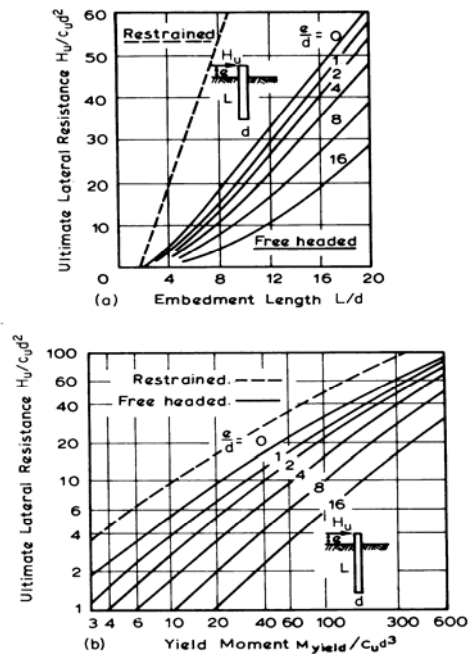


Figure B-4. Ultimate lateral resistance in cohesive soils a) short piles and b) long piles (after Poulos and Davis)

For free headed long piles, the mechanism of failure when a plastic hinge forms at the maximum bending moment is shown in Fig. B-3 (b) and is assumed that failure occurs when $M_y = M_{max}$. The corresponding dimensionless solution for the ultimate lateral resistance is shown in Fig. B-4 (b).

For restrained or fixed head short piles, failure occurs when the applied lateral load is equal to the ultimate lateral resistance of the soil, and the pile moves as a unit through the soil. The ultimate lateral resistance can be calculated by $H_u = 9C_u d[L - 1.5d]$ and the maximum negative moment. $M_{\max(\text{neg})} = H_u(0.5L + 0.75d)$ has to be less than or equal to M_y in order for pile to fail. Fig. B-5(a), (b) and (c) shows the deflection, soil reaction and moment distribution for a short, intermediate and long restrained pile.

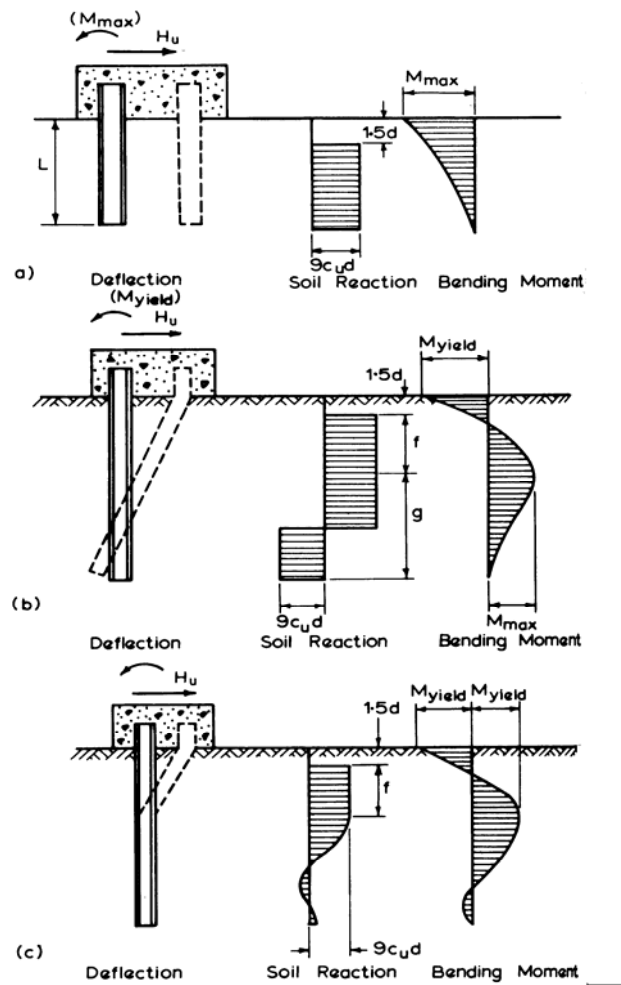


Figure B-5. Ultimate lateral resistance in cohesive soils a) short piles and b) long piles (after Poulos & Davis)

For restrained intermediate length piles, failure occurs when the restraining moment equals to the ultimate moment resistance of the pile section M_y and the pile rotates around a point located at some depth below the ground surface, while the maximum positive bending moment occurs at a section located at a depth $(1.5d + f)$. For the failure to occur $M_{\max(\text{pos})}$ necessarily has to be less than the yield or ultimate moment of resistance of the pile section M_y . Also, the ultimate lateral resistance can be obtained directly by the dimensionless solutions given in the Fig. B-4 (a).

For restrained long piles, failure occurs when two plastic hinges form along the pile, where the first one occurs at the section of the maximum negative and the second one at the section of maximum positive moment. The resulting ultimate lateral resistance can be calculated when the maximum positive bending moment is equal to the ultimate moment resistance of the pile section M_y as

$$H_u = \frac{2M_y}{(1.5d + 0.5f)}. \text{ Also, the ultimate resistance can be determined from Fig. B-4 (b).}$$

Now, for the second case in the cohesionless soil, the assumptions made are: 1) on the back of the pile, action of active earth pressure is neglected, 2) along the front of the pile, distribution of active earth pressure is equal to three times the Rankine's passive pressure, 3) no influence of the shape of the pile section on the distribution of ultimate soil pressure or the ultimate lateral resistance, and 4) the full lateral resistance is mobilized at the movement considered.

The first step is to decide whether the pile is short or long. For this, rotation is assumed to be about a point close to the tip, and high pressure acting near this point are replaced by a single concentrated force at the tip. $H_u = \frac{0.5\gamma dL^3 K_p}{e + L}$ is obtained by taking moment about the toe.

Deflection of the pile and soil reaction and moment distribution for free headed short and long piles

is shown in Fig. B-6 (a) and (b), respectively. Location of the maximum moment is obtained by

$$f = 0.82 \sqrt{\frac{H_u}{dk_p \gamma}} \text{ and the maximum moment by } M_{\max} = H_u \left(e + \frac{2}{3} f \right).$$

results in $M_{\max} \leq M_y$, then the pile is considered as short and the assumption is correct. If the calculated value of H_u results in $M_{\max} > M_y$, then the pile is considered as long and H_u can be calculated taking $M_{\max} = M_y$. Also, the ultimate lateral resistance can be obtained directly from dimensionless solution given in Fig. B-7 (a) and (b).

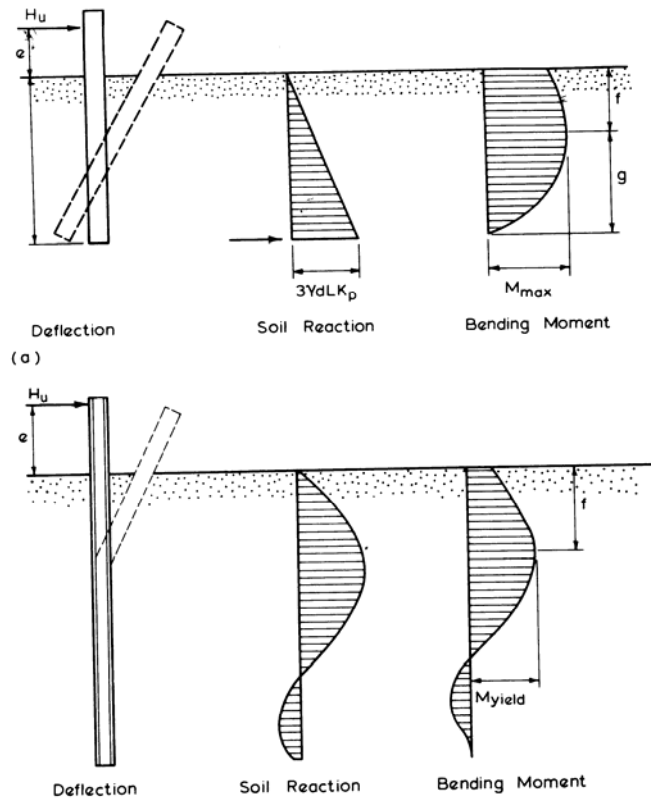
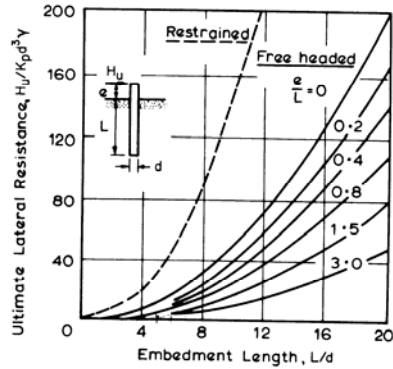
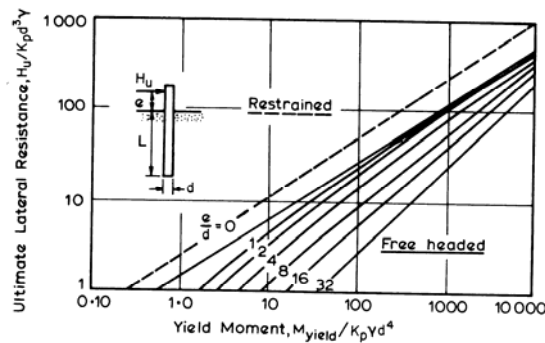


Figure B-6. Free head piles in cohesionless soil (a) short (b) long (after Poulos and Davis)



(a)



(b)

Figure B-7. Ultimate lateral resistance of piles in cohesionless soil

(a) short (b) long (after Poulos and Davis)

For short restrained piles, failure occurs when the load applied to the pile is equal to the ultimate lateral resistance of the soil and is expressed as $H_u = 1.5\gamma L^2 d k_p$. But this is only applicable when the maximum negative moment is less than the M_y of the pile. The ultimate lateral resistance is also plotted in the dimensionless form as shown in Fig. B-7 (a) and the failure mechanism is shown in Fig. B-8 (a).

Failure for the intermediate pile takes place when the $M_{\max(\text{neg})}$ at the head of the pile reaches the yield resistance and is shown in the Fig. B-8 (b). The high negative lateral earth pressure acting

close to the toe of the pile is approximated as the concentrated force as shown in the Fig. B-8 (b). Thus, the equation to calculate H_u is expressed as $H_u = 0.5\gamma dL^2k_p - M_y$. This is applicable only when the $M_{(pos)}$ developed at the depth f is less than M_y . The dimensionless ultimate resistance based on the calculated value is plotted in Fig. B-7 (a).

For long restrained pile, failure takes place when two plastic hinges form and the pile turns into a mechanism as shown in Fig. B-8(c). The two plastic hinges forms when both, $M_{max(pos)}$ at depth f and $M_{max(neg)}$ at the bottom of the pile reach M_y . Considering that the total shear force at the f is equal to zero, we can calculate by the equation $f = 0.82 \sqrt{\frac{H_u}{\gamma dk_p}}$. Therefore, the ultimate lateral

resistance can be obtained from
$$H_u = \frac{M_{max(pos)} + M_{max(neg)}}{e + 0.54 \sqrt{\frac{H_u}{\gamma dk_p}}} = \frac{2M_y}{e + 0.54 \sqrt{\frac{H_u}{\gamma dk_p}}}$$
.

The ultimate lateral resistance as determined from the equation is plotted in Fig. B-7(b) as a function of the dimensionless yield or plastic moment resistance.

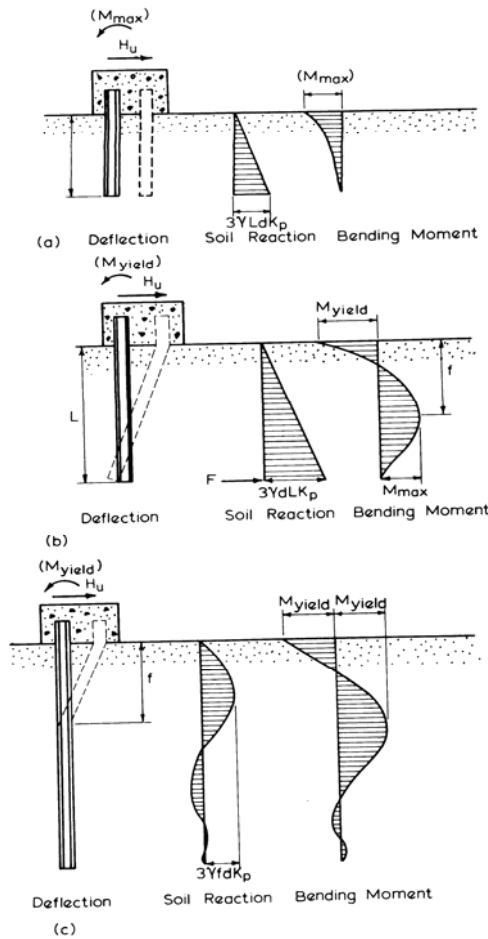


Figure B-8. Restrainted piles in cohesionless soil (a) short (b) intermediate and (c) long (after Poulos and Davis)

3. Sheet Piling Method (AASHTO Specifications)

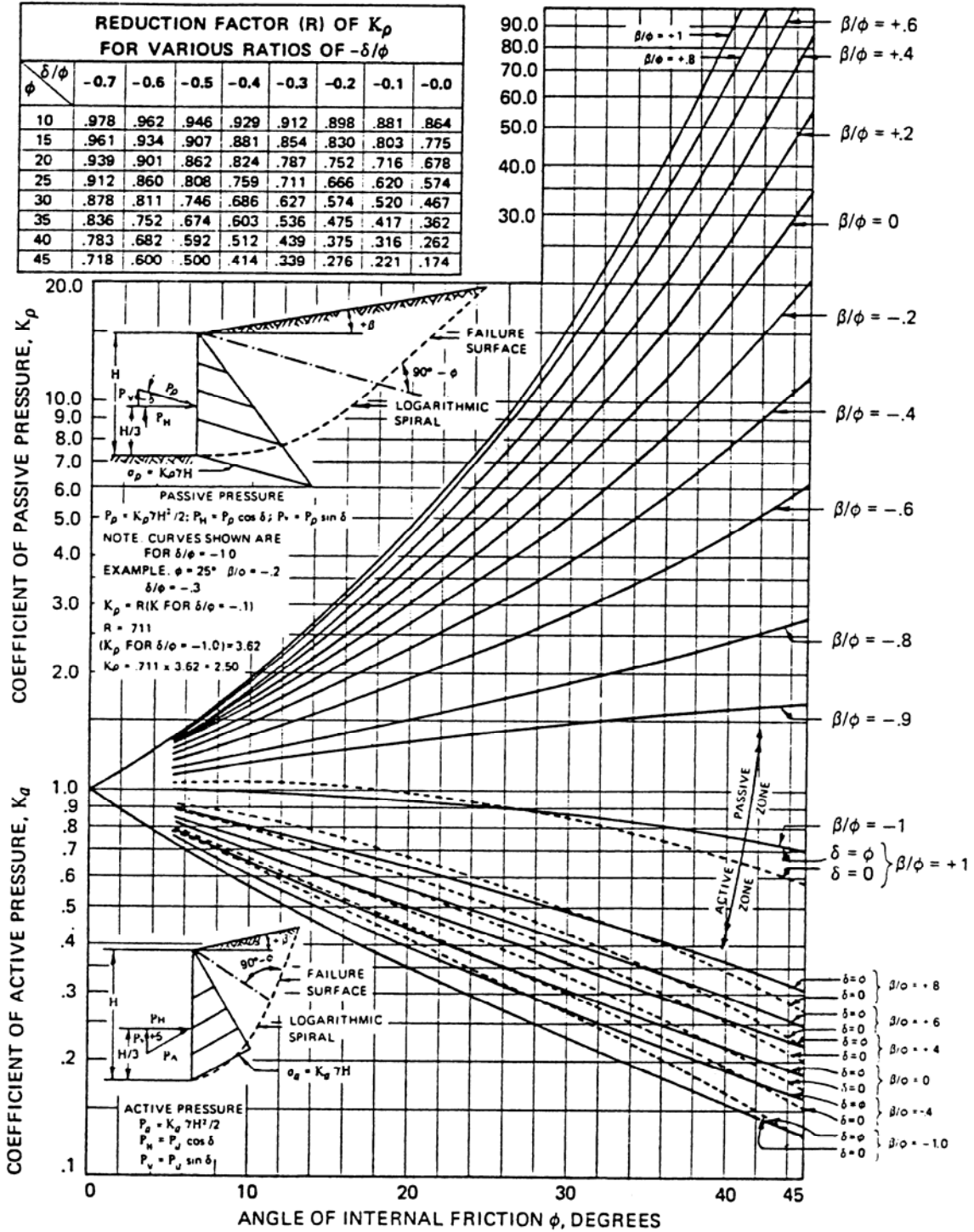
This method was initially developed for sheet piles embedded in cohesionless soils and is based on the earth pressure theory. For cohesionless fills, $\phi > \beta$ (slope angle) and generally fills are designed

for a FS of 1.25, where $FS = \frac{\tan \phi}{\tan \beta}$. Also for cohesive fills, $\tan \phi$ is assumed to be equal to

$1.25 \tan \beta$ and the unit cohesive soil strength of the soil as $c=0$. The wall friction angle δ for concrete piles is considered as $\delta = (2/3)\phi$.

Given the ϕ and γ , the active and passive pressures of slope and/or level ground can be determined using the chart shown in Fig. B-9. It gives the reduction factors for active and passive pressures. Fig. B-10 shows the distribution of active and passive pressures acting on pile.

REDUCTION FACTOR (R) OF K_p FOR VARIOUS RATIOS OF $-\delta/\phi$								
$\phi \backslash \delta/\phi$	-0.7	-0.6	-0.5	-0.4	-0.3	-0.2	-0.1	-0.0
10	.978	.962	.946	.929	.912	.898	.881	.864
15	.961	.934	.907	.881	.854	.830	.803	.775
20	.939	.901	.862	.824	.787	.752	.716	.678
25	.912	.860	.808	.759	.711	.666	.620	.574
30	.878	.811	.746	.686	.627	.574	.520	.467
35	.836	.752	.674	.603	.536	.475	.417	.362
40	.783	.682	.592	.512	.439	.375	.316	.262
45	.718	.600	.500	.414	.339	.276	.221	.174



(Printed with permission from United States Steel)

Active and passive coefficients with wall friction (sloping backfill) (after Caquot and Kerisel²¹)

Figure B-9

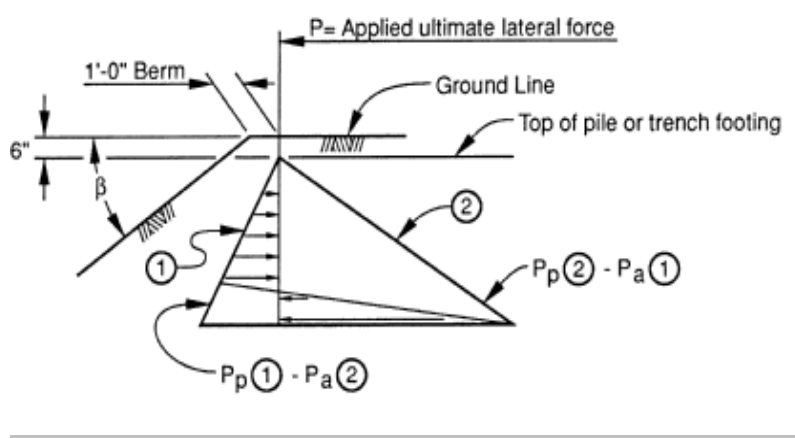


Figure B-10. Pile pressure diagram

Fig. B-11 shows the embedment determination for pile embedded in level ground. Pile diameter and the appropriate isolation factor considered to get the effective passive pressure are used in the calculations.

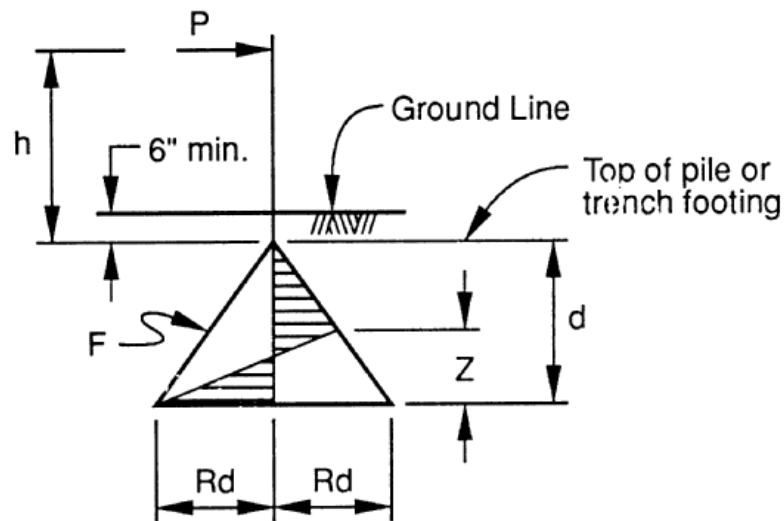


Figure B-11. The calculation schematic diagram for pile embedment depth

The following equations are given in reference to Fig. B-11 to determine the embedment depth;

$$\Sigma F_H = 0 = (2Rd)(1/2)(Z) - (1/2)(Rd^2) + P, \quad (B-2)$$

$$Z = d/2 - P/Rd \quad (B-3)$$

$$\Sigma M = 0 = \frac{Rd^3}{12} - \frac{2Pd}{3} - \frac{P^2}{3Rd} - Ph \quad (B-4)$$

where, h = distance form top of the pile to the point of application of load,

For cohesive soil, Fig. B-12 shows the actual and assumed soil-resistance distributions at failure. The values of the applied lateral load (S) and the bending moment (M) can be found with the following equilibrium equations.

$$S = p_0(2X - D) + (\alpha/2)(2X^2 - D^2) \quad (B-5)$$

$$M = -p_0(X^2 - D^2/2) - (\alpha/3)(2X^3 - D^3) \quad (B-6)$$

where α = slope of the soil resistance diagram,

p_0 = ultimate soil resistance at the ground surface,

D = the pile embedment depth, and

X = the unknown distance to the point of rotation.

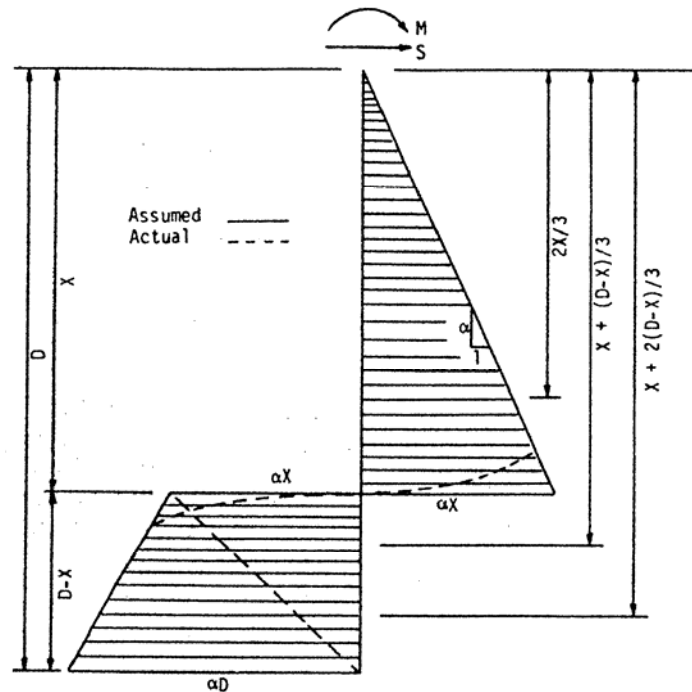


Figure B -13. Ultimate soil resistance for cohesionless soil.

For cohesionless soils, Fig. B-13 shows the actual and assumed soil-resistance distributions at failure. By applying equilibrium conditions to the assumed soil distribution, the equations for S and M can be found as follows.

$$S = (\alpha/2)(2X^2 - D^2) \quad (B-7)$$

$$M = (-\alpha/3)(2X^3 - D^3) \quad (B-8)$$

The soil strength is based on the following equation (Equation 9-7 in “Basic Soils Engineering” by B.K. Hough), which was generated for footing foundation.

$$p_{ult} = K_1 N_c c + K_2 \gamma_1 N_\gamma B + N_q \gamma_2 D_f \quad (B-9)$$

where K_1, K_2 = coefficients dependent on the type of footing,

N_c, N_γ, N_q = bearing capacity factors,

C = unit cohesion,

γ_1 = effective unit weight of soil below footing grade,

γ_2 = effective unit weight of soil above footing grade in depth D_f ,

B = breadth of footing,

D_f = depth of the footing below exterior ground.

The above coefficients of the soil strength equation were calibrated from many testing results with an optimization program developed by Mr. Michael McMullen.

The program can only apply to homogeneous cohesive or cohesionless soil. The program, however, has shown problems when run for cohesive soil conditions. The method cannot provide deflection information.

5. P-Y Method

P-Y method is based on a numerical solution of a physical model based on a beam on Winker foundation shown in Fig. B-14. A number of empirical p-y curves for typical soil conditions based on the field test results have been developed. Reese (1984, 1986) has developed procedures for describing the soil response surrounding a laterally loaded pile for various soil conditions by using

a family of p-y curves. Analytical expressions used for p-y curves are complex and can be found in numerous references, such as Wang, Shih-Tower and Reese, L.C.'s report in 1993.

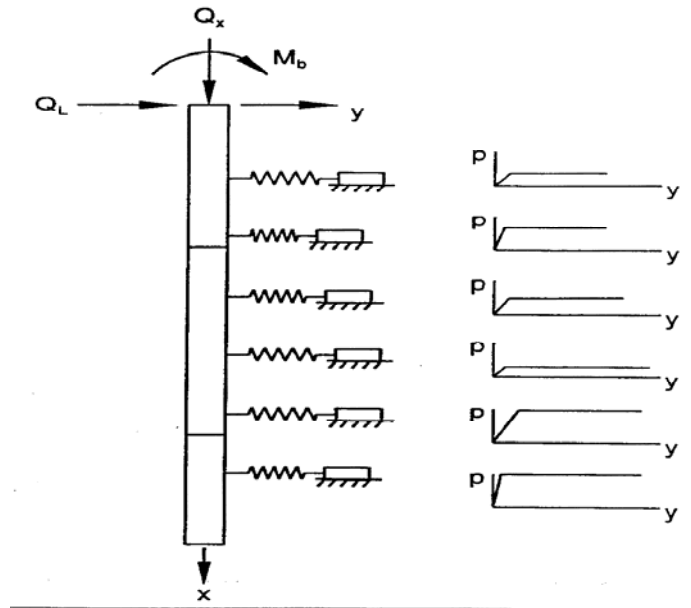


Figure B-14. COM624P Pile-Soil Model

By solving the beam bending equation using finite difference or finite element numerical techniques, solution of pile behaviors can be obtained.

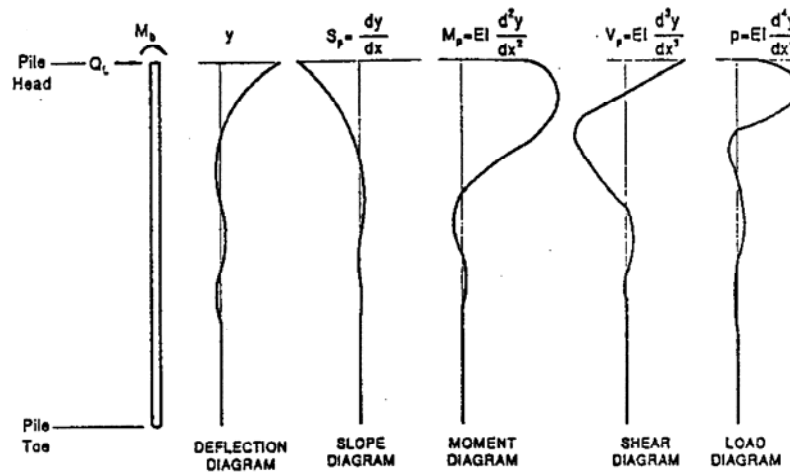


Figure B-15. Graphical presentation of COMP624 results.

Typical output from the computer program COM624P (LPILE) is depicted in Fig. B-15. The advantages of this method are that it accounts for the nonlinear behavior of the soils.

6. NAVFAC DM-7

This approach is based on Reese and Matlock's non-dimensional solutions for laterally loaded piles. Different simplified approaches are used for computing lateral pile-load versus deformation relationship based on complex soil conditions and/or non-linear soil stress-strain relationships. For coarse grained soil, pile deformations can be estimated assuming that the modulus of elasticity (E_s) increases linearly with depth and that the linear increase in coefficient of subgrade reaction k_h is in

accordance with $k_h = \frac{fz}{D}$,

where, k_h = coefficient of lateral subgrade reaction (tons/feet³)

f = coefficient of variation of lateral subgrade reaction (tons/ft³). Chart given in the Fig. 16 is used to select the value of f .

z = depth (feet)

D = width / diameter of loaded area (feet)

For stiff to hard clays, modulus E_s is assumed constant with depth, and the procedure for the conversion of constant modulus E_s to an equivalent modulus E_s that varies linearly with depth is given stepwise as follows:

- Given a value of constant E_s , assume a value of f .
- Compute depth Z to point of zero deflection of pile from the figures shown below
- Recompute f so that value of $f_z=2E_s$.
- Recompute depth z with revised f and alter f again so that $f_z=2E_s$

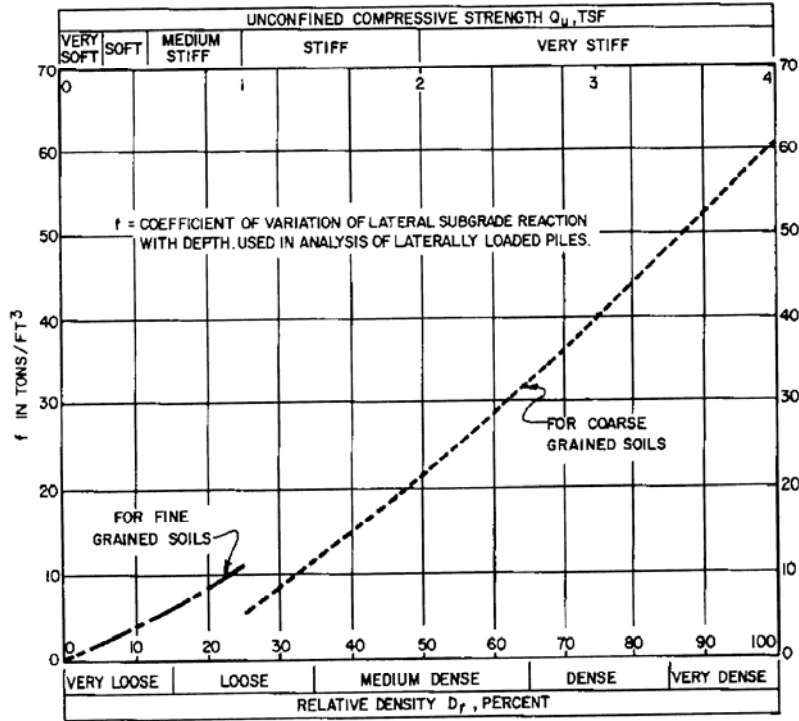


Figure B-16. Coefficient of variation of subgrade reaction

Three principal boundary conditions: flexible cap, rigid cap at ground surface and rigid cap at elevated position, are considered for the method and are explained with the design procedures in Fig. B-17. Fig. B-18 through Fig. B-20 provide the calculation charts for these three boundary conditions. This method provides only elastic solutions. The lateral load cannot exceed about 1/3 of the ultimate lateral load capacity.

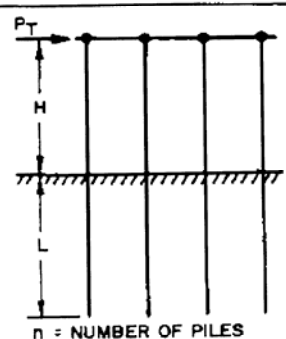
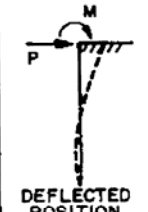
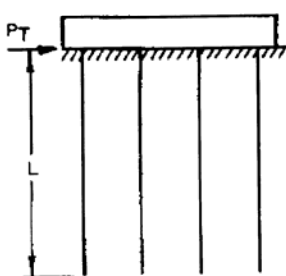

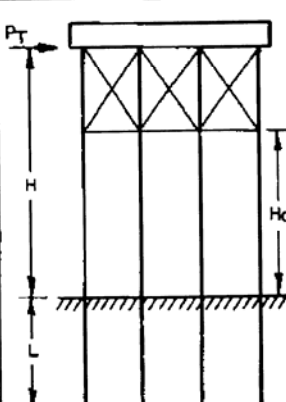
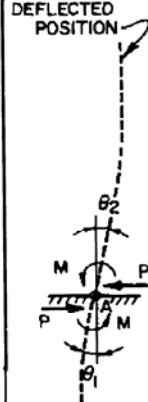
CASE I. FLEXIBLE CAP, ELEVATED POSITION		
CONDITION	LOAD AT GROUND LINE	DESIGN PROCEDURE
 <p>$n = \text{NUMBER OF PILES}$</p>	<p>FOR EACH PILE:</p> $P = \frac{P_T}{n}$ $M = PH$  <p>DEFLECTED POSITION</p>	<p>FOR DEFINITION OF PARAMETERS SEE FIGURE 12</p> <ol style="list-style-type: none"> 1. COMPUTE RELATIVE STIFFNESS FACTOR. $T = (\frac{EI}{P})^{1/5}$ 2. SELECT CURVE FOR PROPER $\frac{L}{T}$ IN FIGURE 11. 3. OBTAIN COEFFICIENTS F_δ, F_M, F_V AT DEPTHS DESIRED. 4. COMPUTE DEFLECTION, MOMENT AND SHEAR AT DESIRED DEPTHS USING FORMULAS OF FIGURE 11. <p>NOTE: "f" VALUES FROM FIGURE 9 AND CONVERT TO LB/IN³.</p>
CASE II. PILES WITH RIGID CAP AT GROUND SURFACE		
		<ol style="list-style-type: none"> 1. PROCEED AS IN STEP 1, CASE I. 2. COMPUTE DEFLECTION AND MOMENT AT DESIRED DEPTHS USING COEFFICIENTS F_δ, F_M AND FORMULAS OF FIGURE 12. 3. MAXIMUM SHEAR OCCURS AT TOP OF PILE AND EQUALS $p = \frac{P_T}{n}$ IN EACH PILE.
CASE III. RIGID CAP, ELEVATED POSITION		
	<p>DEFLECTED POSITION</p> 	<ol style="list-style-type: none"> 1. ASSUME A HINGE AT POINT A WITH A BALANCING MOMENT M APPLIED AT POINT A. 2. COMPUTE SLOPE θ_2 ABOVE GROUND AS A FUNCTION OF M FROM CHARACTERISTICS OF SUPERSTRUCTURE. 3. COMPUTE SLOPE θ_1 FROM SLOPE COEFFICIENTS OF FIGURE 13 AS FOLLOWS: $\theta_1 = F_\theta \left(\frac{PT^2}{EI} \right) + F_\theta \left(\frac{MT}{EI} \right)$ 4. EQUATE $\theta_1 = \theta_2$ AND SOLVE FOR VALUE OF M. 5. KNOWING VALUES OF P AND M, SOLVE FOR DEFLECTION, SHEAR, AND MOMENT AS IN CASE I. <p>NOTE: IF GROUND SURFACE AT PILE LOCATION IS INCLINED, LOAD P TAKEN BY EACH PILE IS PROPORTIONAL TO I/H_0^3.</p>

Figure B-17. Design procedure for laterally loaded piles

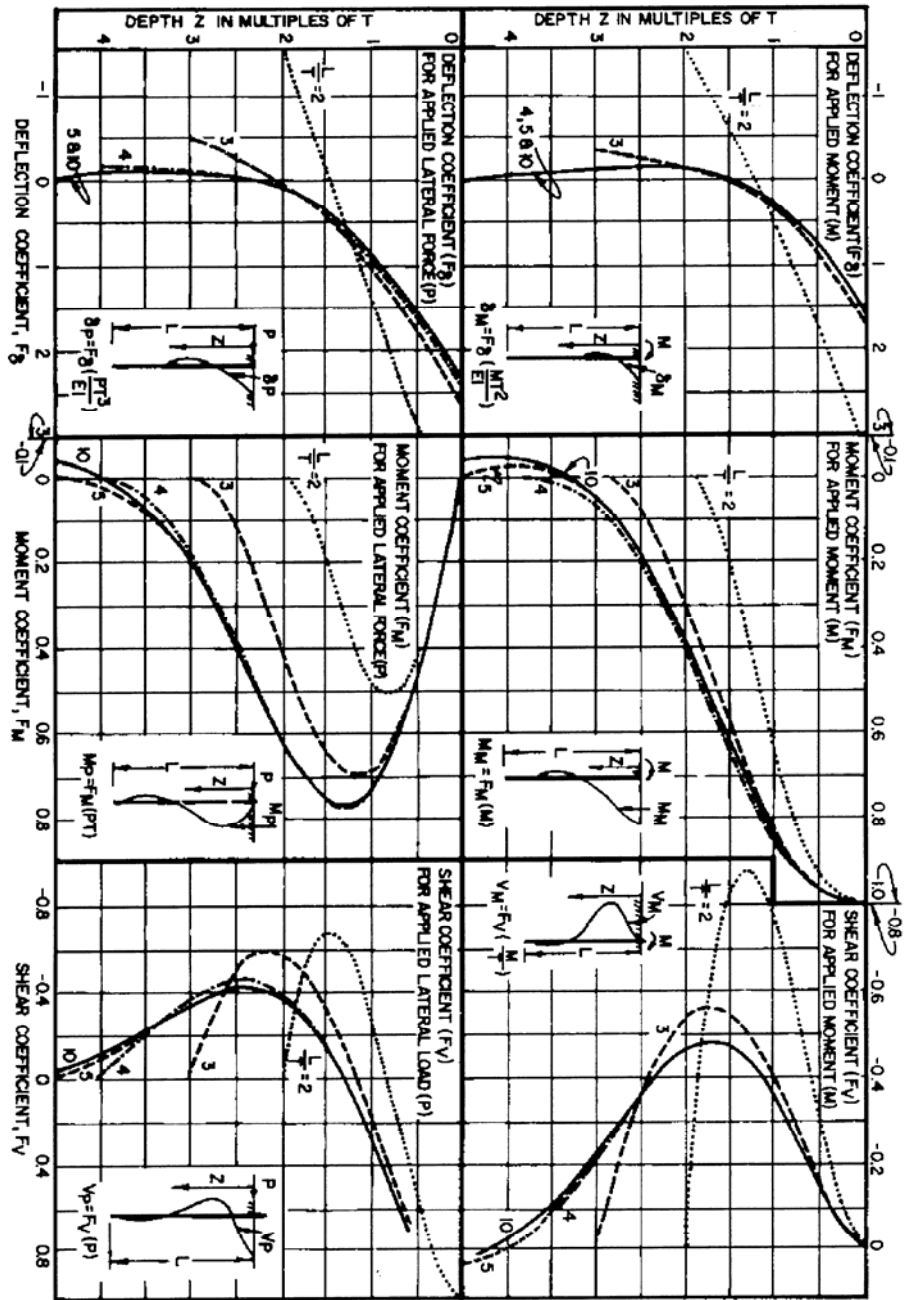


Figure B-18. Influence values for pile with applied lateral load and moment
(Case I. Flexible Cap or Hinged End Condition)

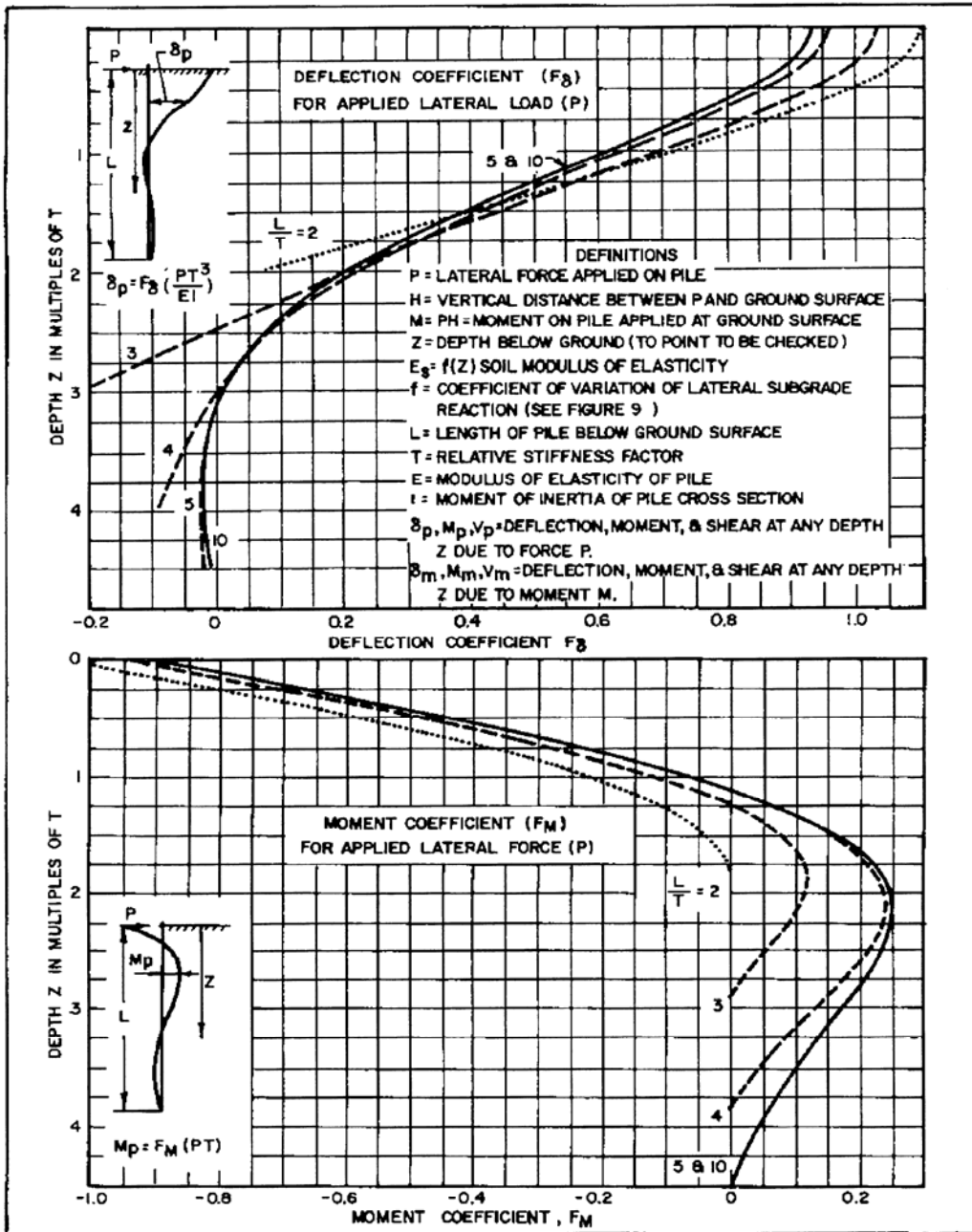


Figure B-19. Influence values for laterally loaded pile

(Case II. Fixed Against Rotation at Ground Surface)

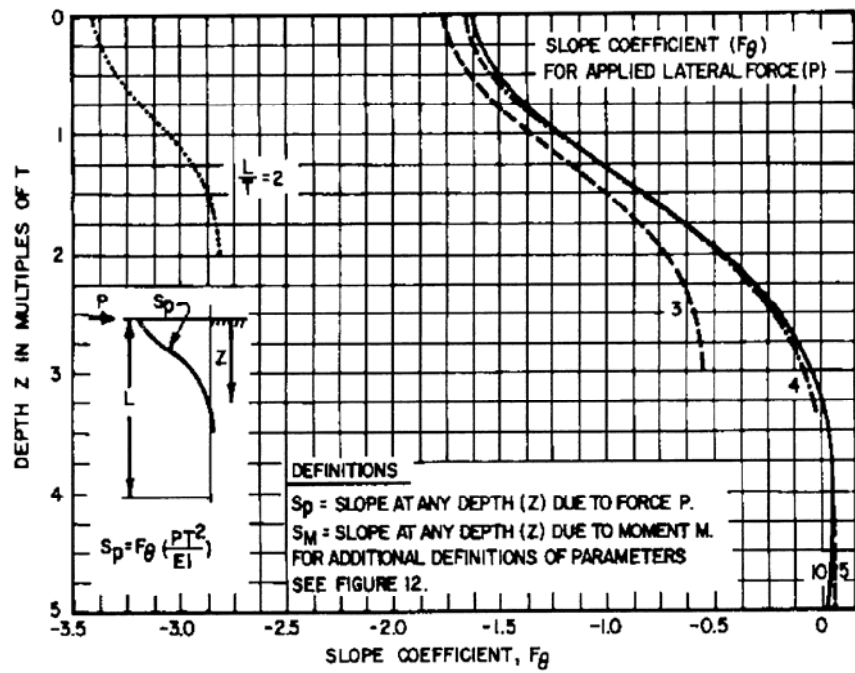
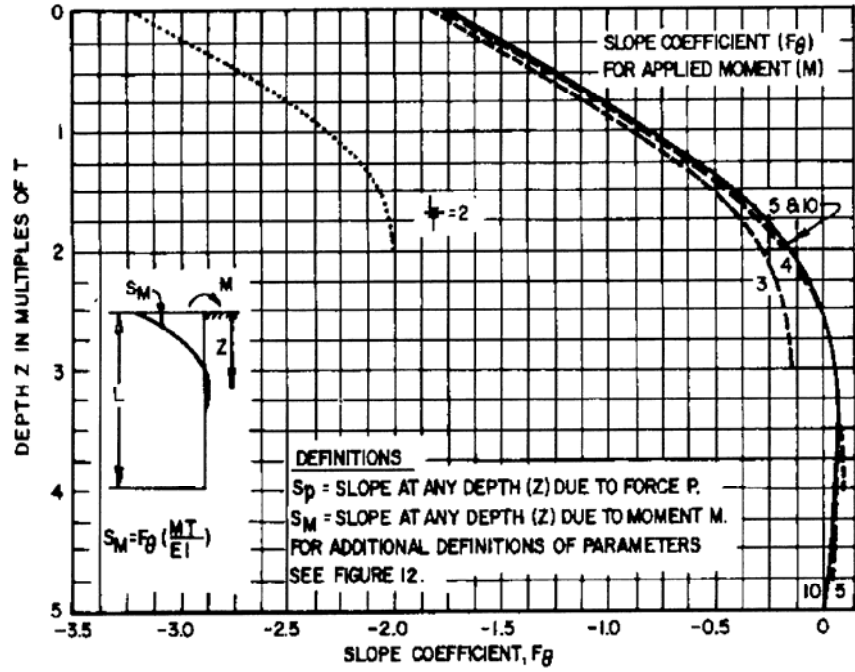


Figure B-20. Slope coefficient for pile with lateral load or moment

Appendix C

Analysis Methods for Torsional Response of Drilled Shafts

Introduction

Structures may be subjected to significant laterally loads due to wind, wave or earthquake actions. These loads may induce torque on piles due to the eccentricity of the lateral loads. During the past few decades, increasing attention is being focused on the torsional response of piles. The researches can be grouped into two schools of thought. The first one pertains to the theory analysis of torsion-twist behavior based on the assumptions that the foundation soil behaves as a linear or non-linear elastic material. The second category focuses on the limit equilibrium analysis where the ultimate capacity of the shaft is governed by the shear strength of the foundation soil.

1. Existing analytical and numerical methods for torsional response of piles

1.1 Methods for all kind of soils

O'Neill (1964) established a closed form differential equation solution for the pile-head torque and twist relationship for the case in which both the pile and the soil are assumed to have linear torque-twist properties.

The linear relationships are expressed as:

$$T(z) = T_0 e^{-z\sqrt{\beta\lambda}} \quad (C-1)$$

$$\left(\frac{T}{\theta}\right)_{\text{pilehead}} = \sqrt{\frac{\lambda}{\beta}} \quad (C-2)$$

in which,

T_0 = The torque applied at the top of the pile

β = The reciprocal of the product of the pile material shear modulus, G_p , and its polar moment of inertia, J

λ = A function of the torsional restraint of the soil = $4\pi r^2 G_s$

r = Radius

G_s = Shear modulus of the soil

The above linear interaction problem is based on the assumption that the torsional restraint of the soil can be represented for all rotations and for all depths by a single

parameter, λ . However, the boundary effects near the top of the pile and non-linear soil response could preclude the use of a value for λ which is constant with depth.

In order to include the non-linearity, O'Neill (1964) suggested a discrete element model that simulates torsional behavior of a circular, prismatic pile. A three-element portion of that model is shown in Figure C-1.

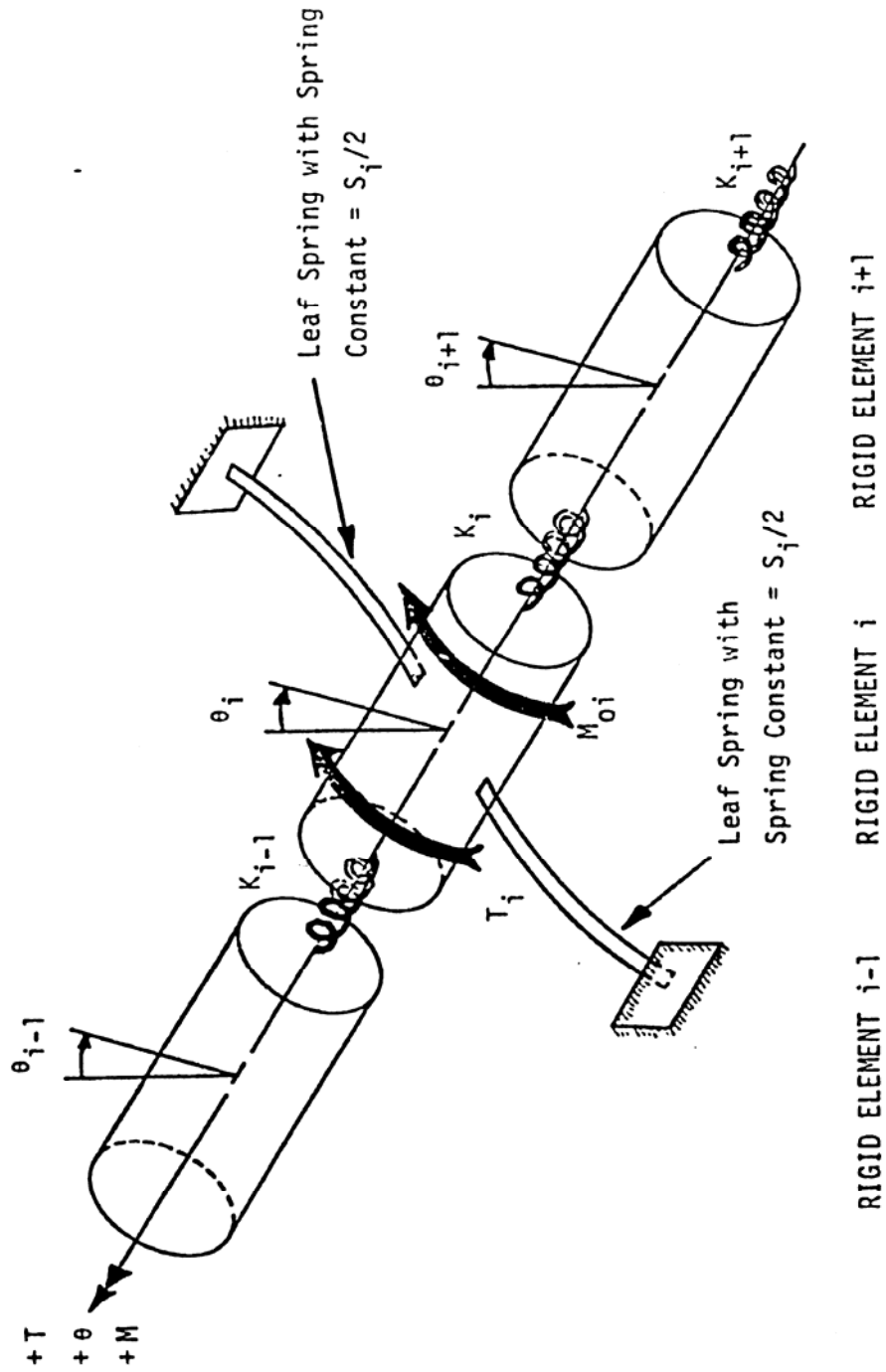


Figure C-1. Mechanical Finite Element Model of Torsionally Loaded Pile for Simulating Torque-Twist Behavior (After O'Neill, 1964)

The mechanical model is composed of rigid elements connected by torsional springs with spring constants k_i . The non-linear torsional resistance of the soil can be represented partially by a spring constant S_i and partially by a fixed moment M_{0i} .

The relationship of twist angle and torque is given by:

$$\theta_i = \frac{(T_i + M_{0i}) + k_{i-1}A_{i-1}}{C_i} + \frac{K_i}{C_i} \theta_{i+1} \quad (C-3)$$

where $C_i = k_{i-1}(1 - B_{i-1}) + k_i - S_i$

$$A_i = \frac{(T_i + M_{0i}) + k_{i-1}A_{i-1}}{C_i}$$

$$B_i = \frac{k_i}{C_i}$$

In order to solving non-linear torque-twist problems, an iterative procedure may be used by successively adjusting the S values and M_0 values to insure compatibility between S and θ everywhere along the pile until closure within a specified tolerance, usually expressed in terms of rotation at the pile head, is achieved.

Poulos(1975) presented a numerical elastic analysis of the response of a single cylindrical pile subjected to torsion by using integral equation techniques. The parametric solutions for the rotation of the pile head are presented, for both a uniform soil and a soil in which shear modulus and pile-soil adhesion increase linearly with depth.

Fig.C-2(a) shows the problem. The pile shaft is divided into n equal cylindrical elements and the base is composed of m annular elements, each element being acted upon by an unknown uniform interaction stress [Fig. C-2(b)].

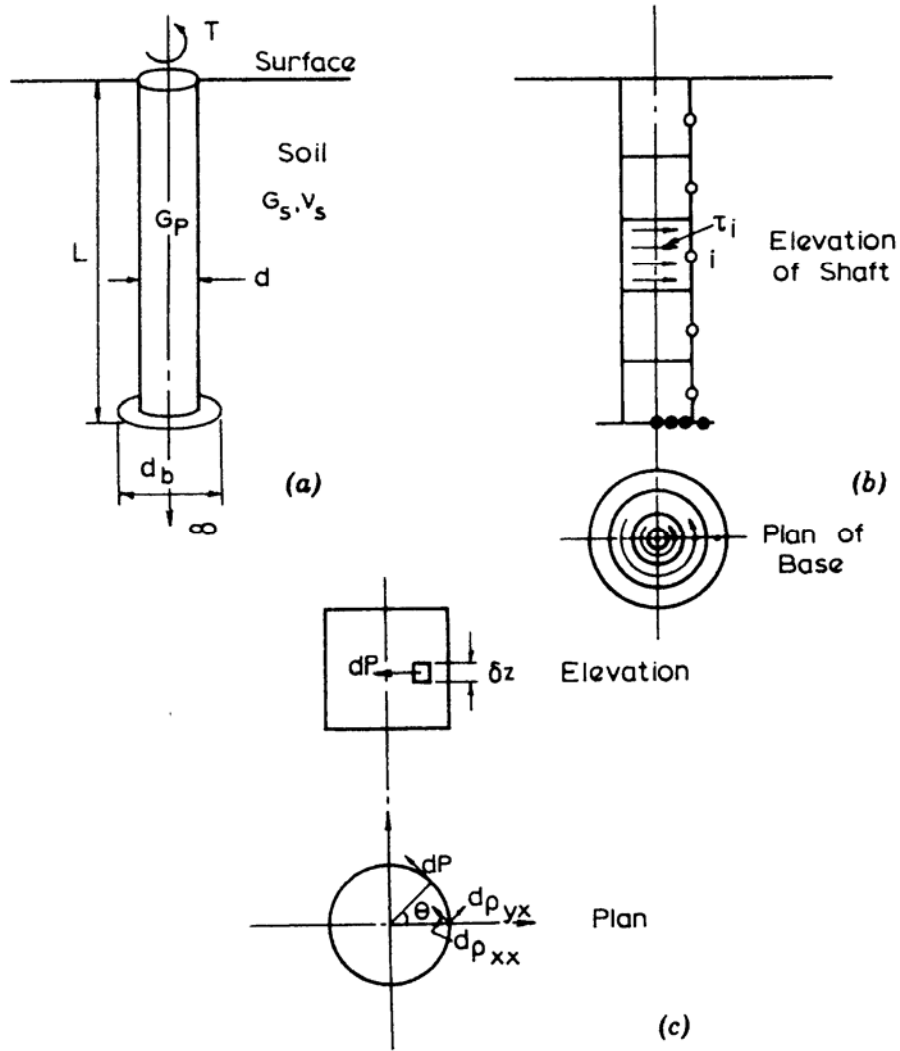


Figure C-2 Definition of Problem:(a) Geometry; (b) Division of Pile into Elements; (c) Detail of Area of Element (After Poulos 1975).

For a uniform-diameter pile in a soil with constant shear modulus and pile- soil adhesion, the top rotation can be expressed as

$$\phi = \frac{T}{G_s d^3} \frac{I_\phi}{F_\phi} \tag{C-4}$$

For a soil having shear modulus and pile-soil adhesion that increase linearly with depth, the top rotation can be given by

$$\phi = \frac{T}{N_G d^4} \frac{I_\phi'}{F_\phi'} \tag{C-5}$$

in which I_ϕ, I'_ϕ = elastic rotation influence factor; G_s = soil shear modulus, and F_ϕ, F'_ϕ = correction factor for the effects of pile-soil slip, N_G = rate of increase of shear modulus with depth ($G_s = N_G z$).

Randolph (1981) presented closed-form solutions for the torsional stiffness of a pile in homogeneous soil and a soil where the stiffness is proportional to depth, based on a simple assumption that the shear stress τ_{z0} is negligible compared to τ_{r0} . The analysis also assumes that the soil deforms in an elastic or pseudo-elastic manner.

For homogeneous soil, the shear modulus of soil G is constant.

For rigid circular pile, the torsional stiffness of pile top is given by

$$\frac{T_t}{Gr_0^3\phi_t} = \frac{16}{3} + 4\pi \frac{1}{r_0} \quad (C-6)$$

in which G = the shear modulus of the soil, r_0 = the radius of pile, Φ_t = the rotation of the pile top, T_t = the torque of pile top.

For flexible pile, the torsional stiffness of pile top is given by

$$\frac{T_{top}}{Gr_0^3\phi_{top}} = \frac{\left(\frac{16}{3} + 4\pi \frac{1}{r_0} \frac{\tanh(\mu l)}{\mu l} \right)}{\left(1 + \frac{32}{3\pi\lambda} \frac{1}{r_0} \frac{\tanh(\mu l)}{\mu l} \right)} \quad (C-7)$$

in which $\mu l = \left(\frac{8}{\lambda} \right)^{1/2} \left(\frac{1}{r_0} \right)$, $\lambda = G_p / G_s$.

When the applied torque approaches ultimate torque, the torsional stiffness of the head of pile can be estimated as:

$$\frac{T_t}{\phi_t} \approx 2 \frac{(GJ)_p}{1} \quad (C-8)$$

For Soil Shear Modulus Proportional to Depth

The assumption is also made that the soil deforms in an elastic or pseudo-elastic manner.

For rigid pile, the torsional stiffness of the pile head is written as

$$\frac{T_t}{mr_0^4 \phi_t} = \frac{1}{r_0} \left(\frac{16}{3} + 2\pi \frac{1}{r_0} \right) \quad (C-9)$$

For flexible pile, the governing differential equation is

$$\frac{d^2 \phi}{dz^2} = \frac{8}{\lambda' r_0^2} \frac{z}{r_0} \phi \quad (C-10)$$

in which $\lambda' = G_p / (mr_0)$.

Solution of this equation is possible in terms of Airy functions. By applying the pile base boundary condition, torsional stiffness can be calculated.

When the applied torque approaches ultimate torque, the torsional stiffness of the head of pile can be estimated as:

$$\frac{T_t}{\phi_t} \approx 1.5 \frac{(GJ)_p}{l} \quad (C-11)$$

Chow (1985) presented a discrete element approach for the analysis of torsional response of piles in nonhomogeneous soil. This approach can deal with complex soil stratification, and arbitrarily varying pile sections. However, the modulus of subgrade reaction is linear, so this method only gives out the solution for linear soil response.

The governing equilibrium equation using the modulus of subgrade reaction approach is given by

$$-G_p J \frac{\partial^2 \psi}{\partial z^2} + k_\psi \psi = 0 \quad (C-12)$$

in which G_p = shear modulus of pile material; J = polar second moment of area of pile section; ψ = angle of twist of pile; k_ψ = modulus of subgrade reaction of soil undergoing torsion; and z = depth coordinate.

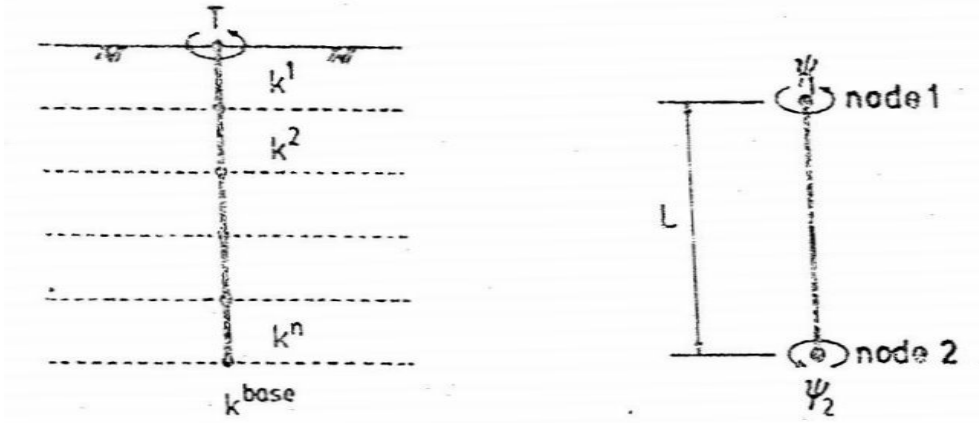


Figure C-3 (a) Discrete Element Model For Torsional Response of Pile (after chow 1985)

(b) Typical Torsional Discrete Element (after chow 1985)

The soil is discretized into a series of elements connected at the nodes. The soil is also divided as horizontal layers, each layer with a modulus of subgrade reaction, k as shown in Fig. C-3(a). Fig.C-3(b) shows the typical element. The continuous variable, ψ , is approximated in terms of its nodal values ψ_1 and ψ_2 through

$$\psi = \{n\}^T \{ \psi \} \quad (C-13)$$

$$\text{in which } \{n\} = \begin{Bmatrix} 1 - \frac{Z}{L} \\ \frac{Z}{L} \end{Bmatrix}, \text{ and } \{ \psi \} = \begin{Bmatrix} \psi_1 \\ \psi_2 \end{Bmatrix}$$

Applying Galerkin method to the governing equation results in the following element matrix equation:

$$[K_p] \{ \psi \} + [K_s] \{ \psi \} = \{0\} \quad (C-14)$$

in which the pile element matrix is

$$K_p = \int_0^L G_p J \left\{ \frac{\partial n}{\partial z} \right\} \left\{ \frac{\partial n}{\partial z} \right\}^T dz$$

and the soil element matrix is

$$[K_s] = \int_0^L k_\psi \{n\} \{n\}^T dz$$

Assembly of the stiffness matrix for the pile-soil system is done element by element. In this way, soils with complex stratification and piles with arbitrarily varying sections can be dealt with.

The modulus of subgrade reaction of soil at the pile shaft is given by

$$k_{\psi}^{\text{side}} = 4\pi G r_0^2 \quad (\text{C-15})$$

in which G = shear modulus of soil; and r_0 = pile radius.

For soil the shear modulus is proportional to depth, $G = mz$, in which m = rate of increase of shear modulus with depth. The modulus of subgrade reaction per unit increase in depth is given by

$$k_{\psi}^* = 4\pi m r_0^2 \quad (\text{C-16})$$

The subgrade reaction modulus of pile tip is given by

$$k_{\psi}^{\text{base}} = \frac{16}{3} G r_0^3 \quad (\text{C-17})$$

Hache & Valsangkar (1988) developed simple mathematical solutions for torsionally loaded pile in a layered soil and nondimensional charts for design purpose. Actually, the nondimensional solutions and charts for two layer soils are similar with Poulos(1975) suggested parametric solution for one layer homogeneous soil. The advantage is this solution can deal with piles in layered soils. The analysis assumes elastic soil response.

The solutions are based on Randolph's (1981) simplified elastic solution. Fig.C-4 depicts the pile-soil analysis model.

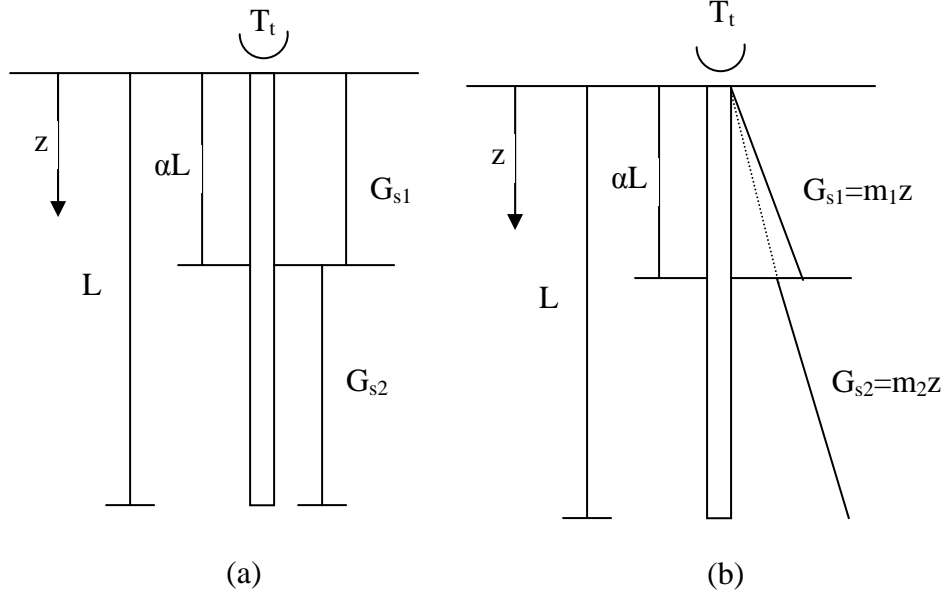


Figure C-4. Pile in Two-Layered Soil: (a) Homogeneous Layers; (b) Nonhomogeneous Layers

For homogeneous layered soil, the governing differential equations are (Randolph 1981; Scott 1981)

$$\frac{\partial^2 \phi}{\partial z^2} - \eta \lambda_2'^2 \phi = 0, 0 \leq z \leq \alpha L \quad (\text{C-18})$$

$$\frac{\partial^2 \phi}{\partial z^2} - \lambda_2'^2 \phi = 0, \alpha L \leq z \leq L \quad (\text{C-19})$$

in which $\lambda_2' = \sqrt{(4\pi r_0^2 G_{s2}) / (GJ)_p}$; $\eta = G_{s1} / G_{s2}$; $(GJ)_p$ = pile torsional stiffness; r_0 = radius of the pile; z = depth from the soil surface; L = length of the pile; and αL = thickness of the upper layer.

The solutions are

$$\phi = C_1 e^{-\sqrt{\eta} \lambda_2' z} + C_2 e^{-\sqrt{\eta} \lambda_2' z}, 0 \leq z \leq \alpha L; \quad (\text{C-20})$$

$$\phi = C_3 e^{-\lambda_2' z} + C_4 e^{\lambda_2' z}, \alpha L \leq z \leq L; \quad (\text{C-21})$$

For a two-layered soil where the shear modulus is linearly varying with depth:

$$\frac{\partial^2 \phi}{\partial z^2} - \eta_1 \lambda_2^3 z \phi = 0, 0 \leq z \leq \alpha L \quad (C-22)$$

$$\frac{\partial^2 \phi}{\partial z^2} - \lambda_2^3 z \phi = 0, \alpha L \leq z \leq L \quad (C-23)$$

in which $\lambda_2 = 3\sqrt{(4\pi r_0^2 m_2)/(GJ)_p}$; $\eta_1 = m_1/m_2$; and m_1 and m_2 are slopes of the soil stiffness variation with depth. The solutions are:

$$\phi = C_1 \beta (\eta_1^{1/3} \lambda_2 z) + C_2 z \xi (\eta_1^{1/3} \lambda_2 z), 0 \leq z \leq \alpha L; \quad (C-24)$$

$$\phi = C_3 \beta (\lambda_2 z) + C_4 z \xi (\lambda_2 z), \alpha L \leq z \leq L; \quad (C-25)$$

Using the pile top and tip boundary conditions and the result equations, nondimensional solutions and charts are developed. The relationship between twist angle of pile top and applied torque is given by

$$\phi_t = \frac{T_t L}{(GJ)_p} (I_\phi) \quad (C-26)$$

Guo & Randolph (1996) presented analytical and numerical solutions for the torsional response of piles embedded in non-homogeneous soil by assuming that the stiffness profile of the soil follows a simple power law with depth.

The soil modulus is assumed as a power law variation of depth, given by

$$G_i = A_g z^n \quad (C-27)$$

in which G_i is the initial shear modulus at depth z ; A_g is a modulus constant; and n is the depth exponent, referred to here as the non-homogeneity factor.

The limiting shaft friction τ_f is also assumed as a power law variation with depth, as

$$\tau_f = A_t z^t \quad (C-28)$$

in which A_t is a constant that determines the magnitude of shaft friction, and t is the corresponding non-homogeneity factor, and $t = n$ is assumed.

Elastic solution

The ratio of torque and rotation can be expressed as

$$\frac{T(z)}{\phi(z)} = \pi_t^{1/2m} C_t(z) \frac{(GJ)_p}{L} \quad (C-29)$$

in which

$$\pi_t = \left(\frac{\pi d^2 A_g L^{n+2}}{(GJ)_p} \right)^m$$

$$C_t(z) = \frac{C_1(z) + \chi C_2(z)}{C_3(z) + \chi C_4(z)} \left(\frac{z}{L} \right)^{n/2};$$

$$C_1(z) = -K_{m-1} I_{m-1}(y) + K_{m-1}(y) I_{m-1}; \quad C_2(z) = K_m I_{m-1}(y) + K_{m-1}(y) I_m;$$

$$C_3(z) = K_{m-1} I_m(y) + K_m(y) I_{m-1}; \quad C_4(z) = -K_m I_m(y) + K_m(y) I_m;$$

I_{m-1} , I_m , K_m , and K_{m-1} are the values of the Bessel functions for $z = L$;

$$\chi = \frac{16G_b r_0^3 L}{3(GJ)_p} \frac{1}{\pi_t^{1/2m}}$$

Elastic-plastic solution

The soil response is modeled as elastic-perfectly plastic. The torque at the pile head, T_t , can be given by

$$T_t = T_e + 0.5\pi d^2 \frac{A_t L_1^{n+1}}{n+1} \quad (C-30)$$

in which,

$$T_e = 0.5\pi_t^{1/2m} C_t(\mu L) \frac{A_t}{A_g} \frac{(GJ)_p}{L};$$

$$\mu = L_1/L;$$

L_1 = the length of pile where slip has occurred.

And the twist angle of the pile head can be expressed as:

$$\phi_t = \phi_e + \frac{L_1}{(GJ)_p} \left(T_e + 0.5\pi d^2 \frac{A_t L_1^{n+1}}{n+2} \right) \quad (C-31)$$

where $\phi_e = \frac{A_t}{2A_g}$.

Pile response with hyperbolic soil model

Non-linear response of the soil is assumed as a hyperbolic stress-strain law, where the secant shear modulus G is written as

$$G = G_i \left(1 - R_f \frac{\tau}{\tau_f}\right) \quad (C-32)$$

in which R_f is the hyperbolic parameter that controls the ratio of the secant modulus at failure, to the initial tangent modulus G_i .

And the angle of twist of the pile will be given by

$$\phi = \left(\frac{v}{r}\right)_0 = \frac{\tau_f}{G_i} \frac{1}{2R_f} [-\ln(1 - \psi)] \quad (C-33)$$

in which $\psi = R_f \tau_0 / \tau_f$, τ_0 the shear stress at the side of pile.

For rigid piles, the angle of twist will be uniform down the pile, so the overall torsional stiffness can be written in the form adopted by Randolph (1981) as

$$\frac{T_t}{A_g L^n r_0^3 \phi_t} = \frac{16}{3} + \frac{4\pi}{n+1} \frac{L}{r_0} \frac{-\psi}{\ln(1-\psi)} \quad (C-34)$$

For flexible piles, it is necessary to use a numerical approach so that the non-linear torque transfer curve can be implemented. A spreadsheet program, GASPILE has been developed for torsional loading.

Lin (1996) proposed a finite element numerical procedure for the analysis of torsional behavior of cracked reinforced concrete pile. A trilinear torque-twist model is employed to represent the torsional response of the reinforced concrete pile element with maximum torsional stresses. The remaining part of the pile is modeled as a linear elastic torsional behavior. Hyperbolic nonlinear model is employed to model the torsional resistance of the soil along the pile shaft. Both linear and nonlinear analyses were performed and showed the importance of taking into account the changing of pile stiffness once concrete has cracked.

1.2. Methods for rock

Carter & Kulhawy (1988) presented an approximate linear elastic solution for torsionally loaded shafts in rock. The solution followed Randolph's (1981) approximate solution for torsional response of piles in soils.

For homogeneous rock, the solutions will be developed for two cases, one for shaft in a "complete" rock socket and one for shaft in a "side shear only" socket.

For complete socket, the torsional stiffness of pile head is given by:

$$\frac{T}{G_r B^3 \phi} = \frac{\left(\frac{2}{3}\right)\left(\frac{1}{\xi}\right) + \pi\left(\frac{D}{B}\right)\frac{\tanh(\mu D)}{\mu D}}{1 + \left(\frac{64}{3\pi\lambda\xi}\right)\left(\frac{D}{B}\right)\frac{\tanh(\mu D)}{\mu D}} \quad (\text{C-35})$$

in which $\xi = G_r / G_b$, D = the length of shaft, $\mu^2 = 32 / (\lambda B^2)$ and $\lambda = G_e / G_r$, $G_e = (GJ)_c / (\pi B^4 / 32)$, B = shaft diameter, $(GJ)_c$ = shaft torsional rigidity, G_r = elastic shear modulus of rock, G_b = the shear modulus of rock below shaft.

For side shear socket, the stiffness can be given by

$$\frac{T}{G_r B^3 \phi} = \pi \left(\frac{\tanh[\mu D]}{\mu D} \right) \left(\frac{D}{B} \right) \quad (\text{C-36})$$

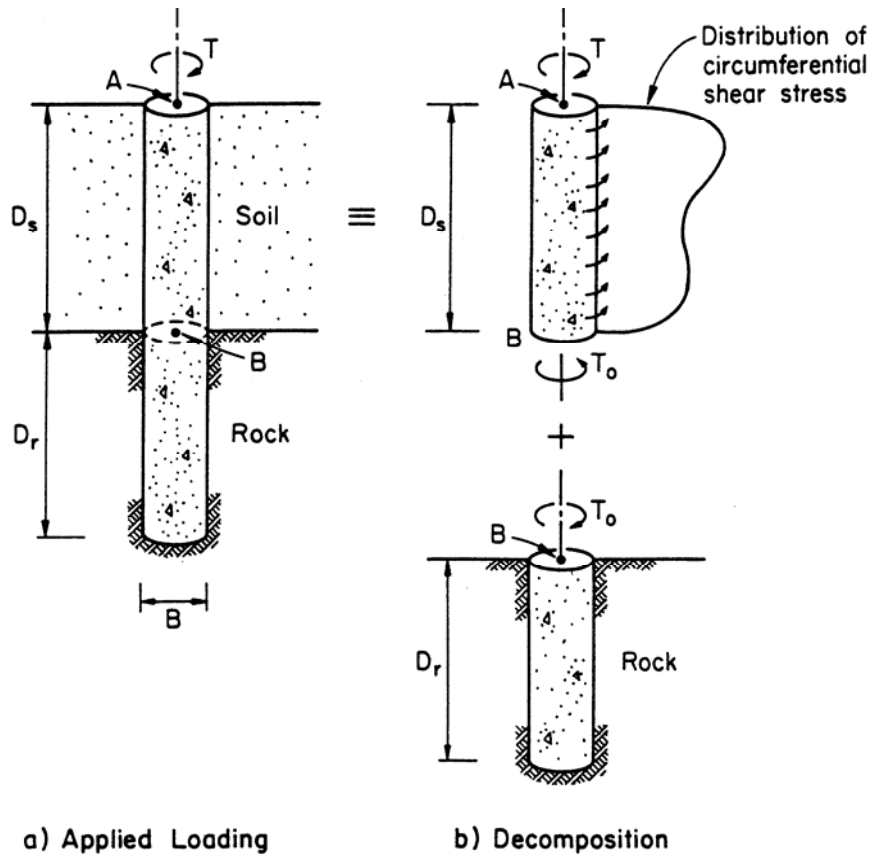


Figure C-5. Rock Socketed Shaft under Torsional Loading with Overlying Soil

For soil overlying rock conditions (Fig. C-5), an assumption is made that the presence of the soil layer could be ignored completely, in which case zero shear stress would be considered at the face of the shaft. Then the twist angle between point A and point B is:

$$\phi_{AB} = \frac{TD_s}{(GJ)_c} \quad (C-37)$$

This quantity combined with the twist of the lower portion of the shaft embedded in the rock would give the overall twist at the groundline, ϕ .

For cohesive soil, the twist of point A relative to B is given by

$$\Phi_{AB} = \frac{1}{(GJ)_c} (TD_s - \pi B^2 D_s^2 \tau_f / 4) \quad (C-38)$$

For cohesionless, Φ_{AB} can be given by

$$\Phi_{AB} = \frac{1}{(GJ)_c} \left(TD_s - \frac{\pi}{12} B^2 D_s^3 \rho \right) \quad (C-39)$$

Florida Pier Analysis Program suggested a hyperbolic curve to model the non-linear T- θ behavior (Fig. C-6). The curve is defined as

$$T = \frac{\theta}{a + b\theta} \quad (C-40)$$

where the coefficients a and b are given by

$$\frac{1}{a} = \text{initial slope} = \left(\frac{dT}{d\theta} \right)_i = 4\pi r_0^2 G_i \Delta L$$

$$\frac{1}{b} = T_{ult} = 2\pi r_0^2 \tau_{ult} \Delta L$$

This hyperbolic model does not consider the pile tip stiffness.

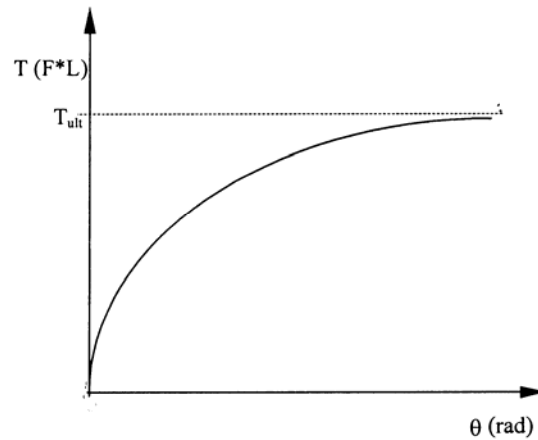


Figure C-6 Hyperbolic representation of T- θ curve

2. Existing methods for ultimate torsional resistance of piles

2.1 Methods For all kind of Soils

FDOT Structural Design Office Method

FDOT Structural Design Office Method only deals with the torsional problem of drilled shaft under simple torsional load, and the method assumes that the soil behaves as a rigid

plastic material, but the soil can be cohesive or cohesionless. By discretizing the drilled shaft, the method can also be applied to stratified soil. For cohesionless soil the method can be applied as follows:

$$T_s = (K_0 \cdot \gamma \cdot 0.5L^2) \cdot \pi \cdot D \cdot \tan \delta \cdot 0.5D \quad (C-41)$$

in which T_s = side torsional resistance, ft-kips,

K_0 = at rest lateral earth pressure coefficient,

γ = effective soil unit weight, lb/ft³,

L = length of drilled shaft foundation, ft,

D = diameter of drilled shaft foundation, ft,

δ = friction angle at the soil-concrete interface, in the case of drilled foundations, it is equal to the internal friction angle of the soil, ϕ of embedded soil.

Additionally, the base torsional resistance can be calculated as:

$$T_b = W \cdot \tan \delta \cdot 0.33D \quad (C-42)$$

in which T_b = base torsional resistance, ft-kips,

W = weight of the drilled shaft foundation, kips,

D = diameter of the drilled shaft foundation,

δ = same definition as above

After determining the side and base frictional resistance, the total torsional capacity of the drilled shaft

$$T_{\text{total}} = T_s + T_b \quad (C-43)$$

Colorado Department of Transportation design methods for torsion.

The torsional design methods for CDOT practice was developed by Richard Osmun. For torsion in cohesive soils, the torsional resistance comes from side resistance and base resistance. The side resistance for the top 1.5D of shaft length is neglected. Then, the total torsional capacity of drilled shaft in clay is given by:

$$T_{\text{clay}} = \pi D(L - 1.5D)c(D/2) + \pi(D^2/4)c(D/3) \quad (C-44)$$

in which, D = shaft diameter, L = the embedment length of drilled shaft, c = cohesion of soil. A 1.25 safety factor for the torsional design of drilled shafts in cohesive soils was used to keep torsion from controlling the shaft depth.

For torsion in cohesionless soils, both the side resistance and base resistance contribute to the total torsional capacity of drilled shaft. For the calculation of the side resistance, the side friction, f , is calculated by

$$f = K\sigma'_v\mu \quad (C-45)$$

in which K = earth pressure coefficient, σ'_v = effective overburden pressure, μ = friction coefficient. For the determination of the value of K , the following procedure is carried out.

The weight of the soil mass in the sliding wedge is larger for a circular configuration than for a planer configuration, therefore, $K = \eta(1-\sin\phi)$ where η = volume of a slice (circular segment) divided by the volume of a wedge (planer segment), and ϕ = friction angle of soil.

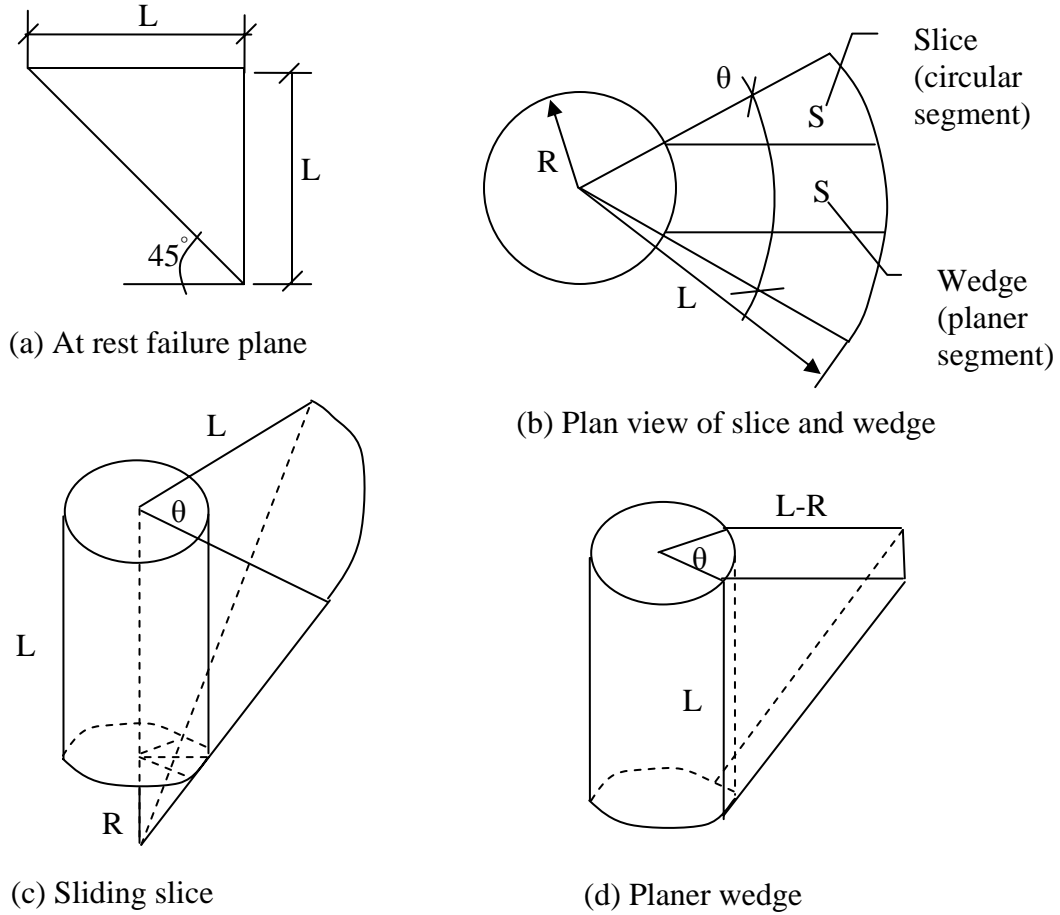


Figure C-7 Sliding Wedge

The volume of slice excluding the shaft volume involved in the slice is:

$$V_L = \frac{1}{3} \pi L^2 (L + R) \frac{\theta}{2\pi} - \frac{\theta}{2\pi} \pi R^2 L - \frac{1}{3} \pi R^2 R \frac{\theta}{2\pi} \approx \frac{1}{6} (L^3 - R^3) \theta - \frac{\theta}{2} R^2 L \approx \frac{1}{6} L^3 \theta \quad (\text{C-46})$$

(If R is small compared to L)

in which L = shaft embedment length, R = the radius of drilled shaft, θ = the slice angle shown in Fig. C-7.

The volume of wedge is:

$$V_R = \frac{R\theta(L - R)L}{2} \approx \frac{R\theta L^2}{2} \quad (\text{If R is small compared to L}) \quad (\text{C-47})$$

Then, the value of η can be calculated as:

$$\eta = \frac{V_L}{V_R} \approx \frac{L}{3R} \quad (C-48)$$

Correspondingly, K can be rewritten as:

$$K = \eta K_0 = \frac{L}{3R} (1 - \sin \phi) \quad (C-49)$$

Therefore, the total torsion capacity of drilled shaft in sand contributed from side resistance and base resistance, can be given by:

$$T_{\text{sand}} = (K\gamma \frac{L}{2})(L)(\pi D)\mu(\frac{D}{2}) + w\mu(\frac{D}{3}) \quad (C-50)$$

in which, $K = \eta(1 - \sin \phi)$, $\eta = 2L/(3D)$ for circular drilled shaft, $\mu = \tan \delta$, $\delta =$ soil friction angle ϕ if the side contact between shaft and soil is very rough, $w =$ the weight of shaft. A 1.25 safety factor for the torsional design of drilled shafts in cohesionless soils was used to keep torsion from controlling the shaft depth.

2.2 Methods For Sands

Florida District 5 Method

Florida District 5 Method uses the ultimate skin friction from the SHAFTUF program to determine the side friction of the drilled shaft. And the side torsional resistance is

$$T_s = Q_s (D/2) \quad (C-51)$$

Also the base torsional resistance is

$$T_b = 0.67 \cdot (W + A_y) \cdot \tan(0.67\phi) \cdot (D/2) \quad (C-52)$$

in which $W =$ the weight of drilled shaft, lbs,

$A_y =$ vertical loading upon the drilled shaft, lbs,

By summing the side and base resistance, the total resistance can be obtained.

Additionally, District 5 proposed to use O'Neill and Hassan approach for shaft subjected to axial loads. And the following equation for cohesionless soil is suggested

$$f_s = \sigma_{vz} \cdot \beta \quad (C-53)$$

in which σ_{vz} = effective vertical stress, β = load transfer ratio and it can be estimated as:

For $N_{spt} < 15$, $\beta = (N/15) \beta_{nominal}$; for $N_{spt} > 15$, $\beta_{nominal} = 1.5 - 0.135 \sqrt{z}$, $1.2 \geq \beta_{nominal} \geq 0.25$, in which z = depth below ground surface, ft.

The total side friction can be described as

$$Q_s = \pi \cdot D \cdot L \cdot f_s \quad (C-54)$$

And the base resistance to torsional loading is

$$Q_b = 0.67 \cdot (W + A_y) \cdot \tan(\delta) \quad (C-55)$$

Thus the total torsional resistance is

$$T = Q_s \cdot (D/2) + Q_b \cdot (D/2). \quad (C-56)$$

Tawfiq (2000) proposed a method for ultimate torsional capacity of drilled shaft in sands under torsional and lateral loading conditions. The method obtains the net lateral soil pressure along the shaft by combining the soil pressure from subgrade reaction method and the threshold lateral pressure from Rankin's theory. Then, the maximum torsional resistance is determined by using limiting shear stress from net lateral soil pressure along the shaft.

Subgrade reaction approach is adopted for determining the lateral soil pressure of drilled shaft under lateral loads. The lateral pressure distribution at each depth was considered as a combination of active pressure and pressure due to the lateral load. The resultant pressure around the shaft perimeter at specified depths was calculated by using Smith's suggestion (Fig. C-8) for the pressure distribution.

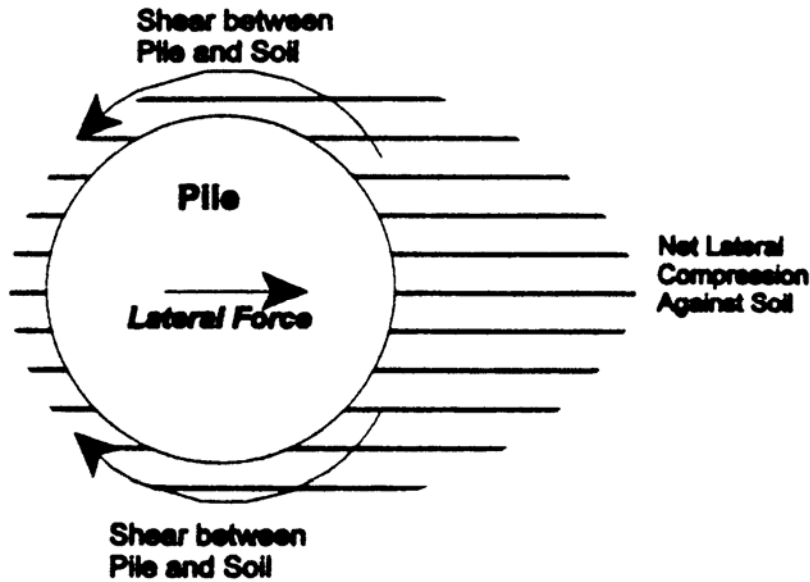


Figure C-8 The soil resistance to lateral pile movement has both compression and shear components. The sum of them is the p in p - y curves (After Smith, 1989)

The Rankin's method is used to set the threshold lateral pressure along the shaft (Fig C-9). Then, the net soil pressure is integrated along the shaft (Fig. C-10).

The limiting side shear stress is determined by

$$\tau = p_h \tan \delta \quad (C-57)$$

in which p_h = integrated net soil pressure along the shaft

δ = soil-shaft angle of friction $\approx \phi$ = soil angle of friction. It is recommended that a factor of 0.5 to 0.6 is used when attapulgate or bentonite slurries are used.

Finally, the ultimate torsional capacity of resistance can be obtained with

$$T = \sum_0^n \sum_0^{\text{rang}} R^2 \frac{2\pi}{\text{rang}} \frac{L}{n} \tan(\delta) \tau \quad (C-58)$$

in which n = segment number of shaft along shaft depth

rang = angle number of shaft section.

MAXIMUM STRESSES ON THE SHAFT

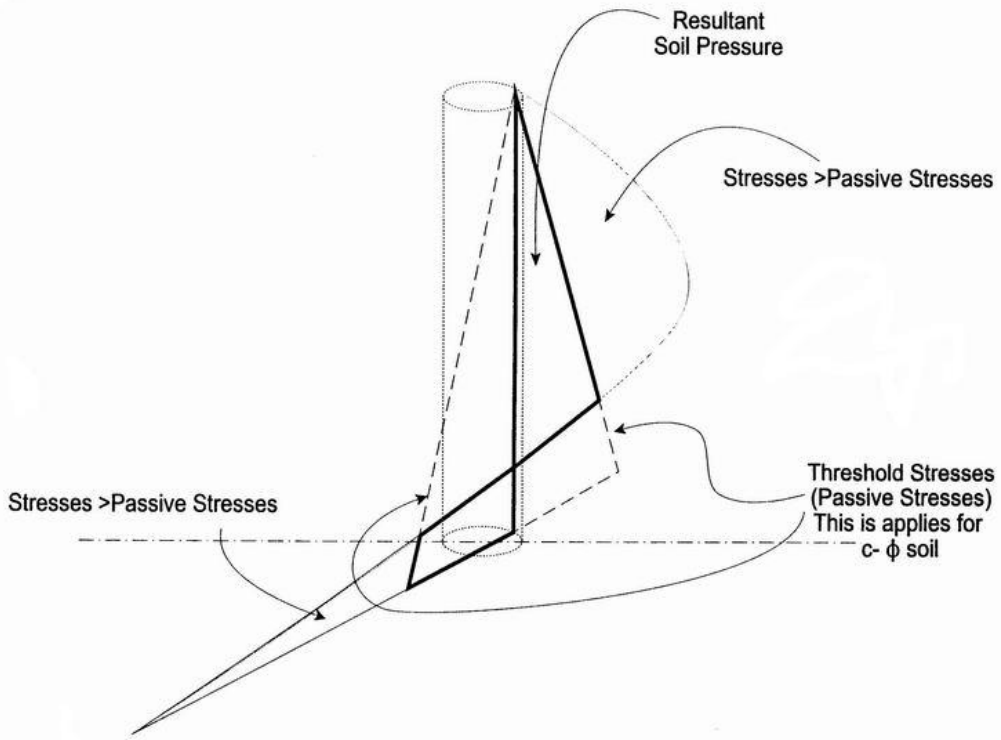


Figure C-9. Setting the threshold pressure (Rankin's Pressure) at each depth along the shaft (after Tawfiq 2000)

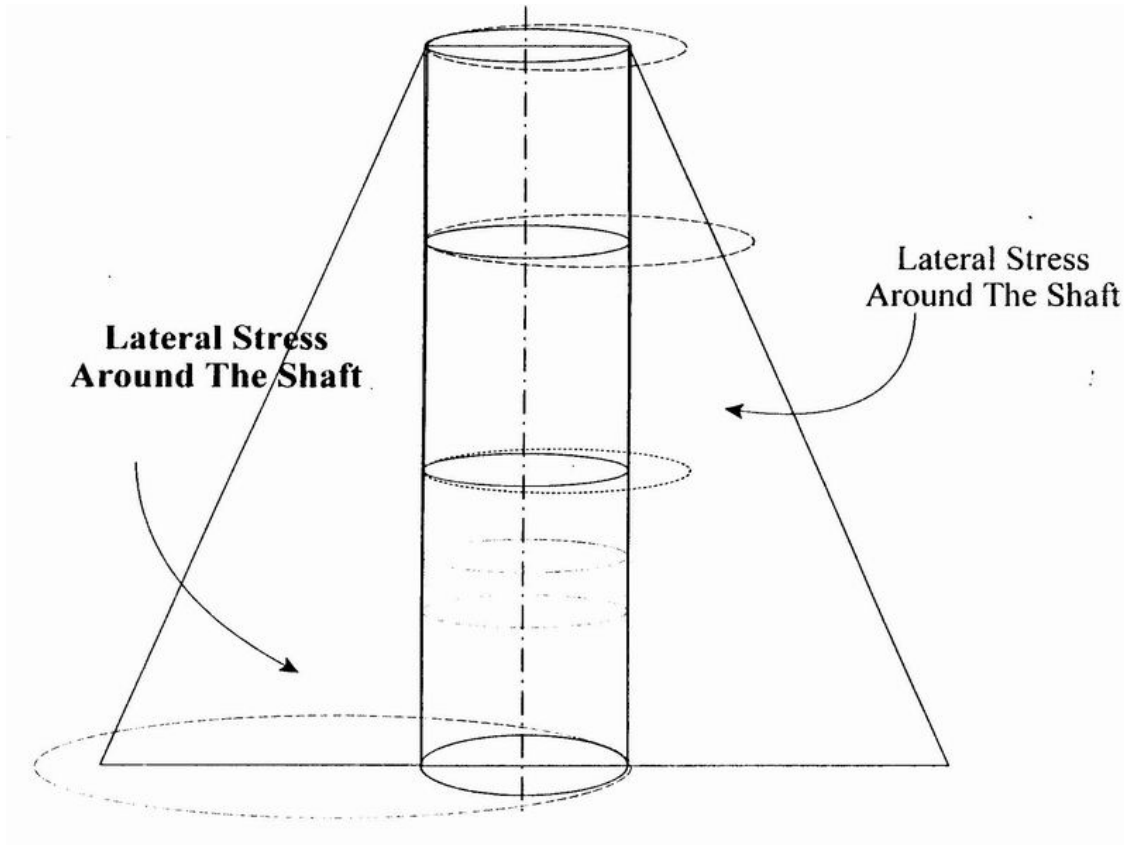


Figure C-10 Final Pressure along the Shaft (After Tawfiq 2000)

2.3 Methods For Clay

Florida District 7 Method

Florida District 7 Method is based on the α method for drilled shaft in clay. According to α method (Tomlinson, 1971), the unit friction is

$$f_s = \alpha \cdot C + \bar{q} \cdot K \cdot \tan \delta \quad (\text{C-59})$$

in which α = the adhesion factor,

C = average cohesion (or S_u) for the soil stratum of interest,

\bar{q} = effective vertical stress on element of the shaft,

δ = effective friction angle between soil and pile material,

K = coefficient of lateral earth pressure ranging from K_0 to about 1.75, values close to K_0 are generally recommended and

$$K_0 = (1 - \sin \phi) \sqrt{\text{OCR}} \quad (\text{C-60})$$

in which OCR = the over consolidation ratio.

The total base resistance is calculated as

$$Q_b = 0.67 \cdot (W + A_y) \cdot \tan(\delta) \quad (C-61)$$

in which W = the weight of the deep drilled shaft, lbs,

A_y = vertical loading upon the drilled shaft, lbs.

Then total base torsion resistance can be calculated as

$$T_b = Q_b (0.67 \cdot D) \quad (C-62)$$

The total torsional side resistance can be obtained by using

$$T_s = p \cdot L \cdot \sum f_s \cdot D / 2 \quad (C-63)$$

in which p = circumferential area of drilled shaft foundation, pD ,

L = length of drilled shaft foundation, ft,

D = diameter of drilled shaft, ft.

Thus, the total torsional resistance is the summation of the side and base torsional resistance.

2.4 Methods For Rocks

N/A

3.The Tests of Pile's Torsional Response

3.1 Torsion Tests --- In Clay

Stoll (1972) devised a field torque shear load test to determine the required penetration depth of friction piles in clay. He conducted two field torsion load tests on steel pipe piles of 0.273m external diameter and 6.3mm wall thickness. Fig.C-11 shows the typical test setup. An early setup includes dial gage and reference beam to measure torque displacement at top of the test pile. Fig.C-12 shows the test results.

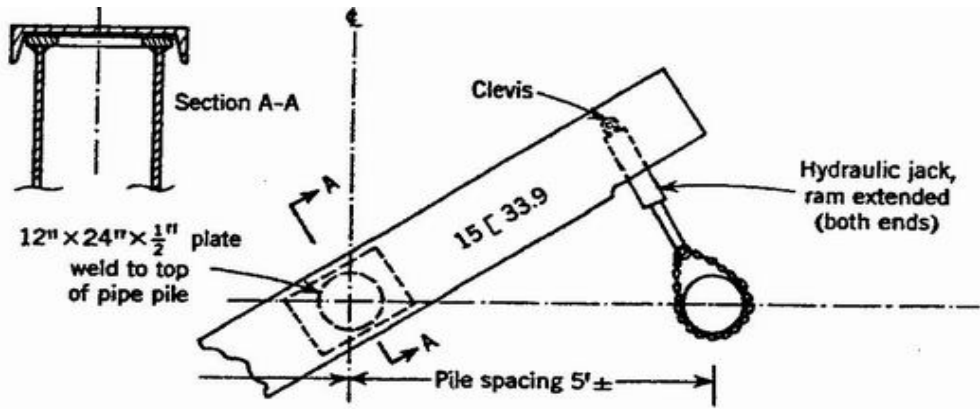
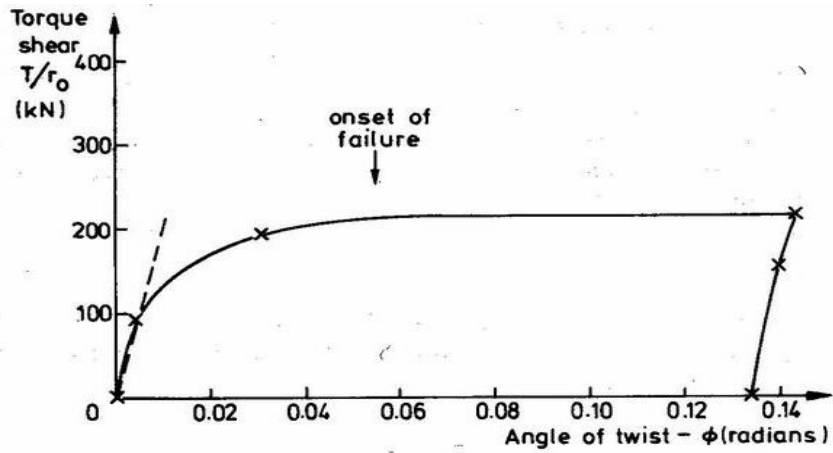
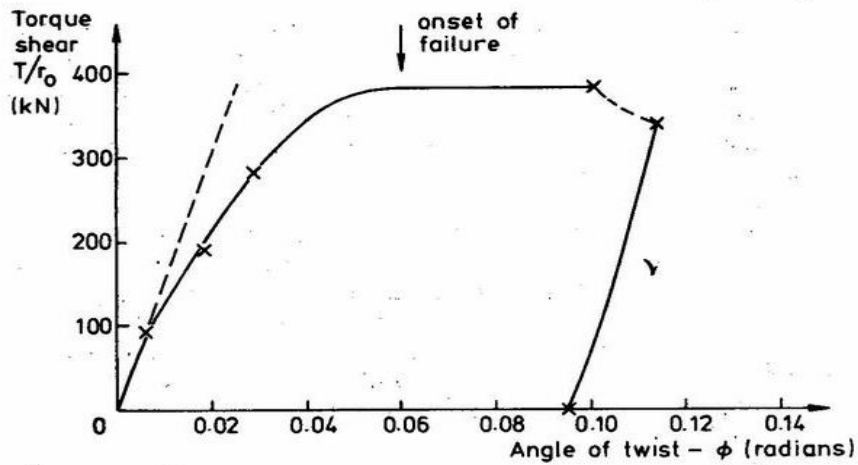


Figure C-11 Pile Torque Shear Test Set Up (After Stoll 1972)



(a) Pile A-3



(b) Pile V-4

Figure C-12 Results from Torsional Load Tests
(After Stoll 1972): (a) Pile A-3 (b) Pile V-4

Poulos (1975) conducted Model Pile Tests. The piles were of solid aluminum, ranging in length from about 6 in. (152mm) to 20 in. (508mm) and in diameter from 0.5 in. (13mm) – 1.5 in. (38mm). The soil used was Kaolin clay. After initial soil consolidation, four piles were installed in each test.

The rotation of the pile was measured by a dial gage mounted on an arm that was bolted to the base of the loading spindle. A pile was considered to have failed after it has rotated through 2 degree. The test results pointed out the possibility of using the shear modulus G from axial load test data to predict both working load and ultimate behavior of piles subjected to torsion. Typical comparisons between calculated and observed torque versus rotation curves to failure are shown in Fig.C-13.

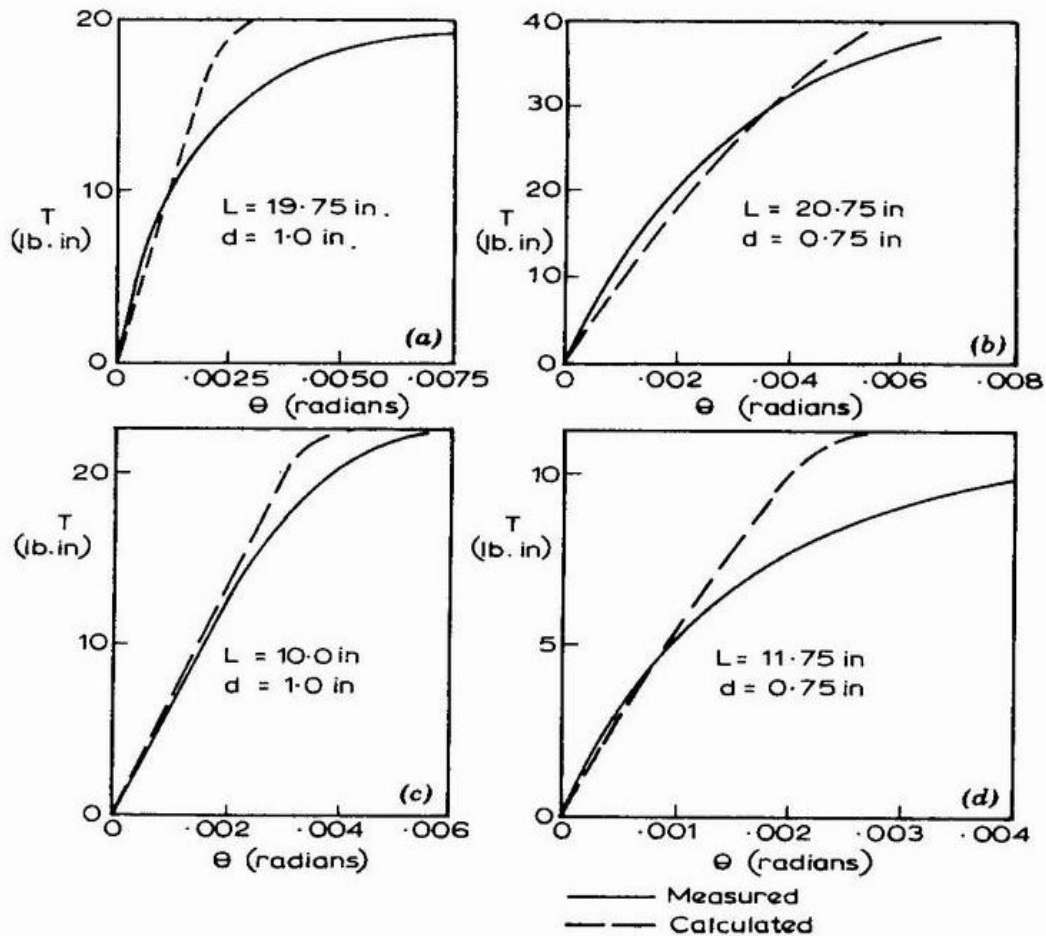


Figure C-13 Typical Comparisons between Measured and Calculated Torque versus Rotational Curves (After Poulos 1975)

3.2 Torsion Tests --- In Sands

Dutt (1976) conducted model tests to investigate the load-deformation characteristics of piles subjected to torsion in relation to the stress-strain behavior of the surrounding soil. And, he tried to establish a method to predict the torque-twist curve by using shear stress-strain behavior of the surrounding soil.

A 1.9 inches (48.3mm) OD circular aluminum pile and a square aluminum pile of 2 inches (50.8mm) outside dimensions were used in this investigation. Strain gages were utilized to measure the distribution of torque along the embedded length of the pile. The twist angle of pile-head was measured through a dial gage. A number of triaxial compression and direct shear tests were performed on samples prepared for torsion tests.

In order to get the torque-twist curves and shear stress-strain curves along the pile length from the measured torque distribution along the length of piles and the pile-head torque-twist curve, Dutt employed a computational procedure depicted in Fig. C-14.

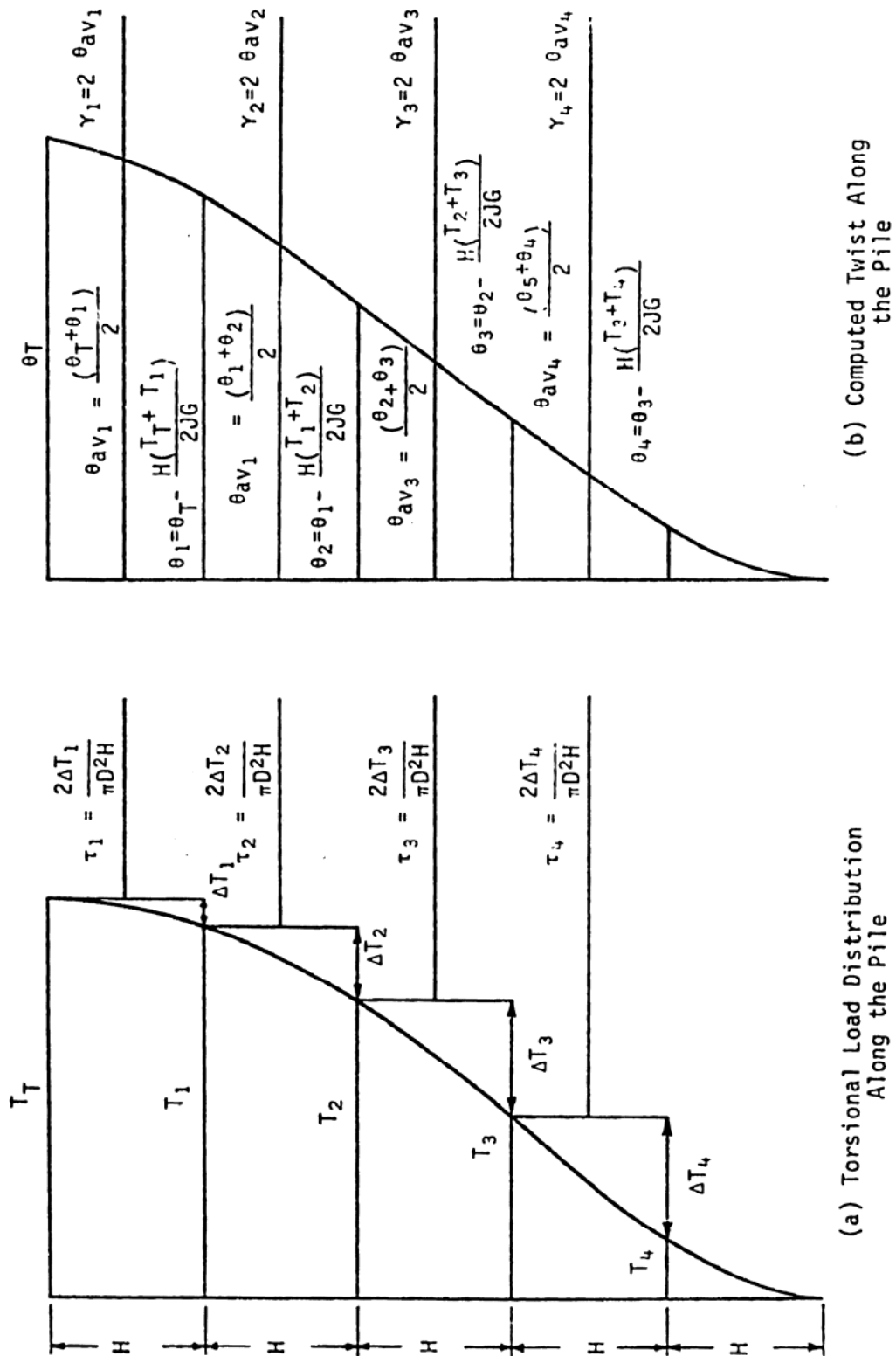


Figure C-14. Example Graphical Illustration for the Development of Mobilized Shear Stress-Strain Curves

In order to establish the correlation between T- ϕ curves with soil properties. Dutt (1976) employed a shear stress-strain relationship suggested by Tucker (1960) to represent soil properties as

$$\gamma = A\tau^n \quad (C-64)$$

where γ is the unit shearing strain due to a unit shearing stress τ . The parameters n and A are properties of the material.

After correlation the measured T- ϕ curves with τ - γ curves, Dutt gives out some suggestions on the determination of A and n . Then, with suggested n and A , the τ - γ curves can be determined to predict T- ϕ curves. The following Equations are employed to compute T- ϕ curves. Here the notation ϕ is the same with θ .

$$T = \frac{\pi D^2 H \tau}{2} \quad (C-65)$$

$$\theta = \frac{\gamma}{2} \quad (C-66)$$

Tawfiq (2000) carried out some scaled model shaft tests for torsional response of drilled shaft in sands. The shaft used for tests is 20 inches long and 4 inches in diameter. The testing setup consisted of a 4' diameter and 5' depth steel chamber where a strain controlled loading system was installed (Fig. C-15). Two 20 gallon buckets were used to apply the constant rate of loading. The torsional displacement was recorded with a dial indicator and a scale.

The model test results show that the rotation resistance dropped by about 65 to 50 percent for the bentonite and attapulgate slurries compared with the dry soil condition. In order to determine the residual frictional resistance, the shaft was rotated back to its original position and another torsional load was applied again in dry soil. The test results show that the frictional capacity was reduced by 70 to 77%.

Additional test was conducted to determine the base resistance by eliminating the side friction. And the test results show that the base resistance has a very small contribution to the total torsional resistance.

Under combined loading conditions, the torsional resistance will increase. Test results show that the torsional capacity increased two folds after adding 20 lb lateral load on the shaft.

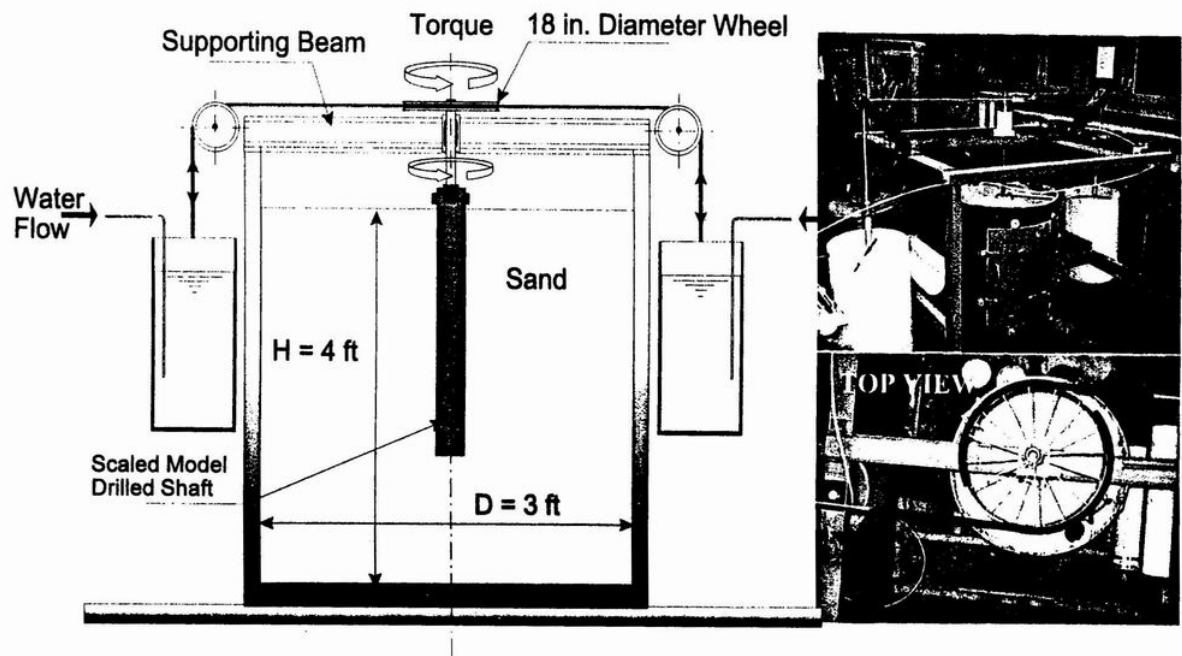


Figure C-15 Scaled Model Torsional Testing Apparatus

Tawfiq (2000) conducted 3 full-scale torsion tests of drilled shafts under combined lateral, overturning and torsional loads in sands. Four drilled shaft with 4' diameter and 20' long were installed, three of them for testing and the other one for supporting. The tested drilled shafts were constructed with polymer slurry, bentonite slurry and dry hole method, respectively. A loading arm consisted of 12" by 12" section and 5/8" thick was constructed to apply lateral loads (Fig. C-16). In order to record the rotation angle, four laser devices were mounted on the shaft and four foam boards were located at 20' from testing setup.

Full-scale field tests show the dry shaft demonstrated the largest capacity, and the shaft was gradually loaded up to structure failure at 490,000 ft-lb torsional loads. The rotation of the shaft was very small.

However for the shaft constructed using bentonite slurry, the rotational displacement was very noticeable at 180,000 ft-lb torsional loads. The load application was stopped at 280,000 ft-lb when no more increase in the loading could be recorded.

For the shaft constructed with polymer slurry, the shaft has similar performance as the dry hole shaft. The maximum load reached to 420,000 ft-lb, and structure failure was occurred.

These tests indicated that the construction method did make the difference in the torsional capacity.

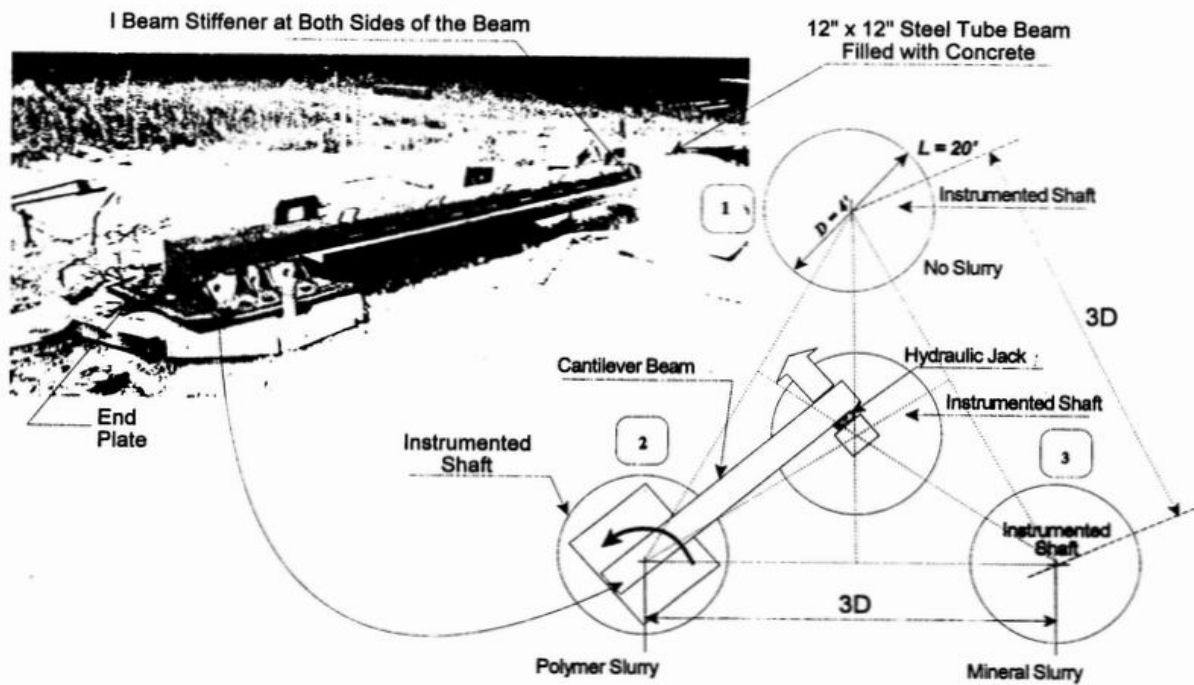
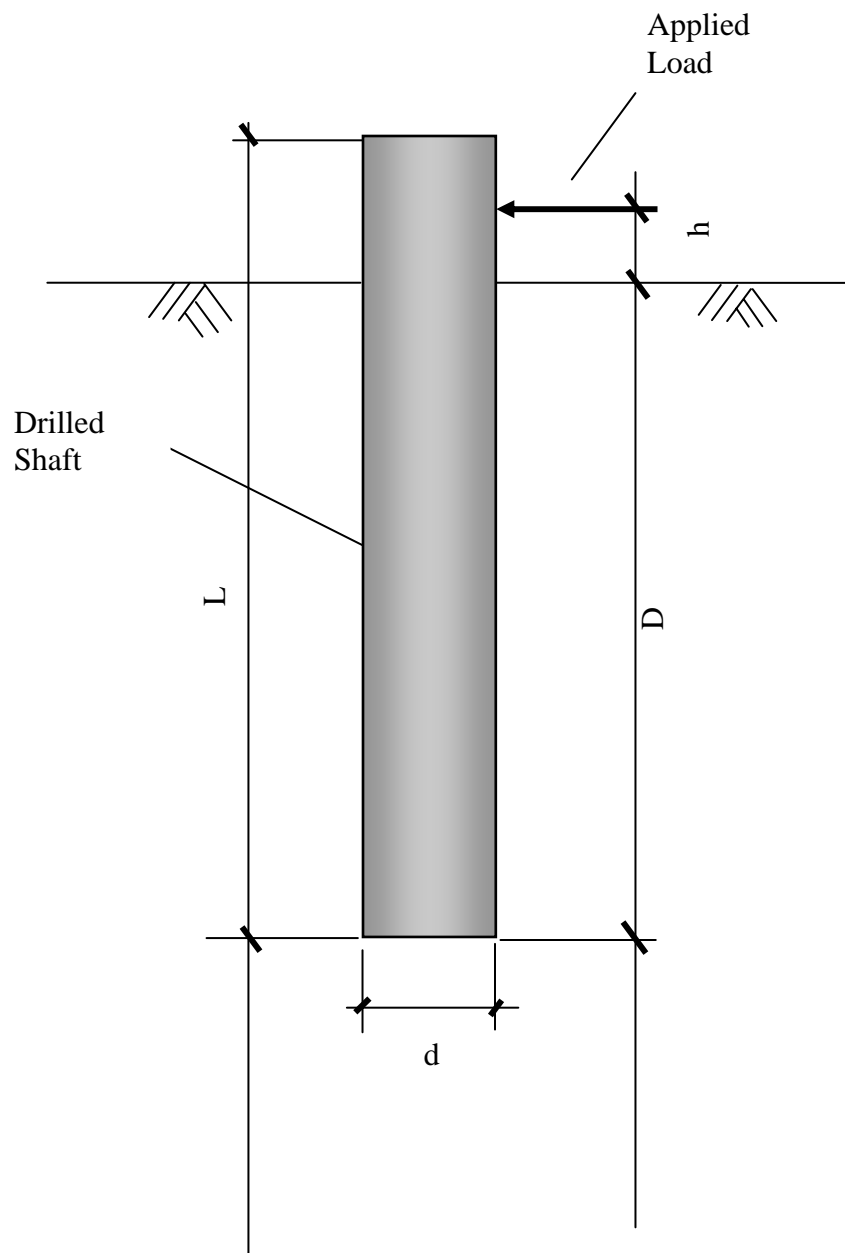


Figure C-16 Field Test Arrangement

Appendix D

The Lateral Load Test Database

Note: Only the drilled shafts embedded in clay are selected and all the tests are conducted in OHIO



The Notations Definition for Lateral Load Test Database

Project Name: I-70 (Columbus, Ohio), Shaft 1 and Shaft 2, Columbus (L=9.5', D=9.5', h=0', d=30")

Depth (ft)	Description	SPT-N/12" Average	COM624P Soil classification	C _u (psi)	φ (deg)	Ks (pci)	ε ₅₀	γ (pci)
0 to 1	Fill Material	22	3	21		1000	0.005	0.078
1 to 4	Stiff Clay	18	3	16		1000	0.005	0.075
4 to 18	Stiff Clay	34	3	27 to 35		1000	0.005	0.075

Project Name: I-90 Sound Barriers Projects, Cuyahoga County, OH, 12ft, Shaft 2, (L=25', D=12', h=10', d=30')

Depth (ft)	Description	SPT-N/12" Average	COM624P Soil classification	C _u (psi)	φ (deg)	K _s (pci)	ε ₅₀	γ (pci)
0 to 3	Brown sand with brick concrete scat fill, MOIST	22	3	19.0		1000	0.005	0.078
3 to 5	Brown very fine sand with some silt, WET	20	3	17.4		1000	0.005	0.077
5 to 7	Brown fine sandy SILT with a trace of CLAY, some possible thin CLAY seams, MOIST	35	3	30.0		2000	0.004	0.078
7 to 9	Brown fine sandy SILT with a trace of CLAY, some possible thin CLAY seams, MOIST	28	3	24.3		1000	0.005	0.082
9 to 12	Brown changing to gray SILTY CLAY with some small ROCK fragment, MOIST	27	3	23.4		1000	0.005	0.081

Project Name: I-90 Sound Barriers Projects, Cuyahoga County, OH, 8ft Shaft 1, (L=21'-8", D=8'-8", h=10', d=30")

Depth (ft)	Description	SPT-N/12" Average	COM624P Soil classification	C _u (psi)	φ (deg)	K _s (pci)	ε ₅₀	γ (pci)
0 to 3	Brown sand with brick concrete scat fill, MOIST	22	3	19.0		1000	0.005	0.078
3 to 5	Brown very fine sand with some silt, WET	20	3	17.4		1000	0.005	0.077
5 to 7	Brown fine sandy SILT with a trace of CLAY, some possible thin CLAY seams, MOIST	35	3	30.0		2000	0.004	0.078
7 to 9	Brown fine sandy SILT with a trace of CLAY, some possible thin CLAY seams, MOIST	28	3	24.3		1000	0.005	0.082
9 to 12	Brown changing to gray SILTY CLAY with some small ROCK fragment, MOIST	27	3	23.4		1000	0.005	0.081

Project Name: I-90 Sound Barriers Projects, Cuyahoga County, OH, 8ft Shaft 2 (L=21'-8", D=8'-5", h=10'-3", d=30")

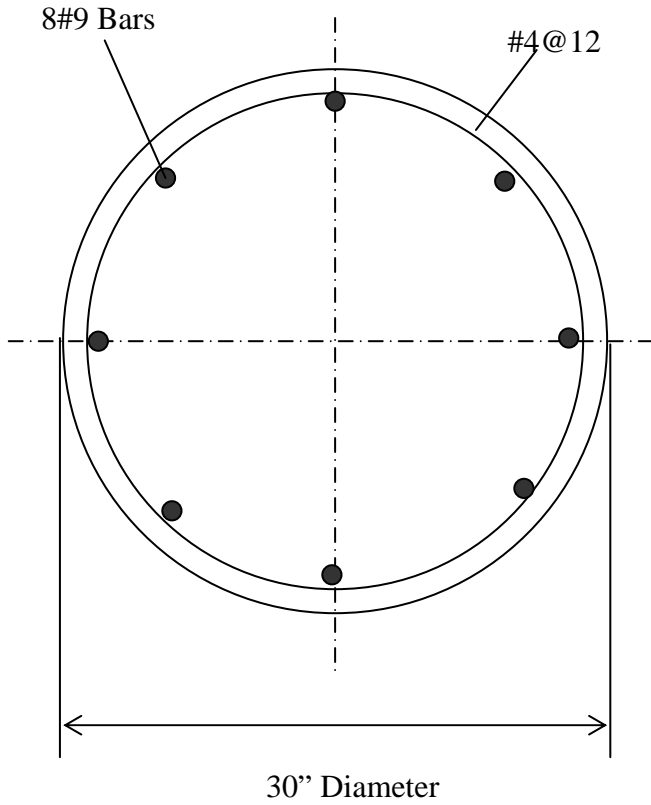
Depth (ft)	Description	SPT-N/12" Average	COM624P Soil classification	C _u (psi)	φ (deg)	K _s (pci)	ε ₅₀	γ (pci)
0 to 3	Brown sand with brick concrete scat fill, MOIST	22	3	19.0		1000	0.005	0.078
3 to 5	Brown very fine sand with some silt, WET	20	3	17.4		1000	0.005	0.077
5 to 7	Brown fine sandy SILT with a trace of CLAY, some possible thin CLAY seams, MOIST	35	3	30.0		2000	0.004	0.078
7 to 9	Brown fine sandy SILT with a trace of CLAY, some possible thin CLAY seams, MOIST	28	3	24.3		1000	0.005	0.082
9 to 12	Brown changing to gray SILTY CLAY with some small ROCK fragment, MOIST	27	3	23.4		1000	0.005	0.081

I-90 Noise Wall Project, OH, Shaft 1 (P 101) and Shaft 2 (P 100) (L=12'/10', D=12'/10', h=0', dim=30"/36")

Depth (ft)	Description	SPT-N/12" Average	COM624P Soil classification	C _u (psi)	φ (deg)	K _s (pci)	ε ₅₀	γ (pci)
0 to 2	Very stiff, gray CLAY (A-7-6), trace sand, trace to no asphalt and wood fragment, moist	24	3	22		1000	0.005	0.08
2 to 8.6	Stiff, gray CLAY (A-7-6), trace sand, trace to no asphalt and wood fragment, moist	11	3	11		500	0.007	0.075
8.6 to 10	Very soft to medium hard, decomposed to weathered, gray SILT SHALE Encountered spoon refusal at 11.3 feet, augered to 11.5 feet and began coring bedrock.	50/0.4	3	50		150	0.004	0.084
10 to 13	Soft, highly weathered to weathered, gray SILT SHALE with nearly horizontal laminar bedding (fissile), good quality as RQD. U. C. Strength at 12.8 feet = 442 psi	50/0.3 RDQ=80 %	3	55		2000	0.003	0.084
	TERMINATION DEPTH = 13.0 FEET							

Shaft Cross Section and Measured Load-Deflection Data for Lateral Load Test Database

I-70 Sound Barriers, Columbus, Shaft 1



$$I = 39760 \text{ in}^4$$

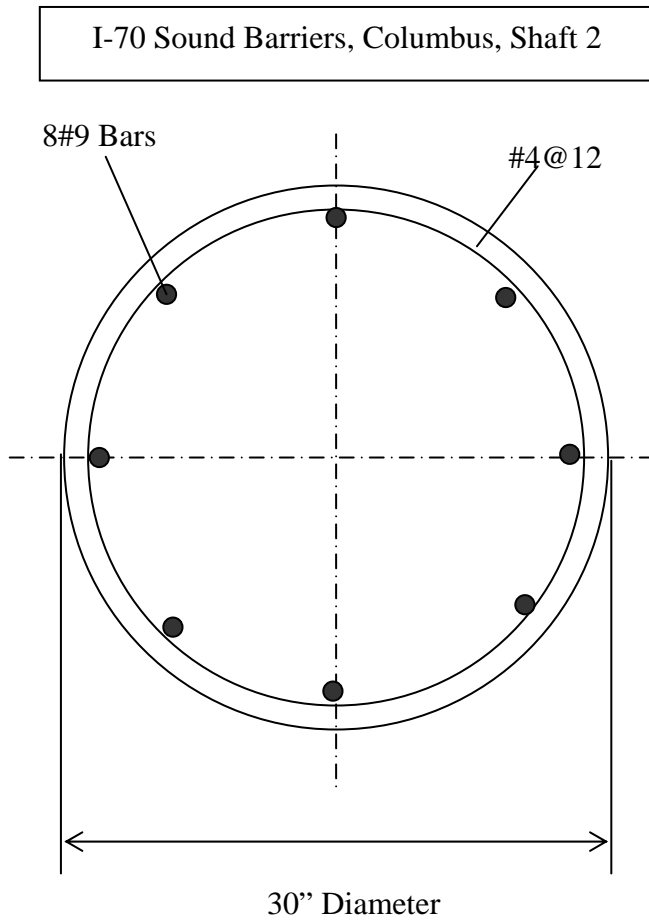
$$A = 707 \text{ in}^2$$

$$E_{\text{concrete}} = 4415201 \text{ lb/in}^2$$

Load (kips)	Deflection (in.)	
	Dial Gage	Inclinometer
0.00	0.000	0.000
2.50	0.012	0.005
3.75	0.015	0.002
5.00	0.021	0.001
7.50	0.031	0.005
10.00	0.036	0.007
15.00	0.061	0.008
17.50	0.076	0.022
22.50	0.094	0.044
27.50	0.116	0.062
30.00	0.135	0.092
32.50	0.154	0.118
37.50	0.213	0.201
40.00	0.239	0.229

Shaft Cross Section and Measured Load-Deflection Data for Lateral Load Test Database

Con.



$$I = 39760 \text{ in}^4$$

$$A = 707 \text{ in}^2$$

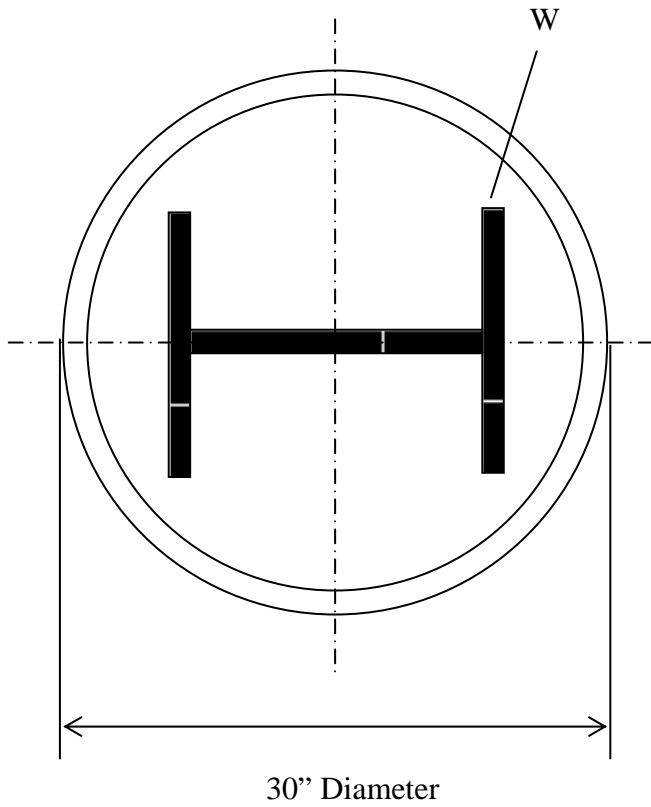
$$E_{\text{avg}} = 4415201 \text{ lb/in}^2$$

Load (kips)	Deflection (in.)	
	Dial Gage	Inclinometer
0.00	0.0000	0.0000
2.50	0.0018	0.0033
3.75	0.0031	0.0075
5.00	0.0066	0.0075
7.50	0.0123	0.0090
10.00	0.0180	0.0084
15.00	0.0237	0.0102
17.50	0.0325	0.0162
22.50	0.0412	0.0267
27.50	0.0553	0.0390
30.00	0.0702	0.0426
32.50	0.0938	0.0627
37.50	0.1149	0.0849
40.00	0.1333	0.1155

Shaft Cross Section and Measured Load-Deflection Data for Lateral Load Test Database

Con.

I-90 Sound Barriers, 12 ft Depth, Shaft 2



$$I = 69471/51471 \text{ in}^4$$

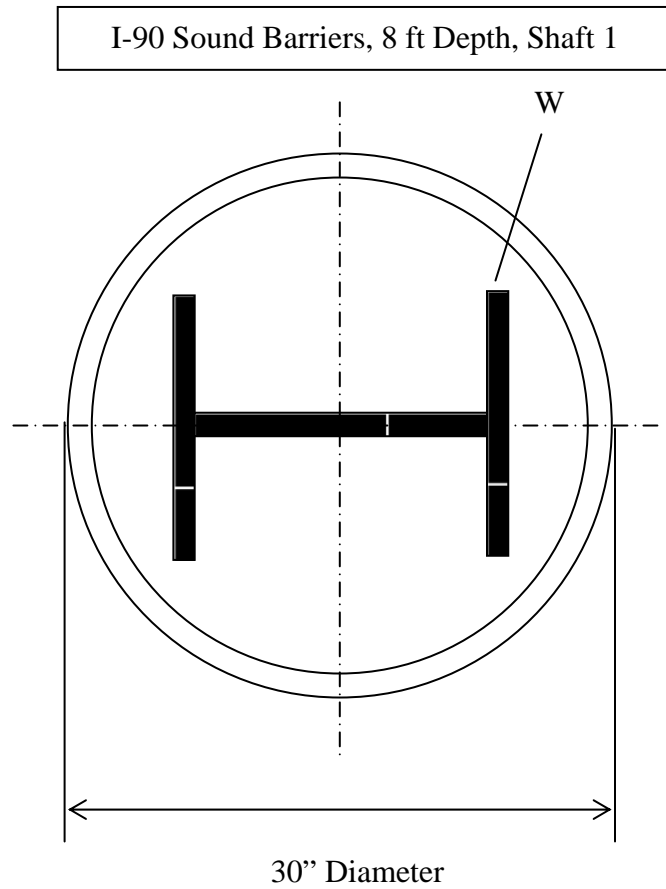
$$A = 804 \text{ in}^2$$

$$E_{\text{avg}} = 6472076 \text{ lb/in}^2$$

Load (kips)	Deflection (in.)	
	Dial Gage	Inclinometer
0.000		0.0000
13.250		-0.0084
26.500		0.1122
53.000		0.5220
79.500		1.0870
37.750		1.0350
0.000		0.4902
39.750		0.8730
84.800		1.1388
53.000		1.1328
0.000		0.7140
106.000		1.6506

Shaft Cross Section and Measured Load-Deflection Data for Lateral Load Test Database

Con.



$$I = 69471/51471 \text{ in}^4$$

$$A = 804 \text{ in}^2$$

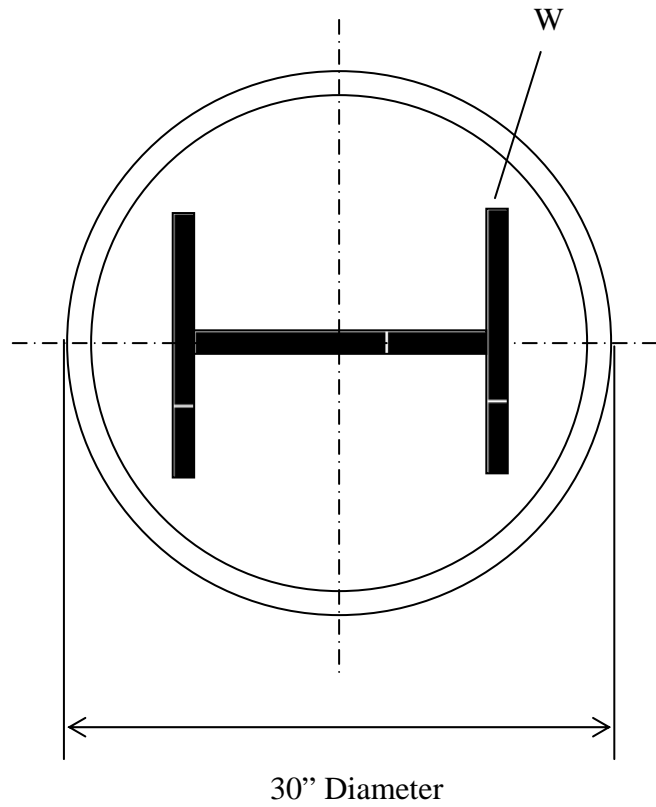
$$E_{\text{avg}} = 6472076 \text{ lb/in}^2$$

Load (kips)	Deflection (in.)	
	Dial Gage	Inclinometer
0.000		0.0000
10.60		0.1080
15.90		0.1869
20.00		0.2760
31.80		0.4773
42.40		1.0089
47.70		1.2375
31.80		1.2309
15.90		1.1697
0.00		0.6891
15.90		0.9270
31.80		1.1307
47.70		1.6116
53.00		1.9047

Shaft Cross Section and Measured Load-Deflection Data for Lateral Load Test Database

Con.

I-90 Sound Barriers, 8 ft Depth, Shaft 2



$$I = 69471/51471 \text{ in}^4$$

$$A = 804 \text{ in}^2$$

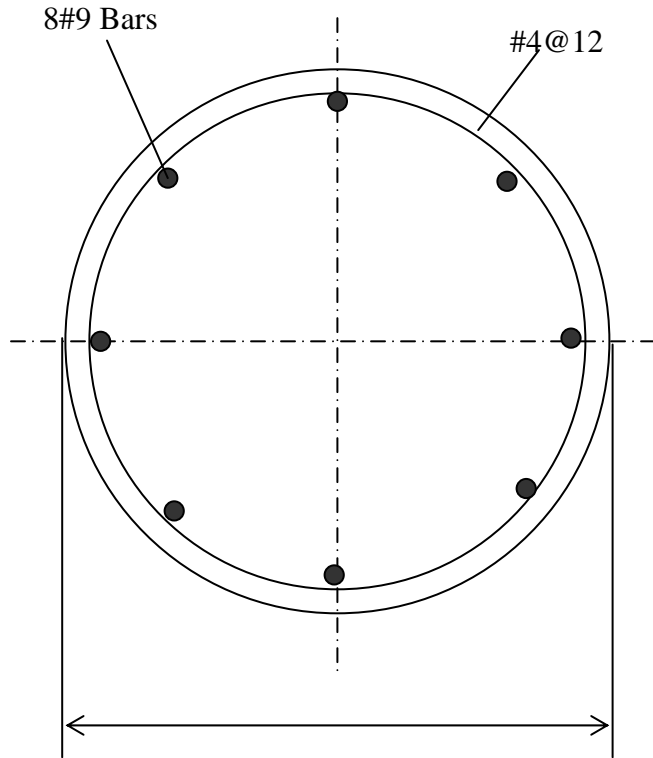
$$E_{\text{avg}} = 6472076 \text{ lb/in}^2$$

Load (kips)	Deflection (in.)	
	Dial Gage	Inclinometer
0.000		0.0000
10.60		0.1254
15.90		0.2106
20.00		0.3162
31.80		0.5475
42.40		1.1775
47.70		1.4427
31.80		1.4379
15.90		1.3752
0.00		0.8544
15.90		1.1358
31.80		1.3446
47.70		1.8894
53.00		2.2335

Shaft Cross Section and Measured Load-Deflection Data for Lateral Load Test Database

Con.

I-90 Sound Barriers, Shaft 100



36" Diameter

$$I = 82448 \text{ in}^4$$

$$A = 1018 \text{ in}^2$$

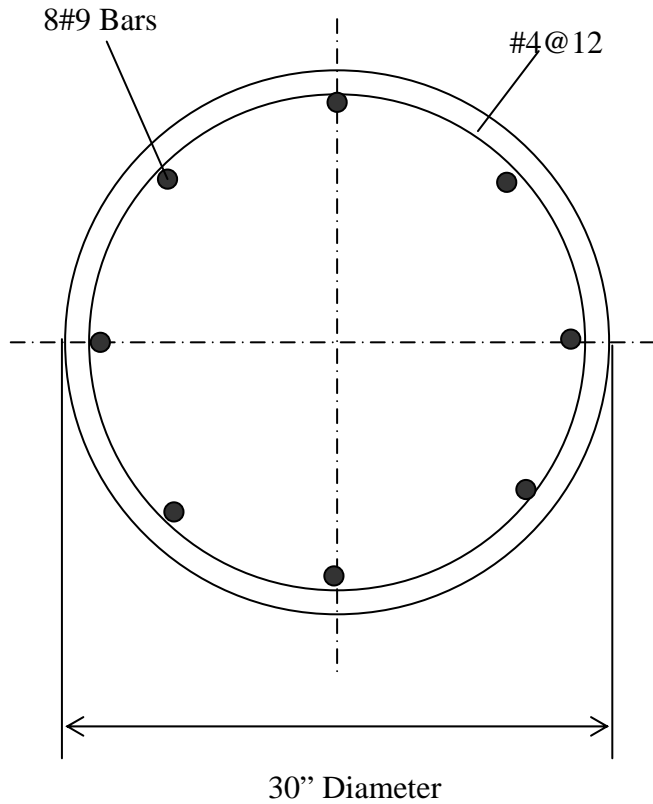
$$E_{\text{avg}} = 4415201 \text{ lb/in}^2$$

Load (kips)	Deflection (in.)	
	Dial Gage	Inclinometer
0.00	0.0000	0.0000
6.25	0.0120	0.0054
12.25	0.0285	0.0270
18.75	0.0550	0.0510
25.00	0.0915	0.0744
31.25	0.1460	0.1218
37.25	0.2200	0.1968
42.50	0.3030	0.2670
45.00	0.3330	0.3108
47.50	0.3945	0.3660
52.50	0.4755	0.4506
58.75	0.5990	0.5382
65.00	0.8200	0.7896
50.00	0.8020	0.7746
37.50	0.8020	0.7668
25.00	0.7750	0.7338
12.50	0.7095	0.6666
0.00	0.4075	0.3720

Shaft Cross Section and Measured Load-Deflection Data for Lateral Load Test Database

Con.

I-90 Sound Barriers, Shaft 101



$$I = 39760 \text{ in}^4$$

$$A = 707 \text{ in}^2$$

$$E_{\text{avg}} = 4415201 \text{ lb/in}^2$$

Load (kips)	Deflection (in.)	
	Dial Gage	Inclinometer
0.00	0.0000	0.0000
6.25	0.0140	0.0180
12.25	0.0355	0.0504
18.75	0.0730	0.0570
25.00	0.1195	0.1110
31.25	0.1870	0.1794
37.25	0.2665	0.2754
42.50	0.3600	0.3390
45.00	0.3910	0.3624
47.50	0.4575	0.4596
52.50	0.5325	0.5250
58.75	0.6530	0.6612
65.00	0.8500	0.8712
50.00	0.8270	0.8610
37.50	0.8255	0.8484
25.00	0.7940	0.8340
12.50	0.7220	0.7650
0.00	0.3755	0.3798

Appendix E

Design Spreadsheet for Lateral Loaded Drilled Shafts Supporting Sound Walls

Design Spreadsheet for Lateral Loaded Drilled Shafts Supporting Sound Walls, - Clay

The numbers with red color or Italic are values of input parameters.

Broms' method, using Unsaturated soil parameters from lab test

1. Parameters

Soil weighted average cohesion $C_u = 14.3$ psi
Embedded length $L = 12$ ft, = 144 in.
Drilled shaft height above ground, $e = 9$ ft, = 108 in.
Drilled shaft diameter $D = 30$ in., = 2.5 ft.

2. Calculate the ultimate capacity P_{ult}

$a = 9C_u D = 3861$
 $b = L - 1.5D = 99$
 $c = e + (L + 1.5D)/2 = 202.5$
 $P_{ult} = (\sqrt{c^2 + b^2/4} - c) * 2a = 46$ kips

3. Check maximum moment in the shaft

$f = P_{ult}/(9C_u D) = 11.9$ in., = 0.994 ft.
 $M_{max} = P_{ult} * (e + 1.5D + 0.5f) = 609.9$ kips-ft < M_y 777 kips-ft
So, the ultimate capacity estimated by Broms' method is 46 kips.
Note: the yielding moment of drilled shaft M_y can be obtained from COM624P analysis

4. Design load

The Factor Safety of 2 is adopted.
Calculated Design Load = 23 kips > required design load = 17.3 kips

Design Spreadsheet for Lateral Loaded Drilled Shafts Supporting Sound Walls - Sand

Suggested New Design for CDOT sound barrier wall's drilled shafts in sand

Broms' method, using soil parameters correlated from SPT N values by using Liang (2002)'s correlation.

1. Parameters

Soil average cohesion $C_u = 0$ psi
Shaft length $L = 12$ ft, = 144 in.
Shaft height above ground, $e = 9$ ft, = 108 in.
Shaft diameter $D = 30$ in., = 2.5 ft.
Friction angle = 33
Unit weight = 0.069 lb/in³ 0.119 kip/ft³

2. Calculate the ultimate capacity P_{ult} :

$K_p = (1 + \sin\Phi) / (1 - \sin\Phi) = 3.4$
 $P_{ult} = 0.5\gamma_d L^3 K_p / (e + L) = 42$ kips

3. Check maximum moment in the shaft.

At $f = 0.82 * (P_{ult} / D * K_p * r)^{0.5} = 5.26$ ft
 $M_{max} = P_{ult} * (e + 0.67f) = 520.6$ kips-ft < $M_y = 555$ kips-ft

$P_{ult} = 42$ kips

Note: the yielding moment of drilled shaft M_y can be obtained from COM624P analysis.

4. Design load

The Factor Safety of 2 is adopted.
Calculated Design Load = 21 kips > required design load = 17.3 kips

Appendix F

Selected Bibliography

References Related to Lateral Response of Drilled Shaft:

O'Neill, Michael W., and Reese, Lymon C. (1999) "Drilled shaft: Construction procedure and design methods" *Publication No. FHWA-IF-99-025*, Vol-I, 1-21

Zhang, L. (1999) " *Analysis and design of drilled shafts in rock.*" PhD thesis, Massachusetts Institute of Technology, Cambridge, Mass.

Broms, B.B.(1964a) "Lateral resistance of piles in cohesive soils" *Journal of the Soil Mechanics and Foundation Division*, Vol. 90, No. SM2, pp27-63.

Broms, B.B.(1964b) "Lateral resistance of piles in cohesionless soils" *Journal of the Soil Mechanics and Foundation Division*, Vol. 90, No. SM3, pp 123-157.

Poulos, H.G., and Davis, E.H. (1980). *Pile foundation analysis and design*. John Wiley & Sons, NY.

Indiana department of Transportation (1996) "General Instructions for Bridge Structure Investigation", *Geotechnical section and division of materials and tests* Indiana department of Transportation.

Mokwa, R.L.(1999) "*Investigation of the resistance of pile caps to lateral loading*", PhD thesis, Virginia Tech, VA.

Sun, K. (1994). "Laterally loaded piles in elastic media," *J. Geotech Engrg., ASCE*, 120(8), 1324-1344

Ashour, M. Member, ASCE, Norris, G. Member, ASCE, and Pilling, P., (1998) “Lateral loading of a pile in layered soil using the strain wedge model” *Journal of geotechnical and geoenvironmental engineering*, pp:303-315.

AASHTO *LRFD BRIDGE DESIGN SPECIFICATIONS*, “Section-10: Drilled Shafts”, Published by the American Association of State Highway and Transportation Officials (AASHTO), First Edition, 1994.

AASHTO, (1989) “*Guide Specifications for Structural Design of Sound Barriers*”, Washington, D.C.

Davidson, J.L., Hays, C.O., Jr., and Hagan, E.M., Jr., (1976) “Design of drilled shafts supporting highway signs”, *Transportation Research Record*, issue 616, pp 62-66.

Hough, B.K., (1969) “*Basic Soils Engineering*”, Publication: John Wiley and Sons.

Liang, R.Y. (1997) “Pressuremeter to Predict Lateral Load Capacity of Drilled Shafts on Slope,” Final Report, FHWA/OH-97/005, ODOT.

Liang, R.Y., (2002) “Drilled Shaft Foundations for Noise Barrier Walls and Slope Stabilization,” Final Report, FHWA/OH-2002/038, ODOT.

ABAQUS Standard User's Manual, Version 5.8, Hibbitt, Karlsson & Sorensen, Inc. 1998.

AASHTO (2001), “*Standard Specifications for Structural Supports for Highway Signs, Luminaries and Traffic Signals*,” 4th Edition.

NAVFAC DM-7 (1971), Department of the Navy, Naval Facilities Engineering Command, “Design Manual – Soil Mechanics, Foundations and Earth Structures” .

Prakash, Shamsheer, and Sharma, Hari (1990) "Pile Foundations In Engineering Practice" pp:322-342, Publication: John Willey & Sons.

AASHTO LRFD Bridge Design Specifications, First Edition, 1994.

Kulhawy, F.H., and Chen. Y.-J., (1995) "A Thirty Year Perspective of Broms' Lateral Loading Models, as Applied to Drilled Shafts," *Bengt B. Broms Symposium on Geotechnical Engineering*, Singapore, pp. 225-240.

Wang, Shih-Tower, and Reese, L.C., (1993) "COM624P-Laterally Loaded Pile Analysis Program for the Microcomputer, Version 2.0," Final Report, Report No. FHWA-SA-91-048.

Bhushan, K., Lee, L.J., and Grime, D.B. (1981) "Lateral Load Tests on Drilled Piers in Sand." *Drilled Piers and Caissons: Proceedings of a Session at the ASCE National Convention*, St Louis, MO, USA. Conference Code: 00225. P. 114-131.

Bhushan, K., and Askari, S. (1984) "Lateral-Load Tests on Drilled Pier Foundations for Solar Plant Heliostats." *Laterally Loaded Deep Foundations: Analysis and Performance*, ASTM STP 835, J.A. Langer, E.T. Mosley, and C. D. Thompson, Eds., ASTM, pp. 140-156.

References Related to Torsional Response of Drilled Shaft:

Carter, J.P., and Kulhawy, F.H., (1988) "Analysis and Design of Drilled Shaft Foundations Socketed into Rock," Cornell University, Ithaca, New York.

Chow, Y. K., (1985) "Torsional Response of Piles in Non-Homogeneous Soil," *Journal of Geotechnical Engineering*, ASCE, Vol. 111, pp. 942-947.

Dutt, R. N., (1976) "Torsional response of piles in sand," Ph.D. thesis, Univ. of Houston, Texas.

Guo, W.D., and Randolph, M.F., (1996) "Torsional Piles in Non-Homogeneous Media," *Computers and Geotechnics*, No. 19, pp. 265-287.

Hache, R.A.G., and Valsangker, A. J., (1988) "Torsional Resistance of Single Pile in Layered Soil," *Journal of Geotechnical Engineering*, ASCE, V. 114, pp. 216-220.

Lin, S.S., and AlKhaleefi, A.L. (1996) "Torsional Behavior of Cracked Reinforced Concrete Piles in Sand," *Journal of The Chinese Institute of Engineers*, Vol.19: (6), pp. 689-696.

O'Neill, Michael Wayne, (1964) "Determination of the Pile-Head, Torque-Twist Relationship for a Circular Pile Embedded in a Clay Soil," Master Thesis, The University of Texas at Austin.

O'Neill, M.W., and Dutt, R.N., (1976) discussion of "Torsional Response of Piles," by Harry G. Poulos, *Journal of Geotechnical Engineering Division*, ASCE, Vol. 102, No. GT6, Proc. Paper 12163, pp. 658-660.

Poulos, Harry G. (1975) "Torsional Response of Piles," *Journal of the Geotechnical Engineering Division*, V. 101, GT10, pp. 1019-1035.

Randolph, M. F. (1981) "Piles Subjected to Torsion," *Journal of the Geotechnical Engineering Division*, American Society of Civil Engineers, Vol.107, issue 8, pp. 1095-1111.

Stoll, U. W. (1972) "Torque Shear Test of Cylindrical Friction Piles," *Civil Engineering*, ASCE, Vol. 42, pp.63-65.

Tawfiq, K. (2000) “ Drilled shaft under torsional loading conditions”, *Final report Federal Highway Administration*, Florida Department of Transportation.

References Related to Strain Rate Effect:

Abrantes, Antonio E., and Yamamuro, Jerry A. (2002) “Experimental and data analysis techniques used for high strain rate tests on cohesionless soil”, *Geotechnical Testing Journal*. v. 25 issue 2, p. 128-141.

Shibuya, Satoru, et al. (1996) “Strain rate effects on stress-strain behaviour of clay as observed in monotonic and cyclic triaxial tests”, *Geotechnical Special Publication*, issue 61, p. 214-227.

Shibuya, Saturo, et al., (1995) “Strain rate effects on shear modulus and damping of normally consolidated clay”, *Geotechnical Testing Journal*, v. 18 issue 3, p. 365-375.

Wedage, A. M.P., et al. (1998) “Strain rate dependent constitutive model for clays at residual strength”, *Canadian Geotechnical Journal*, v. 35 issue 2, p. 364-374.

Nakase, Akio, and Kamei, Takeshi, (1986) “INFLUENCE OF STRAIN RATE ON UNDRAINED SHEAR CHARACTERISTICS OF K_0 -CONSOLIDATED COHESIVE SOILS”, *Soils and Foundations*, v. 26 issue 1, p. 85-95.

Seed, H.B., and Lundgren, R., (1954) "Investigation of the Effect of Transient Loadings on the Strength and Deformation Characteristics of Saturated Sands." *Proceedings of the American Society of Civil Engineers*, Vol. 54, pp. 1288-1306.

Whitman, R.V., and Healy, K.A., "Shear Strength of Sands During Rapid Loading," *Journal of the Soil mechanics and Foundations Division*, ASCE, Vol. 88, No. SM2, PP. 99-132.

Lee, K. L., Seed, H. B., and Dunlop, P., (1969) "Effect of Transient Loading on the Strength of Sand," *Proceedings of the 7th International Conference on Soil Mechanics and Foundation Engineering*, Vol. 1, Mexico City, Mexico, pp. 239-247.

Mesri, G., Febres-Cordero, E., Shields, D.R. and Castro,A., (1981) "Shear stress-strain-time behavior of clays," *Geotechnique*, London, England, 31(4), pp. 537-552.

Kulhawy, F. H., and Mayne, P. W., (1990) "Manual on Estimating Soil Properties for Foundation Design," Rep. No. EL-6800, *Electric Power Res. Inst.*, Palo Alto, Calif.

Casagrande, A., and Wilson, S. D., (1951) "Effect of rate of loading on the strength of clays and shales at constant water content," *Geotechnique*, London, U.K., 2(3), pp 251-263.

Graham, J., Crooks, J.H.A., and Bell, A.L.,(1983) "Time effects on the stress-strain behavior of natural soft clays," *Geotechnique*, London, U.K., 33(3), pp 327-340.

Richardson, A. M., and Whitman, R. V., (1963) "Effect of strain-rate upon undrained shear resistance of a saturated remoulded fat clay," *Geotechnique*, London, U.K., 13(4), pp 310-324.

Lefebvre, Guy, and LeBoeuf, Denis, (1987) "Rate effects and cyclic loading of sensitive clays," *Journal of Geotechnical Engineering*, ASCE, Vol. 113, No. 5, pp 476-489.

Sheahan, T.C., Ladd, C.C., and Germaine, J.T., (1996) "Rate-dependent undrained shear behavior of saturated clay," *Journal of Geotechnical Engineering*, ASCE, Vol. 122, No. 2, pp 99-108.

References Related to Cyclic Degradation

Long, James H., and Reese, Lymon C. (1984) "Testing and analysis of two offshore drilled shafts subjected to lateral loads", *ASTM Special Technical Publication*. p. 214-228.

Long, J. H., and Vanneste, G. (1994) "Effects of cyclic lateral loads on piles in sand" *ASCE Journal of Geotechnical Engineering*, Vol: 120(1), pp: 225-224.

Matasovic, N., and Vucetic, M. (1995) "Generalized cyclic-degradation-pore-pressure generation model for clays" *ASCE Journal of Geotechnical Engineering*, Vol: 121(1), pp: 33-42.

Poulos, H.G. (1982) "Single pile response to cyclic lateral load" *ASCE Journal of Geotechnical Engineering Div*, Vol: 108(GT3), pp: 355-375.

Vucetic, Mladen, and Dobry, Ricardo (1988) "Degradation of marine clays under cyclic loading", *American Society Of Civil Engineers Journal Of Geotechnical Engineering*. v. 114 issue 2, p. 133-149.

Vucetic, M. (1994) "Cyclic threshold shear strains in soils" *ASCE Journal of Geotechnical Engineering*, Vol: 120(12), pp:208-28.

Yasuhara, K. (1994) "Post cyclic undrained strength for cohesive soils" *ASCE Journal of Geotechnical Engineering*, Vol: 120(11), pp:1969-79.

